Enhancing Fighter Aircraft Training: Performance Matching with Thrust and Flap Scheduling

J.S. de Bont

Delft University of Technology

TU Delft

nlr

Enhancing Fighter Aircraft Training: Performance Matching with Thrust and Flap Scheduling

by

J.S. de Bont

To obtain the degree of Master of Science
at the Delft University of Technology.

Thesis Committee:	Dr.ir. R. Vos	Supervisor - TU Delft
	Ir. J.W. Dominicus	Supervisor - Royal NLR
	Dr.ir. E. van Kampen	Examiner - TU Delft
	Dr. C. Varriale	Examiner - TU Delft
Faculty:	Faculty of Aerospace Engineering, Delft	
Student Number:	4268598	
Defense Date:	25-05-2023	
Project Duration:	Jan. 2021 - May 2023	

Cover: Modified version of Lockheed Martin Image [1]

TU Delft

nlr

Preface

This thesis marks the end of my Masters program in Aerospace Engineering at the Delft University of Technology. I chose my BSc and MSc because of my love for aircraft and aviation. I am happy that I got to finish my program here with a thesis subject and internship related to the practical use of aircraft, something I am passionate about. Writing a thesis has been the most significant academic challenge I have faced, and it has taught me a great deal about Aerospace Engineering and myself.

I want to express my gratitude to my supervisors, Dr.ir. R. Vos (TU Delft) and ir. Jacco Dominicus (Royal NLR), for their unwavering support, valuable insights, and constructive feedback. The feedback and brainstorming sessions they provided greatly enhanced the quality of this thesis far beyond what it would have been otherwise.

Lorcan Kelleher, thanks for the brainstorming, support, and fun distractions over the years; you know I appreciate it more than words.

Above all, I want to express my gratitude to my family and extended family for their unwavering support and willingness to lend an ear when I talk about aviation and aircraft. I recognize that I wouldn't be where or who I am today without their backing, and I deeply value them.

J.S. de Bont
Delft, May 2023

Summary

The rapid advancements in fighter aircraft technology, along with the limitations on airspace usage, tight budgets, and constant deployment, have made it challenging to train and maintain pilots' operational effectiveness. During training, pilots typically fly with a clean configuration, even though they are preparing for a combat mission where the aircraft is configured with stores. The impact of stores on aircraft performance is not considered during current training missions. Onboard Training Systems (OTS), such as Embedded Training (ET), can simulate various aspects of a combat mission, including virtual enemies and releasing virtual stores at other physical or virtual targets. OTS has been found to increase training efficacy and improve operational effectiveness. However, the currently available OTS do not simulate the performance impact of stores, resulting in a gap in training realism.

This thesis proposes the Performance Matched Training System (PMTS), which aims to simulate the performance impact of stores in-flight. PMTS intends to achieve the same performance and angle of attack (AOA) of a heavier aircraft carrying stores, on a lighter aircraft without stores, by using thrust and flap scheduling. Thrust scheduling is used to match performance parameters, while flaps are used to match AOA. Negative flap deflections allow the aircraft to fly at a higher AOA without changing flight conditions. The goal is to maintain the current training configuration while improving it to match the performance of a combat-configured aircraft, resulting in increased training efficacy.

Information on defense projects is mostly restricted and classified, making data acquisition difficult. An innovative approach is used to create a model of the F-35 aircraft used during this research. The model is based on data from the F-16, which has a more extended operational history and more available data from research. The creation of this aircraft model required the use of drag polars, thrust plots, lift curves, and store characteristics. The F-16 model is verified to be accurate according to publicly available sources. The F-16 was scaled up to represent the F-35. During the scaling process, specific measures are taken to account for differences in the aerodynamic design of the two aircraft.

The effectiveness of PMTS was tested during three virtual missions, an air-to-air, Close Air Support, and Red Flag mission. These missions represent typical combat or training missions, each with its unique configuration. The configurations ranged from only internal stores to both internal and external. The performance impact of stores is different based on where they are mounted.

PMTS was able to match performance and AOA for all three missions. Furthermore, PMTS was able to reduce fuel burn and provide a derate when compared to the current training configuration. Derates lead to longer maintenance intervals for the engine and lower maintenance costs.

Several limitations exist in the current PMTS implementation. The scope of this thesis restricts PMTS to matching specific performance parameters. There is room to improve PMTS by expanding its performance-matching parameters and adding the effect stores have on angular rates and accelerations. For this thesis, the scope of PMTS was limited to static behavior and certain dynamic maneuvers. Integration with the FCS (Flight Control System) and the PVI (Pilot Vehicle Interface) are not covered.

PMTS shows promise in enhancing fighter aircraft training realism. The combination of PMTS and OTS has the potential to increase training efficacy and operational effectiveness. The simulations and analyses presented in this thesis demonstrate the system's effectiveness in reducing fuel consumption and engine wear, contributing to lower training costs. This research offers a foundation for future studies and developments in PMTS, potentially benefiting the military aviation industry.

Nomenclature

Symbol	Definition	Unit
Latin		
a	Acceleration	[m/s^2]
a_{flap}	Lift Curve Slope for a Finite Wing	
a_0	Lift Curve Slope for an Infinite wing	
AR	Aspect Ratio	[-]
C_D	Drag Coefficient	[-]
C_{D_0}	Zero-Lift Drag Coefficient	[-]
$C_{D_{\text{Flap}}}$	Drag Coefficient due to Flap Deflection	[-]
$C_{D_{i_{\text{Flap}}}}$	Flap induced Drag Increment	[-]
$C_{D_{\text{min}}}$	Minimum Drag Coefficient	[-]
$C_{D_{\text{prof}_{\text{flap}}}}$	Flap Profile Drag Increment	[-]
$C_{D_{\text{Store}}}$	Drag Coefficient of Store	[-]
C_f	Average Friction Coefficient	[-]
C_L	Lift Coefficient	[-]
C_{l_α}	Wing Airfoil Lift Curve Slope	[deg^{-1}]
$C_{L_{\alpha_W}}$	Wing Lift Curve Slope	[deg^{-1}]
$(c_{l_\delta})_{\text{theory}}$	Lift Effectiveness of a Plain Flap	[RAD^{-1}]
$C_{L_{\text{min.drag}}}$	Lift Coefficient at minimum Drag	[-]
$c_{l_\delta}/(c_{l_\delta})_{\text{theory}}$	Correction Factor for Plain Flap Lift	[-]
D	Drag	[N]
DI	Drag Index / Drag Count	[-]
e	Oswald Factor	[-]
g	Gravitational Acceleration	[m/s^2]
h	Height	[m]
K_b	Flap-Span Factor	[-]
$k^{'}$	Non-linearities correction factor for Flap	[-]
K^2	Empirical Constant for Flap Drag calculation	[-]
KE	Kinetic Energy	[J]
L	Lift	[N]
m	Mass	[kg]
$N_{Z_{\text{Turn}}}$	Load Factor in Turn	[-]
P_S	Specific Excess Power	[feet/second]
PE	Potential Energy	[J]
R	Turn Radius	[m]
S_{Ref}	Wing Surface Reference Area	[m^2]
S_{Wet}	Wetted Area	[m^2]
S_{wf}	Flapped Wing Area	[m^2]
T	Thrust	[N]
T_{factor}	Thrust Scaling Factor	[-]
t	Time	[seconds]
TR	Turn Rate	[deg/second, RAD/second]
$TSFC$	Thrust Specific Fuel Consumption	[(mg/s)/N]
v	Velocity	[m/s]
W	Weight	[N]

Symbol	Definition	Unit
Greek		
α	Angle of Attack	[deg]
$\alpha_{L=0}$	Zero-Lift Angle of Attack	[deg]
α_T	Thrust Angle relative to Chord line	[deg]
$\frac{(\alpha_\delta)_{C_L}}{(\alpha_\delta)_{c_l}}$	Ratio of three-dimensional to the two dimensional flap effectiveness parameter	[-]
γ	Flight Path Angle	[deg]
$\Delta C_{d_{p_{\Lambda_{c/4}=0}}}$	Two-dimensional profile drag increment due to flaps	[-]
$\Delta C_{L_{\text{flap}}}$	Incremental Lift Coefficient due to flap	[-]
δ_f	Flap Deflection	[deg, RAD]
θ	Flight Path Angle	[deg]
$\Lambda_{C/4}$	Quarter Chord Sweep Angle	[deg, RAD]
ρ	Air Density	[kg/m^3]

List of Figures

List of Tables

Contents

1 Introduction

Fighter aircraft are designed to be used during combat operations, but thankfully the majority of the time, they are used for training and show of force. A show of force, which involves deploying troops and equipment to conflict-prone regions to deter further escalation, comprises a significant portion of fighter aircraft deployment worldwide [2]. The actual use of fighter aircraft during a combat situation is rare, which means pilots need adequate training to stay proficient. High-quality training is critical to ensure operational effectiveness in case actual combat deployments occur. The traditional way of training fighter pilots is expensive and limited by geography, airspace, and infrastructure.

Additionally, training is often inaccessible during a pilot's deployment. Traditional fighter pilot training consists of a couple of different approaches. The most realistic training would be using physical aircraft representing enemy and friendly aircraft. These aircraft are called red and blue air, representing enemies and friendlies. These aircraft act as physical allies or foes and offer high-quality realistic training. However, these red and blue aircraft would be physical aircraft that require pilots, maintenance, and fuel, making them expensive [3]. The 'tactical training' section of Figure 1.1 illustrates what training with red and blue aircraft would look like. It is not always possible to offer a realistic enemy that can mimic the characteristics of the current enemy systems. These characteristics include radar cross-section, targeting capabilities, or aircraft performance.

Furthermore, modeling Surface-to-Air threats is a significant challenge. Ground-based simulators offer some training benefits, especially in procedure and system training, but lack training in airmanship [3, 4]. Airmanship covers a broad range of skills to fly the aircraft, ranging from navigation to the pilot's awareness of the aircraft and their capabilities.

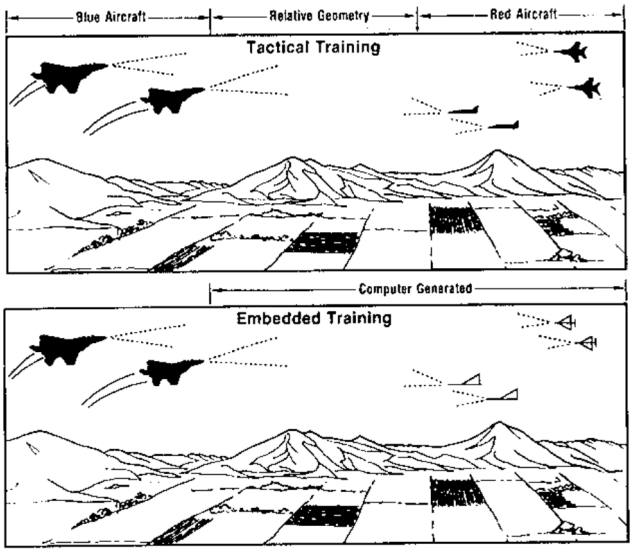

Figure 1.1: Embedded Training Methodology [5]

A number of these training limitations have already been solved, or partially solved, by modern Onboard Training Systems (OTS). For example, the 'SIM' mode on modern fighter aircraft allows the pilot to train as if they had stores on the wings. This enables a pilot to go through the entire process of finding, locking on and eventually releasing a virtual store at a virtual or physical enemy [6]. Technologies like Embedded Training (ET) offer another significant step in training realism. In the last couple of decades, the extended deployment of pilots limited the pilots' access to training time and facilities. In response to this issue, researchers and developers explored the concept of ET to facilitate training anywhere and anytime. ET simulates a virtual overlay in the cockpit, enabling in-flight virtual interactive combat training [7]. Royal NLR has been at the forefront of ET and developed the prototype. ET was first tested on a Royal Netherlands Air Force (RNLAF) F-16 and introduced on the F-35 from the Block-3 version. ET can simulate virtual threats in air, land, or sea environments. The threats can also release virtual ordinance in the simulation. ET can also work together with friendly aircraft, virtual or physical, flying in the same training mission [4]. Figure 1.1 visualizes how training with ET compares to regular training. Since modern fighter aircraft can engage beyond visual range, the airspace required to train would be too large for most countries to accommodate. ET can simulate both friendly and enemy participants virtually. This keeps the physical airspace small while offering a large virtual airspace for training [3]. Since ET can replace red/blue air and ground infrastructure for many mission types, it reduces training costs. ET is predicted to save F-35 users almost three billion dollars over the program's lifetime, making it an incredibly interesting product for developers and users [7].

Training with live munitions is logistically challenging and increases training costs even further, stores are expensive. On top of that, the area where you can deploy live munitions is very limited [8]. Several different arguments lead to the same conclusion: real-life flying is still required to prepare pilots for combat and maintain operational effectiveness. Onboard Training Systems like ET represent a significant advancement in pilot training, enhancing realism and addressing many challenges associated with traditional methods. However, there is a lot of room for improvement. This thesis explores one of the potential improvements.

During a combat mission, aircraft carry various stores such as missiles, bombs, or sensors. These stores, along with their adapters, add weight and affect the aircraft's drag. Modern fighters can carry stores both internally and externally. Internal stores increase the aircraft's weight, leading to a rise in induced drag and the angle of attack (AOA) at which the aircraft must fly. External stores add weight and contribute to drag due to the presence of stores and adapters, further increasing total drag and AOA.

Although OTS allows for virtual store configurations and the releasing of these virtual stores, it does not account for the performance impact these stores would have in an actual combat situation. Pilots flying an aircraft with OTS enabled feel no difference in aircraft performance between the configurations, even though these differences would be noticeable during actual missions. This presents an opportunity to enhance OTS by simulating the performance impact of different configurations in-flight.

Figure 1.2: RNLAF Lockheed Martin F-35A [9]

This thesis proposes a system to account for the performance impact of stores, called the Performance Matched Training System (PMTS). PMTS would limit the performance of an aircraft to make it behave like a heavier configuration of the same aircraft. The heavier configuration produces more drag due to its stores, limiting performance. Since the aircraft is heavier and produces more drag, its AOA will also be higher, PMTS will use flaps to match the AOA of the heavier configuration. By matching performance, the training realism will increase as the aircraft behaves more like it would during a combat mission. Added benefits are the potential for fuel savings, aircraft airframe life, and a derate on the engine, which could reduce engine wear.

PMTS will be developed for the F-35 but could also be used on other platforms. The F-35 is the latest generation fighter aircraft and represents a significant step up in capability, survivability, and mission effectiveness compared to the previous generation. The first RNLAF F-35A is shown in Figure 1.2. There are several reasons the F-35 has been chosen as the aircraft for this thesis. First, the Flight Control System (FCS) of the F-35 is particularly well suited for this type of training system. The F-35 uses a Nonlinear Dynamic Inversion based FCS. This type of FCS is model-based. Pilots command an aircraft to perform a specific movement using their controls, this command is then fed to an onboard model, which takes into account the current flight condition and configuration and determines what the most efficient control surface solution is to fulfill the requested command. If PMTS proves effective, implementing this on an F-35 should be relatively straightforward. Instead of feeding the command to the actual model in the NDI FCS, it is first fed to the heavier configurations model, after which the heavier configurations response is taken as a new command. The pilot's commands would be translated into the aircraft response of a heavier aircraft. The second reason the F-35 was selected for this thesis is the prevalence and longevity of the aircraft. It will be the main fighter for many air forces worldwide for a long time, including the Royal Netherlands Air Force (RNLAF), which the NLR and TU Delft work with.

This thesis investigates the feasibility of such an improvement through the development of a Performance Matched Training System (PMTS). The proposed PMTS would employ thrust scheduling and flap deflections to match performance and AOA throughout the mission, providing a more accurate and immersive training experience.

1.1. Research Objective

This thesis aims to enhance the realism and effectiveness of current fighter aircraft training missions by investigating whether a system based on flaps and thrust scheduling can enable a lighter aircraft without stores to match the performance of a heavier aircraft with stores. Thrust scheduling is used to match performance, while flaps scheduling is used to match AOA. Quantifying increased training realism is only possible by evaluating pilots flying with the system. Since this is impossible for this thesis, matching AOA and performance will indicate increased training realism and demonstrate the effectiveness of PMTS.

This research is relevant due to constraints on training cost, airspace, and availability. These constraints have only increased in recent years. A system like PMTS would be a valuable addition to the current OTS. Furthermore, improving operational capability is a desire for any defense department worldwide. Developing a way to do this while, not increasing training costs would be a great addition to the currently available training options.

The research method involves creating an F-35 aircraft model and simulating specific combat missions. Each mission will be flown by three aircraft configurations; loaded, clean, and matching. The loaded aircraft represents a combat aircraft with stores and will set the performance target for the matching aircraft with PMTS. The clean aircraft represents the current training configuration. The matching configuration is a clean aircraft that will use PMTS to derate its performance to match the performance of the loaded aircraft. These three missions will provide data on how effectively performance and AOA can be matched and the impact PMTS has on fuel burn and engine life. The missions are modeled on real-life air-to-air (A/A), close air support (CAS), and Red Flag (RF) missions. Each mission has a unique configuration, with the A/A and RF missions having only internal stores and the CAS also using external stores. The missions will be described in detail, they cover various missions the F-35 performs today. They differ in total weight, altitude, and flight profile. This provides an opportunity to test PMTS in a diverse set of missions.

Before using PMTS on these three missions, three smaller PMTS tests will be used to display its effectiveness. These tests consist of basic aircraft maneuvers completed by all three configurations described earlier. They will show how effective PMTS can be even in smaller tests that only last a few minutes. These tests will make it easier to understand how PMTS functions and the benefits it can offer.

Creating an F-35 model poses challenges due to the classified nature of defense projects. Therefore, a model of the F-16 will be created, which will then be scaled to represent the F-35. The F-16 model can be constructed using publicly available research papers, manuals, and other documents. All data sources used to create the F-16 model are obtained from publicly available sources and will be shown in the reference section. The scaled-up F-35 cannot be verified due to that data being classified. Since the F-16 model can be verified to be accurate, it is anticipated that the F-35 model will produce results within a reasonable range of accuracy. If PMTS proves effective, it will enhance training realism while reducing fuel burn, maintenance costs, and engine wear.

1.2. Research Questions

This study investigates whether training realism could improve using a thrust and flaps scheduling method to match a heavier aircraft's performance and AOA. The following main research question is established based on the literature review, NLR requirements, and gaps in current training methods.

What is the potential impact of implementing a flap and thrust scheduling system on enhancing training efficacy for fighter aircraft?

To answer the main research question, it has been divided into different parts, each addressing a crucial aspect of the problem:

1. How can the effect of stores on aircraft performance be simulated with a clean aircraft?
2. How successful is the performance matching system in terms of matching aircraft performance parameters?
   (a) What is the reduction in fuel use on a typical mission?
   (b) What is the effect on engine wear?
3. How does software-enhanced training compare to the current methods of training?

By addressing these research questions, this thesis aims to explore the feasibility and effectiveness of the proposed PMTS in enhancing training efficacy for fighter aircraft. The effectiveness of PMTS with respect to the clean configuration is especially interesting, as it represents the currently most flown training configuration.

1.3. Report Outline

This thesis is divided up into multiple parts. Chapter 2 is the literature study on the F-35, current training methods, and the unique flight control system. After the literature study, the main part of the thesis is again divided into blocks. The structure is shown in Figure 1.3. Chapter 3 is the first block that revolves around collecting data for the F-16 model, creating it, and verifying its performance. This chapter will also cover the methodology of how the model is made and how it functions. The second block, covered in Chapter 4, is where the model is scaled to represent the F-35 and where PMTS is created and tested. This chapter also covers the methodology behind PMTS. The missions and configurations are introduced in Chapter 5, and the results from flying these missions are shown in Chapter 6. The conclusion and recommendations for future research are provided in Chapter 7. Finally, additional information and figures are shown in the Appendixes.

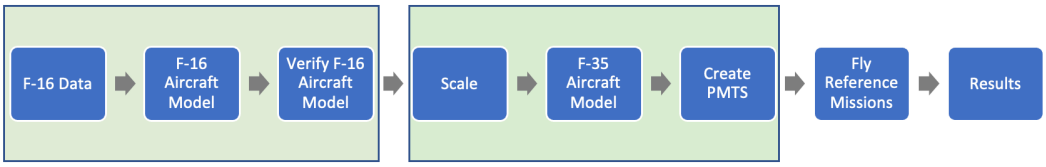

Figure 1.3: Thesis Methodology Structure

2

Background Information

This chapter provides the necessary background information to understand the scope, aim, and purpose of the research proposed in this thesis. The F-35 program will be introduced, highlighting why this aircraft is suited to answer the research questions. Background information regarding the flight control system, current training techniques, issues with the current F-35 program are covered, and how PMTS could mitigate these problems. For more detailed background information

2.1. The Joint Strike Fighter program

The end of the Cold War saw drastic cuts in defense budgets worldwide. These budget cuts, an aging fleet, and the introduction of stealth aircraft forced Western countries to collaborate on the next generation of aircraft. Historically, each defense department would have its specific requirements for an aircraft. This necessitated the development of a tailor-made aircraft for that defense branch. For example, the F-18 was designed for the U.S. Navy, while the F-22 was created for the U.S. Air Force. This design philosophy resulted in a large variety of aircraft types, which became difficult and expensive to procure and maintain. The Joint Strike Fighter (JSF) program was formed to create a single platform for all defense branches. The winner of the JSF competition would replace the aircraft used by Western countries at that time, shown in Figure 2.1.

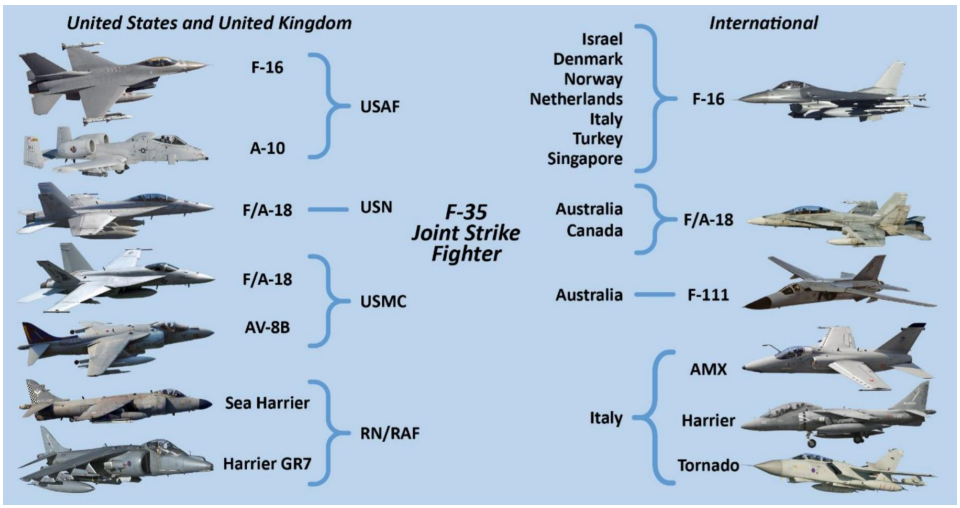

Figure 2.1: Legacy fighter types that are expected to be replaced by JSF [10].

The winner of the JSF competition was the X-35, which became the Lockheed Martin F-35 Lightning II. To fulfill the requirements of three defense branches, three different versions of the F-35 were developed: the conventional take-off and landing variant (CTOL) (F-35A), the short take-off and vertical landing variant (STOVL) (F-35B), and the carrier take-off and landing variant (CV) (F-35C). The F-35

represents a significant leap forward in fighter aircraft technology. Most countries purchasing the F-35 are upgrading their third and fourth-generation aircraft to this fifth-generation aircraft. The transition from fourth-generation aircraft, known for their dogfighting ability, close-range combat, and maneuverability, to fifth-generation aircraft has necessitated a different approach to training and operations. Fifth-generation aircraft, like the F-35, are renowned for their stealth, sensor fusion, network-centric warfare, and electronic warfare systems [11]. Besides the outstanding capabilities of the F-35 itself, it is also a force multiplier, enabling older aircraft flying alongside it to benefit from its sensors and data for improved situational awareness [12].

The F-35's success is indisputable, with the program becoming the largest defense project in history [13]. Over 3,000 orders have been placed for the F-35, divided among three primary U.S. services, which account for most orders, and 15 international allies. The Netherlands has also chosen the F-35 as its next fighter, with an order of 46 aircraft and more planned. The war in Ukraine has drastically increased F-35 orders, with countries like Germany and Canada signing on in recent months [14]. By replacing over thirteen legacy aircraft types, the F-35 has the potential to streamline global fleets and reduce acquisition and maintenance costs [10].

2.1.1. The F-35A

This thesis will focus on the F-35A, the most popular variant with the highest number of orders and the primary platform chosen by the RNLAF. Some specifications are provided in Table 2.1. From this point forward, any mention of the F-35 in this thesis will refer to the F-35A.

Table 2.1: Basic Specification of the F-35A [15]

Length [m]	Wingspan [m]	Wing Area [m^2]	Aspect Ratio	Max. Takeoff Weight [kg]
15.7	11	43	2.66	29,900

2.2. The Current State of Training

Recent training strategy and technology developments have led to significant jumps in training effectiveness [16]. Fourth-generation aircraft rely heavily on a pilot's skill in combat. Designed for Within Visual Range (WVR) combat, 4th generation aircraft require a high level of pilot skill to be effective in battle. WVR combat is often portrayed in aviation-themed films such as Top Gun. There are multiple ways to train pilots for this type of flying.

RNLAF training missions involve multiple aircraft practicing WVR maneuvers without stores attached. The missions consist of red and blue air components, with red air representing enemy aircraft. However, the training benefit for red air pilots is limited, and operating and maintaining these aircraft can be costly [3]. Additionally, this training requires specific infrastructure and can only be done in certain areas. Nonetheless, it remains an effective way to train for WVR combat and applies to air-to-air and air-to-ground missions.

Live training exercises allow pilots to use actual stores and simulate combat configurations. However, this method is expensive and rules out flights over populated areas. The RNLAF is limited to dropping 70 stores per year on its designated weapon range [8], limiting training availability. Air-to-air training with live stores is even more challenging and can involve using drones, which further increases costs [17]. Given the high costs, developing virtual training options is worth considering. An hour-long air-to-air training mission with four blue and four red F-35s cost over 280.000 dollars, highlighting the need for more cost-effective training methods [18].

Ground-based simulator training is a cost-effective alternative to live training, and simulators have long been a valuable tool for commercial pilots to learn and practice essential skills. However, simulators cannot replicate the g-forces experienced by pilots in fighter aircraft, with the Desdemona simulator being the only one capable of simulating constant g-forces up to 3.5 g. Airmanship, essential for combat readiness, cannot be fully trained on the ground. Flying and training in the air remain a critical part of pilot training, as it enables pilots to develop their feel and awareness of the aircraft [19, 20].

2.2.1. Fifth Generation Training

The introduction of fifth-generation aircraft, such as the F-35, has led to significant changes in combat strategies and tactics. Beyond Visual Range (BVR) combat has become the preferred method for completing missions, offering numerous benefits over traditional WVR combat, particularly against lower-generation adversaries. BVR combat relies heavily on advanced sensors, data fusion, and interoperability. This shift in mission execution demands a new approach to training.

While traditional training methods like using red air as targets can still be used for BVR training, the improvements in radar and targeting range provided by the F-35 require a significantly larger training airspace, which may not be feasible for countries with limited airspace [3]. Additionally, replicating modern adversarial aircraft for training purposes is challenging and expensive. Therefore, there is a need for innovative training solutions to effectively prepare pilots for BVR combat while overcoming traditional training limitations.

Onboard Training Systems

Onboard Training Systems (OTS) for the F-35 have improved training methods by simulating an aircraft's combat mode. Pilots can practice releasing a store by locking onto a physical or virtual aircraft in SIM mode, simulating the sequence of actions during a combat scenario [6]. OTS also allows training with other aircraft to avoid virtual missiles and report hits or misses on targets. However, this method still requires the presence of physical aircraft for a realistic experience.

Embedded Training (ET) is a virtual simulation system that enhances training realism by mimicking incoming signals on sensors, requiring the pilot to employ countermeasures, fire stores, or perform evasive maneuvers against almost any platform. With ET, pilots can train for specific missions against enemy platforms and engage in multiplayer scenarios. This overcomes some challenges and limitations of traditional training methods, providing a more effective and cost-efficient solution for preparing F-35 pilots for modern warfare scenarios.

OTS like ET offer cost-effective and versatile solutions for preparing pilots to operate fifth-generation aircraft like the F-35. ET eliminates the need for physical red or blue air, significantly reducing the cost of live training exercises. ET outperforms traditional methods in terms of training effectiveness for various mission aspects, allowing for virtual simulation of large airspace while only requiring a small physical space. ET enables realistic simulation of ground and air threats, providing more dynamic and tailored training scenarios. Pilots receive immediate feedback, enhancing the overall training experience [3, 21]. ET's benefits will continue to grow as technologies develop, making it an increasingly effective training tool for next-generation aircraft.

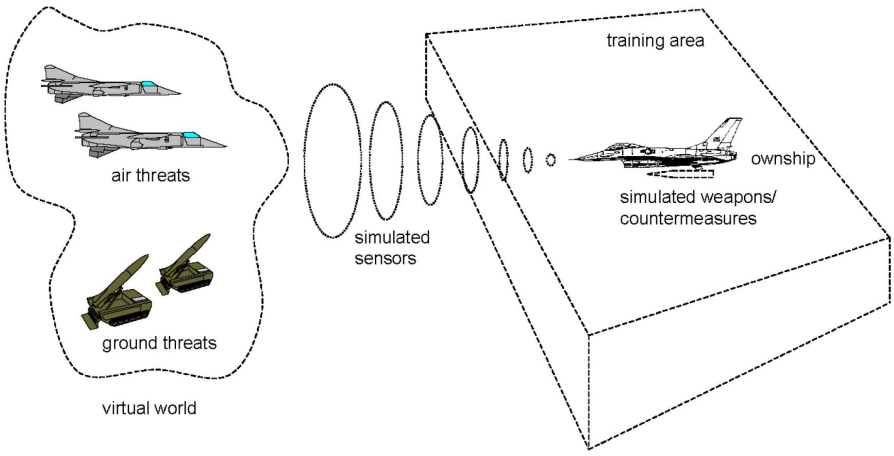

Figure 2.2: Airspace use for fighter aircraft with Embedded Training [3]

Research has demonstrated that Embedded Training (ET) has significantly impacted training effectiveness, with its potential first demonstrated on an F-16 where it increased training efficiency by $30\,\%$ [3, 4, 22]. This convinced Lockheed Martin to add ET to the F-35, with expanded capabilities over the F-16 version. ET outperforms live and simulator training for most mission types and is now onboard every F-35 thanks to research and development by Airbus and NLR [3].

Training with ET can be carried out anytime and anywhere. ET is estimated to save nearly three billion dollars in training costs over the lifetime of the F-35, with most of these savings coming from air-to-air training [23]. Although ET may underperform in some categories compared to live training, its ability to improve training effectiveness across various other aspects while reducing costs makes it a crucial component of the F-35 training package.

OTS like ET demonstrate the potential for virtual training systems to enhance training realism and efficiency. PMTS could be integrated as another training system for the F-35, offering similar training procedures as current methods but with limitations on the aircraft's performance for increased realism. Safety measures, such as altitude floors and the system being disabled during landings and descents, would still apply to ensure safety during training.

In conclusion, Onboard Training Systems have revolutionized how pilots train, providing a more realistic and efficient training experience that resembles actual combat missions. As technology advances, OTS will likely play an increasingly important role in preparing pilots for modern warfare and maintaining operational effectiveness between deployments.

Current Training Limitations and the Performance Gap

Currently, OTS does not account for the differences in aircraft behavior when carrying various virtual payloads, which can significantly affect the performance of the F-35. As pilots predominantly train with clean aircraft due to the limited availability of live training, they may not be fully prepared for real combat scenarios where the aircraft carries payloads, such as weapons or fuel tanks. The delta between training and actual combat conditions can be large for specific store configurations.

To address this performance gap and enhance the realism of OTS, this thesis will focus on developing a Performance Matched Training System (PMTS). The PMTS aims to accurately represent the aircraft's behavior under various payload configurations during training, preparing pilots for real combat situations. In addition, by simulating the impact of different configurations on the aircraft's performance, PMTS could reduce fuel consumption and engine maintenance requirements, further contributing to cost savings in the training process.

In conclusion, while OTS has significantly improved pilot training, there remains room for enhancement through developing and integrating a system like PMTS. By closing the performance gap and providing a more realistic representation of aircraft behavior under different configurations, PMTS promises to advance the capabilities of OTS further and increase the operational effectiveness of pilots. PMTS can be used together or independently from the current OTS available on the F-35. Allowing multiple OTS to work together enhances training efficacy, but it is also possible to train with just PMTS.

2.3. Performance Matched Training System

This thesis aims to find a possible solution to close or reduce the performance gap during training missions. The proposed solution is called the Performance Matched Training System (PMTS). PMTS will reduce the performance of a clean training aircraft to match the performance of a loaded combat aircraft. PMTS will also use flaps to match the higher angle of attack of the loaded aircraft. A flight-ready PMTS system would impact the Engine Management System (EMS), Flight Control System (FCS), and Pilot Vehicle Interface (PVI) and would interface with the current OTS.

2.3.1. Engine Management System

The EMS translates a throttle input by the pilot into an engine setting, depending on several inputs and flight condition variables. The F135 engine, selected for the F-35, is an afterburning turbofan based on the F119 engine used in the F-22 [24]. Currently, the F135 engine operates at its design limit and maybe even a little over, which has led to premature cracks in the turbine blade coating. Although these cracks do not pose an immediate safety hazard, they reduce the engine's operational life and necessitate early maintenance [25]. This, in turn, impacts the operational readiness of the aircraft, a crucial factor for defense departments. In 2022, the U.S. Department of Defense reported that 5 % to 6 % of its F-35 fleet would be without engines due to maintenance [26]. Pratt and Whitney are working on an engine core upgrade, which could help alleviate some of the issues the F135 faces today [27]. By upgrading the engine core, the F135 should be able to operate further away from its design limit during normal operations, increasing engine life.

The Impact of derating on engines

Derating an engine, which involves running the engine at a lower power setting and reducing thrust production, can be a potential solution to the issues faced with the F135 engine. High-pressure turbine (HPT) temperature is typically the limiting factor for engines, as the turbine blades are the most stressed parts and suffer the highest degradation [28]. Derating is common practice in commercial aviation, with some fantastic results. A 25 % derate can lead to an order of magnitude increase in cycles to failure [29]. This results in an increase in maintenance interval and a reduction in costs. Derating can reduce overall fuel use due to the lower power setting.

Research into the effect of derating on military aircraft is limited. The military prioritizes operational effectiveness over potential savings in fuel and maintenance. Research indicates that even a 5 % derate on a military engine leads to an up to 50 % increase in HPT blade life [28]. The data show that even a slight derate can significantly impact the longevity of an aircraft engine.

Quantifying the exact savings in maintenance cost, engine replacements, or maintenance intervals is challenging and would warrant its own research. However, with the data presented in this section, the derate percentages that will follow from implementing PMTS can be put into perspective. A few percent derate can substantially impact the longevity and should not be dismissed. That small percentage of derate could improve the operational readiness of the F135 engine and, indirectly, that of the F-35.

PMTS will use the EMS to reduce engine performance, allowing the PMTS-equipped aircraft to match the flight conditions of a heavier target aircraft with more drag while using a lower thrust setting. The pilot can set the throttle to full power in the cockpit, and PMTS will limit the engine's performance without requiring cockpit adjustments, resulting in more realistic training. This engine derating will reduce fuel and maintenance costs, potentially alleviating some of the issues currently faced by the F135. Maintenance intervals and lifetime will increase, reducing the need for spare parts.

2.3.2. Flight Control System

The Flight Control System (FCS) of the F-35 is a first of its kind. When Lockheed Martin proposed the design of three different variants of the F-35, they were hoping to use a unified FCS for all three variants, despite their significant differences. Traditional FBW systems, which relied on PID-like controllers using precalculated scheduled gains, struggled to guarantee closed-loop performance in highly nonlinear regimes that fighter aircraft often encounter, such as high angle of attack, high angular rates, and transonic flight [30]. These nonlinear regimes make guaranteeing closed-loop performance with a legacy FBW system challenging and sometimes impossible [31, 32]. Nonlinear propulsion characteristics add even more complexity to legacy FBW systems [33].

NDI uses nonlinear equations of motion, aircraft aerodynamics, mass properties, and an engine model to create an onboard model. This model provides live control surface solutions for the desired aircraft responses the pilot asks for. This allows for closed-loop performance, even in nonlinear regimes where traditional FBW systems may fail. The F-35 is the first production fighter to incorporate NDI as the FCS for its FBW system [34, 35, 36, 37].

NDI utilizes an inverse model with the equations of motion and aerodynamic behavior characteristics to simulate all possible control effector combinations until one solution can efficiently fulfill the pilot's commands [38]. NDI can determine the most efficient combination of control surface deflections needed to produce the desired response. According to F-35 test pilot Dan Canin, "NDI allows the aircraft

to determine a control solution on the fly, based on a detailed onboard model of the aircraft's mass properties and stability and control characteristics" [39].

NDI simplifies the pilot's role by translating their hands-on throttle-and-stick (HOTAS) input into the desired aircraft response. It does this regardless of the flight condition the aircraft is in. Figure 2.3 provides a simplified illustration of how an input becomes a control surface deflection. If PMTS is used, the pilot's input passes through the loaded aircraft model first, and the response will then become the required response for the clean, PMTS-equipped aircraft. The pilot can then fly the clean aircraft with the response of a heavier aircraft without changing their cockpit behavior.

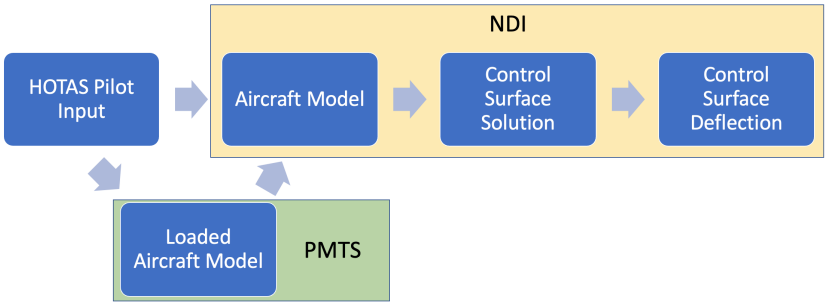

Figure 2.3: NDI with PMTS implementation

There have been examples of FCS being adapted to facilitate in-flight simulation of other aircraft. Projects like X-62 VISTA, DLT ATTAS, and the Shuttle Training Aircraft have shown that in-flight simulation of another aircraft's performance and handling characteristics are possible [40, 41, 42, 43]. Given PMTS is simulating a different configuration of the same aircraft, the F-35 is expected to accommodate this well. NDI's model-based control system allows for a simple implementation of PMTS by changing the onboard model NDI uses. A process step would be added to calculate the simulated response of the loaded aircraft and then translate it to the desired control effector combination for a clean aircraft.

2.4. Scope

Implementing PMTS would affect many aspects and systems of the F-35. To keep the scope of this thesis in line with the expectations of the TU Delft and NLR while also considering the timeline, certain aspects of this thesis are limited. For this thesis, the scope of PMTS is limited to the aircraft's performance and angle of attack. To do this, PMTS will only use the engine management system and the trailing edge flaps. These two combined will allow for the control of the aircraft's flight condition (velocity, climb rate, acceleration) and the aircraft's angle of attack. The aircraft does not take off, land, or descend during missions. Furthermore, it does not consider any structural limitations besides the max load factor on the airframe.

Dynamic movements like angular rates or accelerations are not considered in this thesis. The aircraft can accelerate, climb, turn, or perform a combination of these options. Descending flight, landing, take-off, or any flight activity below $10\,000$ ft is not treated. This altitude is the training floor, a common practice during training missions. Creating a model for the F-35 is not possible due to the classified nature of defense projects, a workaround is scaling an F-16 model up to represent an F-35.

3

The Aircraft Model

To create the Performance Matched Training System (PMTS), an aircraft model of the F-35 has to be created. Because of the classified nature of defense projects, the decision has been made to create an F-16 model based on publicly available information and then scale that model to represent an F-35. This chapter covers the creation and validation of the F-16 model.

3.1. Regulation and Workarounds

Regulations like the International Traffic in Arms Regulations (ITAR)[1] severely restrict what information is publicly available for defense and military-related technologies. The F-35 falls under ITAR, so the aircraft's operational capabilities are classified. Creating an F-35 model for this thesis requires a workaround that does not violate any regulations.

For this thesis, the decision was made to base the F-35 model on an F-16 model. Using an F-16 model as a basis for an F-35 model has limitations and potential inaccuracies but offers a viable solution to answering the research questions. The F-16 has been flying since 1974, and many research papers have been published on its performance and capabilities. This thesis uses two key data sources for F-16 flight performance data. The first is a highly regarded F-16 simulator: Falcon 4.0, which is based on research papers and provides drag polars, lift, and thrust curves [44]. The second data source is a paper that compares the wind tunnel performance with flight-test data of the YF-16 and F-16. The flight test and wind tunnel data comparing the two aircraft show that they only differ a couple of percent in performance. Therefore, using the YF-16 flight test data for the F-16 model in this thesis is deemed reasonable. The YF-16 research paper consists of data like the drag polar, thrust settings, lift curves, and some other parameters [45].

Stores and adapters also fall under ITAR. Store Drag Index (DI) data is related to the aircraft the store or adapter is attached to, so an adjustment will be made to get the correct DI for stores mounted on the F-35. Data like the drag index and weight of certain stores and adapters are available in the public domain from government data sources even though they fall under ITAR [46, 47, 48, 49].

3.2. F-16 vs. F-35

While the F-16 and F-35 are both multi-role fighters and comparable in size, they significantly differ in design, technology, and operational capability. These aircraft can do everything from close air support (CAS), air-to-air (A/A), or even electronic warfare missions. The F-35 is significantly more advanced, incorporating the latest technology, radar, and mission systems. The F-35 is a stealth aircraft designed to minimize its radar signature, making it harder to detect and track. The F-16 is not a stealth aircraft. While hard to quantify, creating a stealth aircraft can significantly impact the aircraft's aerodynamic design. Since the radar cross section becomes one of the most critical design parameters, other parameters like aerodynamic efficiency might suffer due to this prioritization.

The F-16 was designed with dogfighting in mind, while the F-35 is optimized for beyond-visual-range combat. The F-35 relies on its stealth, sensors, and advanced radar to engage enemies from a distance

[1] `https://www.pmddtc.state.gov/ddtc_public?id=ddtc_public_portal_itar_landing`

before they can detect its presence. These differences in design and operational capability are reflected in each aircraft's training missions, as discussed in Section 2.2.1. Despite these differences, using the F-16 as a basis for constructing an F-35 model in this thesis provides a valuable starting point for addressing the research questions, as both aircraft share similarities and are multi-role fighters.

Figure 3.1: F-16 v.s. F-35, true to scale [50]

Figure 3.1 shows a to scale comparison of the F-16 and F-35. The F-16 has an aspect ratio of 3.56 while the F-35 has an aspect ratio of 2.66. The F-35's lower aspect ratio affects maneuverability, the lift curve, and the overall aerodynamic efficiency of the aircraft. The wing area increases from $28\,\mathrm{m}^2$ on the F-16 to $43\,\mathrm{m}^2$ on the F-35 [51]. This is a significant increase that will also affect aircraft performance. The combination of a lower aspect ratio and higher wing surface area means the F-35 will produce more induced drag and lose more energy in high-load turns.

3.3. Equations of Motion

In Figure 3.2, an aircraft is depicted in-flight, with the flight path represented by an angle γ with respect to the horizontal axis. The angle of attack, α, is the angle between the chord line and the flight path direction. Four primary forces are acting on the aircraft, starting with the Lift, which is perpendicular to the flight path direction. The Drag is parallel to the flight path and opposes the aircraft's forward motion. Thrust, which is inclined to the angle of the flight path with an angle of α_T. Finally, the weight (W) that acts vertically towards the Earth.

Considering these forces and their interactions in a free-body diagram (FBD) and kinetic diagram (KD), the equations of motion for the aircraft can be established. These equations will help to model the aircraft's performance.

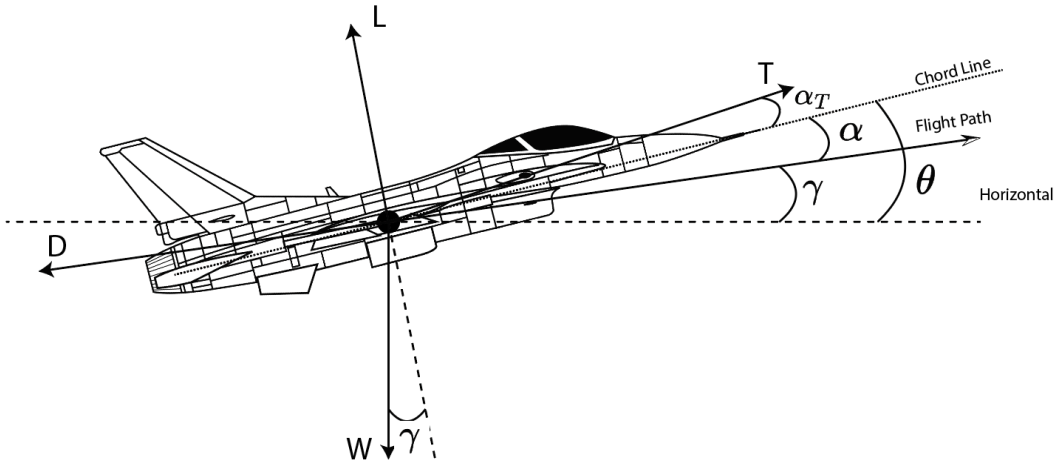

Figure 3.2: Force diagram for an airplane in-flight

Some assumptions are made to simplify the FBD. The first assumption is that the flight path angle is 0° during straight and level flight. The second assumption is that the thrust acts in line with the chord line of the aircraft, resulting in α_T becoming 0°. Considering these assumptions, Figure 3.3 displays the updated FBD and the corresponding KD. Equation (3.1) shows the vertical force equilibrium for the flight condition shown in Figure 3.3, Equation (3.2) displays the horizontal equation of motion for the same condition.

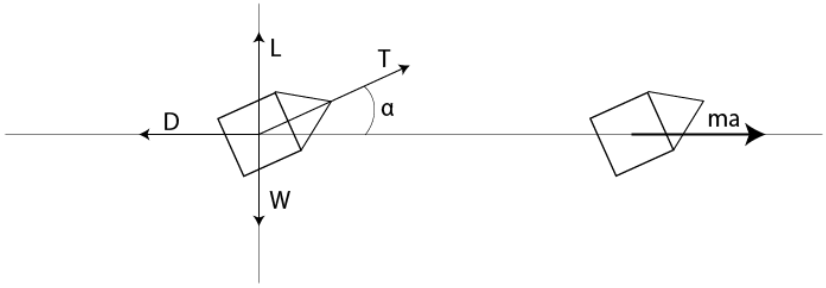

Figure 3.3: Force diagram and Kinetic Diagram for an aircraft in-flight

$$L + T\sin(\alpha) = W \tag{3.1}$$

$$T\cos(\alpha) - D = m\frac{dv}{dt} \tag{3.2}$$

3.3.1. The Energy Method

The energy method is preferred for aircraft such as the F-16 and the F-35 that can fly at highly accelerated rates of climb. The energy method uses the aircraft's specific energy (H_e), also known as energy height. The energy height is the sum of the potential and kinetic energy of the aircraft per unit weight, as displayed in Equation (3.3) [52]. The equation indicates that if an aircraft maintains its energy state, it can exchange velocity for altitude or vice versa. Thrust can be used to increase the energy height. The energy height is essential to a fighter jet during a dogfight. With everything else equal, the aircraft with the highest energy height has an advantage in air combat maneuvers [52].

$$H_e = \frac{PE + KE}{W} = \frac{mgh + \frac{1}{2}mv^2}{mg} \tag{3.3}$$

For an aircraft to climb, the flight path angle needs to be greater than 0°; this changes the assumptions made to obtain the previous equations of motion. The equation of motion along the flight path is shown in Equation (3.4).

$$T - D - W\sin(\gamma) = m\frac{dv}{dt} \tag{3.4}$$

With m being equal to $\frac{W}{g}$ and the multiplication of both sides with $\frac{v}{W}$ the equation can be rewritten as Equation (3.5).

$$\frac{Tv - Dv}{W} = v\sin(\gamma) + \frac{v}{g}\frac{dv}{dt} \tag{3.5}$$

$\frac{Tv-Dv}{W}$ is defined as the specific excess power (SEP). $v\sin(\gamma)$ is defined as the rate of climb, also denoted as $\frac{dh}{dt}$. Equation (3.5) can be rewritten as Equation (3.6).

$$P_s = \frac{Tv - Dv}{W} = \frac{dh}{dt} + \frac{v}{g}\frac{dv}{dt} \tag{3.6}$$

The energy method is a versatile tool that can be applied to various flight conditions, including climbs, cruise, and combat scenarios. Using this method, aircraft performance can be evaluated throughout the entire duration of a mission. The energy method requires models for Drag, Thrust, and Angle of Attack.

3.4. Drag

The drag polar is instrumental in understanding aircraft performance. The drag polar relates drag production and lift production at various Mach numbers. For the F-16, two different drag polars are publicly available. The drag polar used for the aircraft model, and subsequent scaling, will be constructed using the YF-16 flight test data [45]. The drag polars from the YF-16 flight test are shown in Figure 3.4b. The doghouse plots in the Falcon 4.0 sim manual are the only option to verify the complete aircraft model. Therefore, a drag model based on the drag polar from the Falcon 4.0 manual is also created [44]. The Falcon 4.0 polars, shown in Figure 3.4a, are only used during verification. The YF-16 polars are used as a base during scaling, testing, and missions since they represent more accurate data. Larger versions of these drag polars are shown in Appendix A.1.

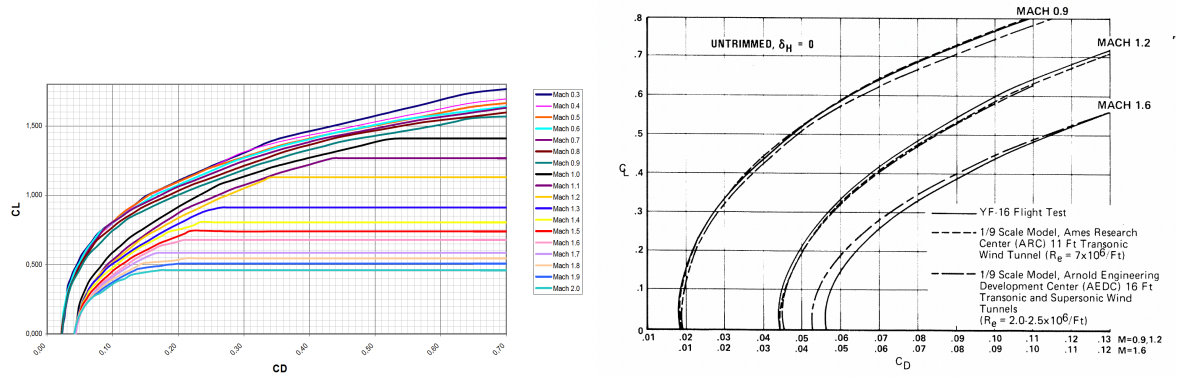

(a) F-16 Drag polar [44]

(b) YF-16 Drag polar [45]

Figure 3.4: Two drag polar models for the F-16

A different method of digitizing is required for both drag polars. Digitizing the Falcon 4.0 drag polars is done by adding all the data points from Figure 3.4a to an array and then using linear interpolation to calculate all the values between the curves. The Falcon 4.0 drag polar is limited by the maximum lift coefficients of the aircraft, avoiding the 'infinite' drag values present in the original data.

The YF-16 data consists of three drag polars at three different Mach numbers: 0.9, 1.2, and 1.6. The gap in data between the Mach numbers of 0.9 and 1.2 needs to be addressed. A linear interpolation between these curves would not account for the transonic drag rise. The book *Design for Air Combat* by *R. Whitford* contains a drag-rise plot for the $C_{D_{\text{min}}}$ value of an F-16 [53]. Using the shape of Whitford's transonic drag rise data but fitting that shape to the $C_{D_{\text{min}}}$ values obtained from the YF-16 drag polars provides a solution to the lack of transonic data in Figure 3.4b. To model the drag polar correctly across

the flight envelope, Equation (3.7) will be fitted to the flight test polars [52]. This requires determining the three unknown variables in Equation (3.7): $C_{D_{\text{min}}}$, e and $C_{L_{\text{min.drag}}}$. What the variables in Equation (3.7) represent visually in a polar is shown in Figure A.3.

$$C_D = C_{D_{\text{min}}} + \frac{(C_L - C_{L_{\text{min. drag}}})^2}{\pi e AR} \tag{3.7}$$

$C_{D_{\text{min}}}$ represents the minimum drag coefficient on the drag polar. $C_{L_{\text{min.drag}}}$ is the lift coefficient that corresponds with the $C_{D_{\text{min}}}$. To find the Oswald factor, a nonlinear regression function in MATLAB is used to fit Equation (3.7) to the three digitized polars, using the Oswald factor as the only unknown variable [52]. The other two variables can be determined visually from the drag polar data. The three Oswald factors calculated have an average R^2 of 0.997, indicating a good fit. The variables are shown in Table 3.1.

Table 3.1: Data for YF-16 Drag Polars

Mach	0.9	1.2	1.6
e	0.65	0.51	0.37
$C_{D_{\text{min}}}$	0.018	0.044	0.046
$C_{L_{\text{min drag}}}$	0.028	0.027	0.015
R^2	0.992	0.999	0.999

A custom data fitting method is employed to model the transonic drag rise accurately. The shape of the F-16 $C_{D_{\text{min}}}$ data from *Design for Air Combat* by *R. Whitford* is preserved, but it is adjusted to match the $C_{D_{\text{min}}}$ values from the YF-16 flight test data in Figure 3.4b. This approach ensures that the transonic drag rise fits both the shape of the F-16 data from *R. Whitford* and the specific values from the YF-16 flight tests. The custom fit for $C_{D_{\text{min}}}$ is shown in Figure 3.5. The black line represents the F-16 drag rise shape from *Design for Air Combat* by *R. Whitford* [53]. The drag rise data is fitted to the blue line, which represents the three data points from the YF-16 drag polars, as displayed in Table 3.1.

The Oswald Factor and $C_{L_{\text{min.drag}}}$ are linearly interpolated between Mach numbers and assumed to stay constant in the subsonic regime. This approach ensures a comprehensive and accurate drag model for the F-16. The three variables modeled for this thesis to be able to use Equation (3.7) are shown in Appendix A.3. Using these three distributions, the drag can be calculated for any flight condition within the flight envelope.

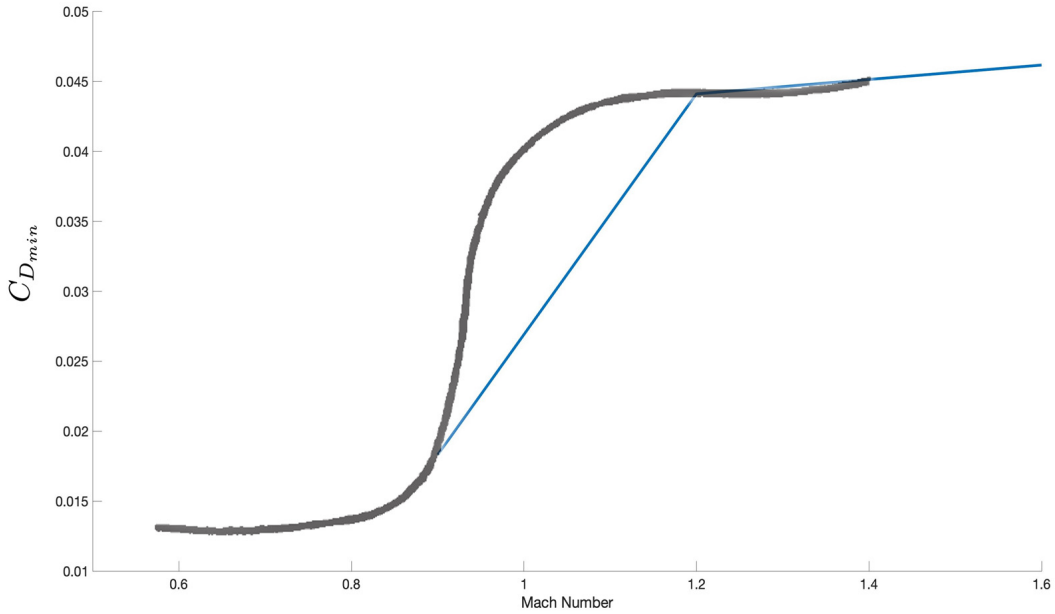

Figure 3.5: Custom fit $C_{D_{\text{min}}}$ [45, 53]

To summarize, there are two different drag models. The first model, based on Falcon 4.0 data, will be used to verify the F-16 model. The second model, based on the YF-16 flight test data, is more accurate and realistic and is used when the F-16 is scaled up to represent the F-35. The YF-16 data lacked information in the transonic region, so the transonic drag rise was manually added based on data that modeled an F-16's transonic drag rise. Both models have safeguards in place to not exceed the flight envelope.

3.5. Thrust

The thrust an engine can produce changes with altitude and Mach number [52]. The engines on both the F-16 and F-35 can use an afterburner to increase thrust production by injecting fuel behind the turbine. A model is created to calculate the thrust production across the flight envelope. The thrust plots for the F-16 can be found in the Falcon 4.0 sim flight manual and are shown in Appendix A.5. The engine used for the F-16 model in this thesis is the F110–GE–129, commonly used in the F-16 Block 50 model [44]. The thrust plots from the manual are digitized and linearly interpolated between Mach numbers. The afterburner setting can be triggered manually in the model, depending on whether that mission phase requires the afterburner. Most fighter aircraft have two distinct engine settings: military power and afterburner. The engine operates like a typical jet engine during the military power setting. When the afterburner is activated, extra fuel is injected behind the final turbine stage, drastically increasing thrust production at the cost of a significant increase in fuel burn rate. Safeguards have been implemented to ensure minimum and maximum thrust production is not exceeded. The fuel consumption of the F-16 model does not need to be determined, as fuel use is only important for the missions and final results that the F-35 flies.

3.5.1. Thrust at High AOA

Fighter aircraft can operate at very high angles of attack. The thrust plays a significant role in the vertical force equilibrium at these high angles of attack. Figure 3.3 illustrates the FBD for this condition. Usually, an aircraft flies at a relatively small angle of attack, allowing for the use of the small angle approximation. This results in the thrust having no vertical component. This approach is valid for most commercial aviation and even parts of military aviation. But, when fighter aircraft operate at high AOA, this assumption is no longer valid, and the thrust's vertical component must be considered. To solve this problem, the relationship between the thrust, lift, and drag must be iterated until a force equilibrium is reached for that specific moment in-flight. Equation (3.1) shows the effect thrust at a high AOA can have on the force equilibrium. The AOA is determined using the lift coefficient, as covered in Section 3.6.

At the start of the iteration, the sum of the vertical component of the thrust and the lift is too high, which would result in the aircraft climbing. The iteration Module iterates the lift coefficient and thrust till it finds a suitable solution. It does this by first reducing lift, resulting in less drag and, consequently, a lower thrust setting. Reducing lift production also reduces AOA, further reducing the vertical component of the thrust. The iteration might overshoot its target, which will increase lift production again. The module goes through this iterative process until it converges on a solution. This solution consists of a thrust setting and a lift coefficient, with which it can fly at the required flight condition.

3.6. Angle of Attack

A large part of the realism gains provided by PMTS depends on matching the AOA of a loaded aircraft. To achieve this, it is essential to determine the AOA for the aircraft at different speeds and weights. The YF-16 flight test data provides three different AOA curves for three Mach numbers: 0.9, 1.2, and 1.6. These lift curves are used for the F-16 model. As before, it is assumed that the AOA curve remains constant in the subsonic regime. For any value between the curves, the AOA is linearly interpolated. Figure 3.6 shows the AOA curves for the YF-16. By digitizing this data, the AOA can be calculated when the lift coefficient and Mach number are known. A larger version of Figure 3.6 is shown in Figure A.12.

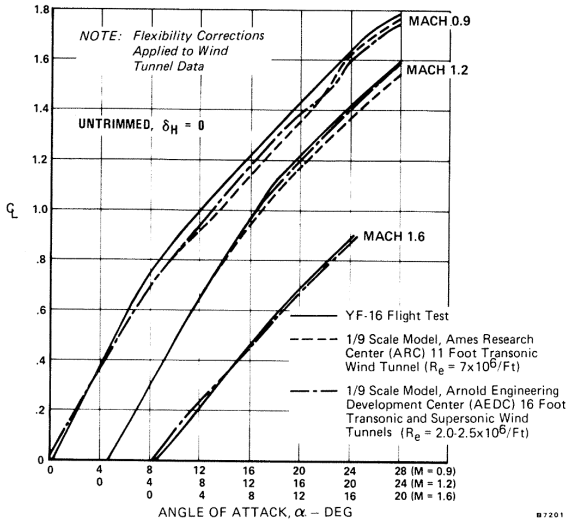

Figure 3.6: Comparison of Flight Test with Wind Tunnel Lift Curves for YF-16 [45]

3.7. The effect of stores on aircraft performance

Modeling the performance impact of stores is a critical part of this thesis. Stores, such as missiles, rockets, bombs, sensors, and fuel tanks, are equipment an aircraft carries to complete a mission. Stores are part of mission configurations, but their effect on aircraft performance must also be considered during the verification of the model. Thus, the effect of stores on aircraft performance is covered in this chapter. The stores an aircraft is equipped with are the main driver behind the performance gap that PMTS is trying to match.

Stores can be attached externally or internally, depending on the aircraft type. The F-16 only has external storage, while the F-35 has both external and internal storage. The location of stores plays a critical role in an aircraft's total radar cross-section (RCS), especially important for stealth fighters like the F-35. The location of stores changes depending on the mission requirements, where internal storage is chosen to minimize RCS. A larger RCS means the aircraft will be visible on enemy radar at a greater distance, reducing the chances of completing the mission [53].

Adding stores to the aircraft affects its performance, which can be represented by changes to the equations of motion. The effect of stores on aircraft performance can be quantified into Lift-induced drag and the Drag Index (DI). The DI, sometimes called the drag count, is a way to normalize the ΔC_D the store adds with respect to the reference surface area of the aircraft [54]. The DI only represents the extra aerodynamic drag of the store. The effect of the stores' weight still must be considered regardless of the DI. All stores use adapters to be mounted to the aircraft. These adapters do not separate from the aircraft when a store is dropped. This means that even after dropping all stores, an aircraft that carried stores at the beginning of the mission will still have a slightly higher DI and weight penalty due to the adapters [46]. The two main effects of stores will be covered below in separate sections.

Lift-induced drag

The increase in weight due to stores can significantly affect an aircraft's performance. When fully loaded, the F-35 can carry almost $10\,000$ kg of internal and external stores, representing more than 30 % of its maximum take-off weight (MTOW). In stealth mode, with only internal stores, this drops to 2600 kg, which is still about 10 % of the stealth configuration take-off weight [55, 56, 57]. To carry this extra weight, the aircraft must produce more lift, which leads to increased lift-induced drag. Lift-induced drag is a main contributing factor to total drag during subsonic flight. Even for supersonic flight, lift-induced drag is a significant factor of the total drag [58]. Flying at supersonic speeds is challenging when external stores are present due to the extra drag.

Drag Index
The Drag Index (DI) is a helpful metric for quantifying the aerodynamic drag created by external stores on an aircraft. External stores are exposed to the airflow and therefore produce aerodynamic drag. Since the DI is aircraft specific, it needs to be scaled when a store is used on another aircraft Scaling is done using the ratio of wing surface areas of two aircraft [46]. Scaling of DI for the F-35 is covered in Section 4.1.4. Scaling is not required here, as the verification data for the F-16 specifies a DI that the configuration has. Equation (3.8) shows how to calculate the drag coefficient increase for a specific Drag Index. External store adapters also have a DI.

$$\Delta C_{D_{\text{store}}} = \frac{\text{Drag Index}}{10^4} \tag{3.8}$$

Updated Force Equilibrium and Equations of Motion
The force equilibrium and equations of motion can be updated to account for the effect of stores on aircraft performance. Equations (3.1) and (3.2) become Equations (3.9) and (3.10). The equation for the energy method also changes, Equation (3.6) becomes Equation (3.11). The effect external stores would have on the lift curve of the aircraft is not considered.

$$L + T\sin(\alpha) = (W + W_{\text{Stores + Adapters}}) \tag{3.9}$$

$$T\cos(\alpha) - (D + D_{\text{Stores + Adapters}}) = (m + m_{\text{Stores + Adapters}})\frac{dv}{dt} \tag{3.10}$$

$$P_s = \frac{Tv - (D + D_{\text{Stores + Adapters}})v}{W + W_{\text{Stores + Adapters}}} = \frac{dh}{dt} + \frac{v}{g}\frac{dv}{dt} \tag{3.11}$$

3.8. Doghouse Plots

A doghouse plot shows the SEP as a function of the Mach number and turn rate in a contour plot. These plots provide an efficient way of displaying the performance of an aircraft at a specific altitude for a specific engine setting and configuration. They also provide a way of verifying the entire aircraft model, since almost every aspect covered in this chapter is required to create an accurate doghouse plot, this is seen as an accurate means to verify the entire model. To verify the F-16 model, doghouse plots created using the model will be compared with plots from data sources. A doghouse plot contains a lot of information: load factor, turn radius, and the SEP. All this information is plotted for a range of Mach numbers and turn rates.

First, the constant load factor and turn radius lines are plotted for the flight envelope. A range of load factors are selected, all within the aircraft's flight envelope. To calculate the turn rate as a function of the load factor, Equations (3.12) and (3.13) are combined and rewritten to get Equation (3.14). A range of turn radii are selected, and the turn rate per turn radius is calculated using Equation (3.13) [59].

$$\text{Turn Radius} = R = \frac{v^2}{g\sqrt{N_Z^2 - 1}} \tag{3.12}$$

$$\text{Turn Rate} = TR = \frac{360}{2\pi}\left(\frac{v}{R}\right) \tag{3.13}$$

$$\text{Load Factor in Turn} = N_{Z_{\text{Turn}}} = \sqrt{\left(\frac{2\pi \cdot v \cdot TR}{360 \cdot g}\right)^2 + 1} \tag{3.14}$$

$$C_L = \frac{2N_{Z_{\text{Turn}}}W}{\rho v^2 S_{ref}} \tag{3.15}$$

The final calculation required to create the doghouse plot is the SEP per turn rate and Mach number. Using Equation (3.15), the lift coefficient per load factor can be calculated, and this load factor corresponds with a specific turn rate [59]. Once the lift coefficient is calculated, Drag can be calculated using the method described in Section 3.4. Finally, the maximum thrust at that specific flight condition is calculated. The SEP can be calculated using Equation (3.11). The effect of thrust at high

AOA is not considered here. The thesis on doghouse plots by *John Robert Wilson* provides a detailed method to construct doghouse plots, and the effect of thrust at high AOA is not accounted for [59].

3.9. Turns

The equations provided above to calculate the data to make a doghouse plot can also be used to calculate turn performance. During missions, fighter aircraft often fly max sustained turn rates. This is the maximum turn rate the aircraft can fly constantly, and at this turn rate, the SEP is zero. Finding this maximum sustained turn rate is relatively straightforward. First, the load factors are calculated using Equation (3.14) for a range of turn rates. This is done for a specified Mach number, which is fixed for turns during the missions in this thesis. Then, using Equation (3.15), the lift coefficient for that load factor and turn rate combination can be calculated. Once this is known, the drag coefficient is calculated, and the SEP can be determined for that turn rate. The maximum sustained turn rate will be the turn rate with zero SEP. The option to set a maximum load factor is also available in the model to ensure the aircraft's structural or operational envelope is not exceeded.

3.10. Verification

The accuracy of the F-16 model created in this chapter was verified using doghouse plots from the Falcon 4.0 F-16 sim manual [44]. The plots were specific to an F-16C Block 50 configuration with an F110-GE-129 engine, a DI of 38, and a gross weight of $13\,000$ kg. Doghouse plots were created at three different altitudes: $10\,000$ ft, $20\,000$ ft, and $30\,000$ ft, representing the entire range of altitudes for the missions covered in Chapter 5. The plots were created using the Falcon 4.0 drag polar, as mentioned in Section 3.4. The MATLAB-generated data is overlaid on the doghouse plots from the Falcon 4.0 manual, and if the specific excess power lines overlap, the model is considered accurate.

Although multiple data sources would have been preferred, this is extremely challenging for fighter aircraft. Moreover, doghouse plots fall under ITAR restrictions due to their comprehensive performance information. For that reason, the plots from the Falcon 4.0 manual were used for verification.

The three doghouse plots are shown in Figures 3.7 to 3.9, with full-page versions in Appendix A.10. In each figure, the black and white doghouse plot from the Falcon 4.0 manual serves as the background, with colored lines from the MATLAB-generated data overlaid on top. The MATLAB-generated data, derived from the constructed F-16 aircraft model, closely follows the doghouse plot, indicating sufficient accuracy for this thesis.

Not all SEP lines are plotted for the aircraft model, as the aircraft will not fly at negative SEP during the missions or tests in this thesis. Therefore, it was deemed unnecessary to include very negative SEP values for verification. The SEP data from the model does not go below a SEP of $-600\,\mathrm{ft\,s^{-1}}$. At these negative SEP values and higher Mach numbers, the model and verification data start to deviate. However, these differences were not considered significant since the aircraft will not operate in that part of the flight envelope in the analysis for this thesis.

Additionally, at $30\,000$ ft, the aircraft model is unable to reach the same maximum airspeed as the doghouse plot, falling just short of Mach 1.8. As the drag model used for verification is based on interpolating digitized data, it could be that this part of the dataset was not digitized entirely accurately, leading to this slight deviation. However, this is not a concern since the model will be scaled to represent an F-35, which has a maximum Mach number of 1.6.

In the most critical area (at the zero SEP line and between Mach numbers 0.5 and 1.6), the model was deemed accurate enough to answer the research questions. The following steps include scaling the model to represent an F-35 and flying missions with the aircraft model. Below each figure will be discussed in more detail.

10,000ft

The first verification plot is displayed in Figure 3.7. This plot was created using the previously mentioned configuration and flown at an altitude of $10\,000$ ft. The overlay accurately matches the source data. However, slight deviations can be observed at larger negative values near Mach 1.0, where the thesis model exhibits a larger SEP for that flight condition. These deviations could be attributed to a slight overestimation of engine performance or a minor underestimation of drag. This could also be due to the custom transonic drag-rise model not being completely accurate or needing further fine-tuning. Although the model closely matches the source data in subsonic flight regimes, there are slight discrepancies at supersonic speeds and high negative SEP values. Nevertheless, this does not impact the thesis findings, as the thesis model will not be operated in-flight conditions with negative SEP values. Overall, the first verification plot displays a successful verification of the thesis model for this flight condition.

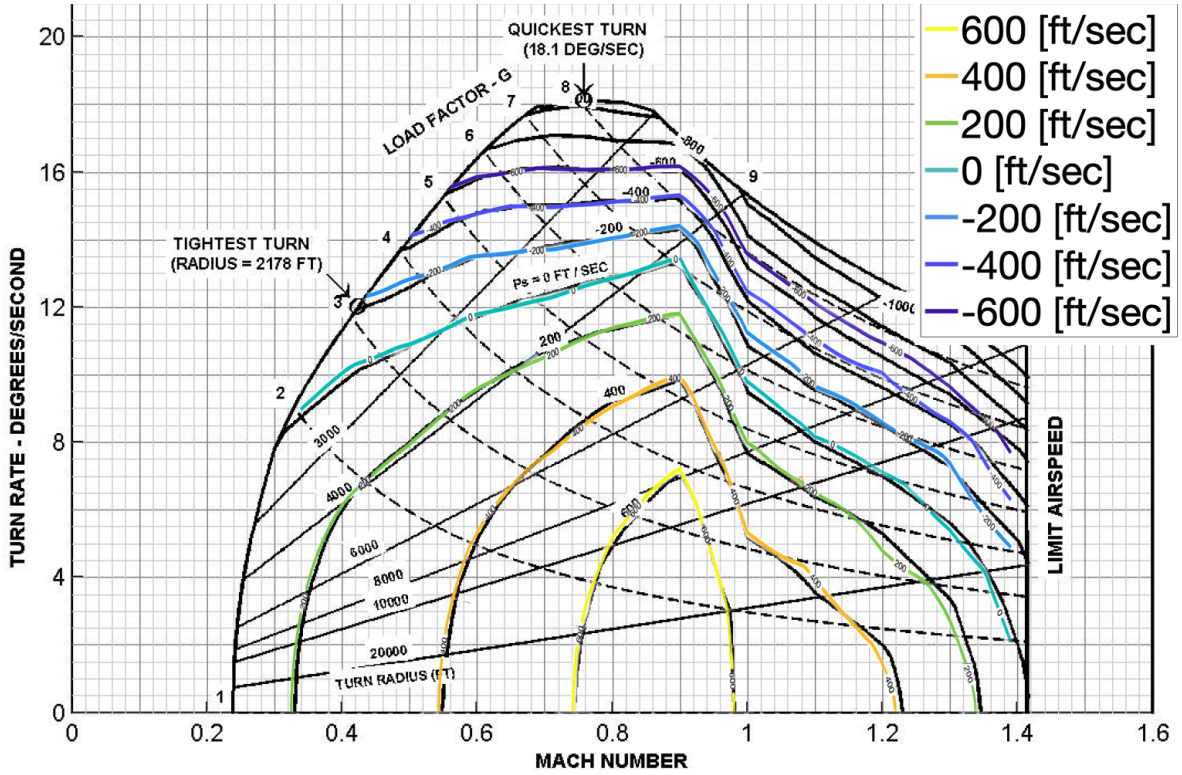

Figure 3.7: Doghouse plot overlay at $10\,000$ ft

20,000ft

The second verification plot is displayed in Figure 3.8. This plot was created using the previously mentioned configuration but flown at a higher altitude of $20\,000$ ft. As expected, the aircraft performance is reduced at this altitude compared to the $10\,000$ ft altitude. The same trends observed at $10\,000$ ft are evident here, with minor deviations between the models occurring at Mach 1.0 and negative SEP values. In subsonic flight regimes, the models exhibit a close match, while slight discrepancies can be seen at supersonic speeds and larger negative SEP values. Overall, the second verification plot displays a successful verification of the thesis model for this flight condition.

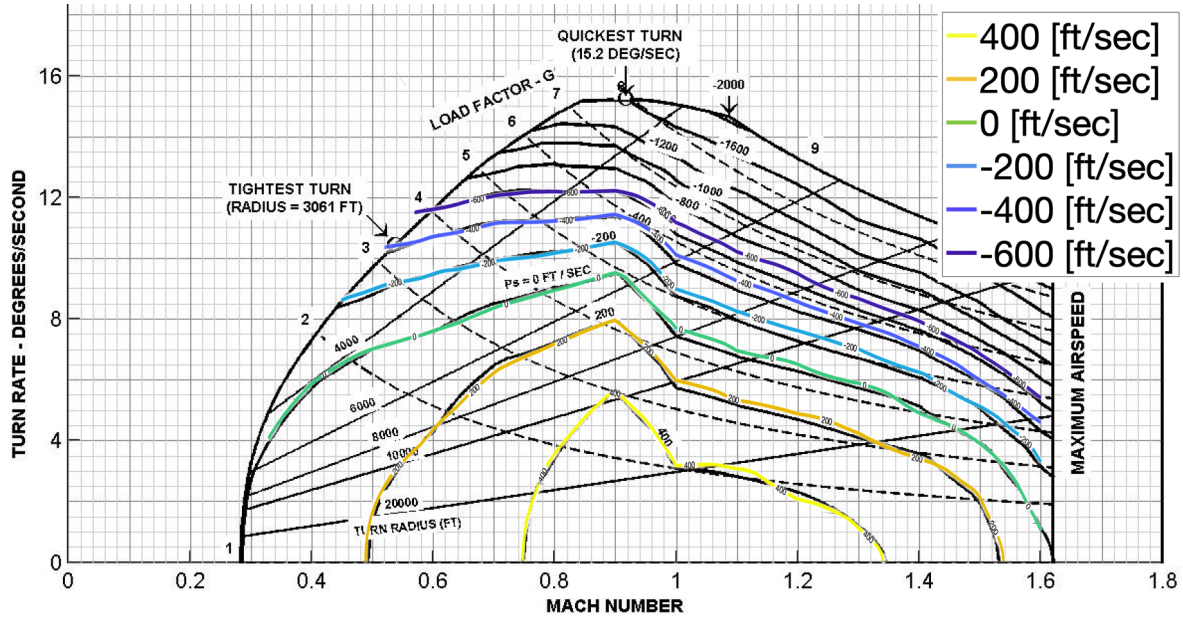

Figure 3.8: Doghouse plot overlay at 20 000 ft

30,000ft

The third and final verification plot is displayed in Figure 3.9. As expected, the performance degrades further compared to that shown in Figures 3.7 and 3.8, due to the increased altitude. The same deviations observed in the previous two figures are evident here as well, with minor discrepancies occurring at supersonic speeds and negative SEP values. However, as mentioned earlier, the aircraft will not be flown at negative SEP values during this thesis. Despite these minor deviations, the third verification plot demonstrates a satisfactory match between the models, indicating that the thesis model is accurate.

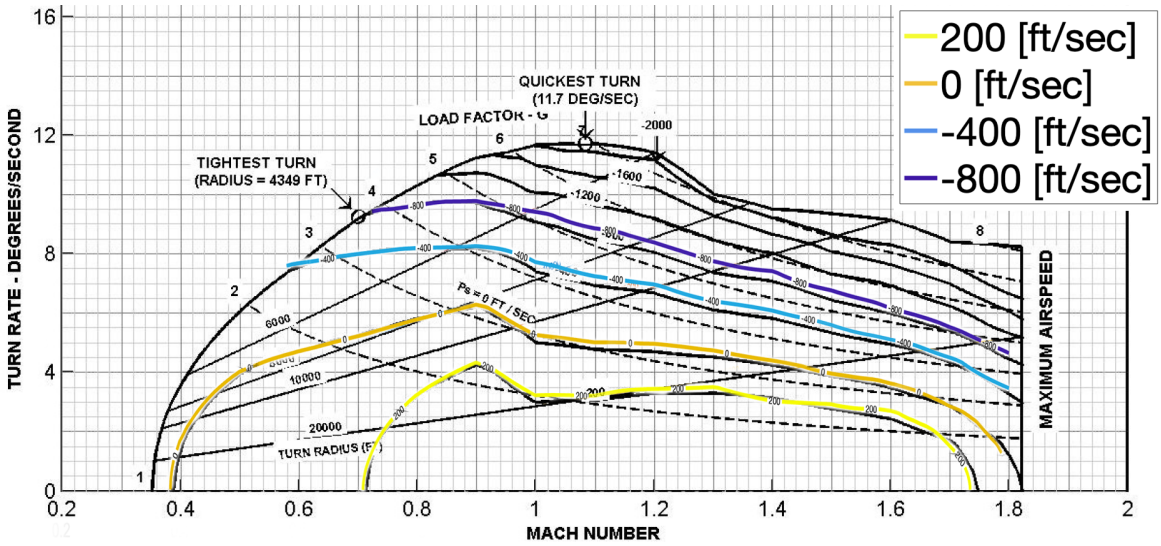

Figure 3.9: Doghouse plot overlay at 30 000 ft

4

The F-35 and Performance Matched Training System

In Chapter 3, the data sources, modules, and calculations required to make the F-16 model were discussed. The model has been verified and shown to be accurate using doghouse plots. The next step is to scale the F-16 model to represent an F-35; how this is done will be covered in this chapter. Once the F-35 model is finished, the calculations necessary for PMTS will be discussed. Finally, a couple of small tests are done to show the effectiveness of PMTS on a small scale.

4.1. Scaling up to the F-35

The process of scaling the F-16 model to represent an F-35 will take into account the significant differences between the two aircraft. The F-35 is larger, stealthier, and designed to operate beyond visual range, while the F-16 is smaller, more maneuverable, and not optimized for low observability. Due to the limited availability of publicly accessible information on defense projects, the scaling process will rely on the F-16 model as a starting point. A true-to-scale comparison of the two aircraft is shown in Figure 3.1.

Scaling is split into several different modules, as not every part of the model can be scaled similarly. As mentioned in Section 3.1, getting publicly available information on defense projects is very challenging. For the F-35, it is not possible to find publicly available performance data besides the generic information that can be found on Wikipedia or Lockheed Martin's website. While the scaling process will not yield a perfect F-35 model, it will provide a close enough approximation for this research, given the limited availability of public data on the F-35's performance.

4.1.1. Drag

The most important part of the aircraft model to scale accurately is the drag model. The drag model is based on Equation (3.7), and the three variables that were calculated/determined for it in Section 3.4. As mentioned before, the drag polar model used from now on will be based on the flight-test data of the YF-16. The Oswald factor and $C_{L_{\text{min.drag}}}$ values are not scaled; it is assumed they stay constant. $C_{D_{\text{min}}}$ could be scaled by assuming that the average friction coefficient of the aircraft remains constant. $C_{D_{\text{min}}}$ would then be scaled based on reference and wetted area ratios between two aircraft, as indicated in Equation (4.1), which is used to calculate the average friction coefficient. This works well for commercial aircraft since their design goals are consistent over time and between models. Because the aircraft and design choices are similar, scaling based on a constant average friction coefficient is an accurate method for commercial aircraft.

Fighter jets exhibit significant variations in design criteria across generations and models, as these criteria profoundly impact the decisions made during the design process. For instance, the F-16 was designed before low-observability (LO) was a design requirement. Designing a LO aircraft means the design team must adhere to specific aircraft shapes. These shapes are not always the most preferred for aerodynamic performance [60]. The F-117 is a great example, it does not look aerodynamically optimized or sleek, the main design criteria was having a low radar cross section (RCS), and the cost

of this design choice is a less favorable aerodynamic shape. Similarly, the F-35 was designed with LO in mind, even though it appears more streamlined than the F-117, it still required aerodynamic compromises to minimize its RCS.

$$C_F = C_{D_0} \cdot \frac{S_{\text{wet}}}{S_{\text{ref}}} \tag{4.1}$$

Given these differences in design criteria, scaling between a non-LO and an LO aircraft using a constant average friction coefficient would be an inaccurate method. Due to distinct design requirements, the F-35's average friction coefficient is likely higher than that of the F-16. Consequently, $C_{D_{\text{min}}}$ is assumed to remain constant between the two aircraft, implying that the drag polar does not change. While the values are maintained, the size and geometry of the aircraft differ, as shown in Figure 3.1. In summary, drag scaling is based on differences in aspect ratio and wing surface area, with all other variables remaining constant. Theoretically, there may be more accurate methods for scaling between these two distinct aircraft, as retaining the same drag polar might not be entirely accurate. However, after extensive discussions and deliberation between TU Delft and NLR and considering available data and examples, this approach has been deemed the most accurate without a specific model or data set for the F-35.

The drag model for the F-35 can be summarized with the following two equations. Equations (4.2) and (4.3) show how the drag coefficient for the F-35 is calculated and then how that drag coefficient is used to calculate the total drag. A number of variables shown in Equation (4.2) are a function of the Mach number the aircraft is flying at. These relations have been described in Chapter 3 and are also shown in Appendix A.

$$C_{D_{\text{F-35}}} = C_{D_{\text{min}_{\text{F-16}}}}(M) + \frac{(C_L - C_{L_{\text{min.drag}_{\text{F-16}}}}(M))^2}{\pi \cdot AR_{\text{F-35}} \cdot e_{F-16}(M)} \tag{4.2}$$

$$D_{\text{F-35}} = 0.5\rho v^2 C_{D_{\text{F-35}}} S_{\text{F-35}} \tag{4.3}$$

The method to construct the drag model for the F-35 has been covered in this section. Figure 4.1 shows the final drag polar used for the F-35 for four different Mach number. This drag polar was created by digitizing the YF-16 drag polar, then adding the effect of transonic drag rise manually, and finally using the F-35 aspect ratio in Equation (4.2). The comparison between the F-16 and F-35 drag polar for this thesis is shown in Figure A.7.

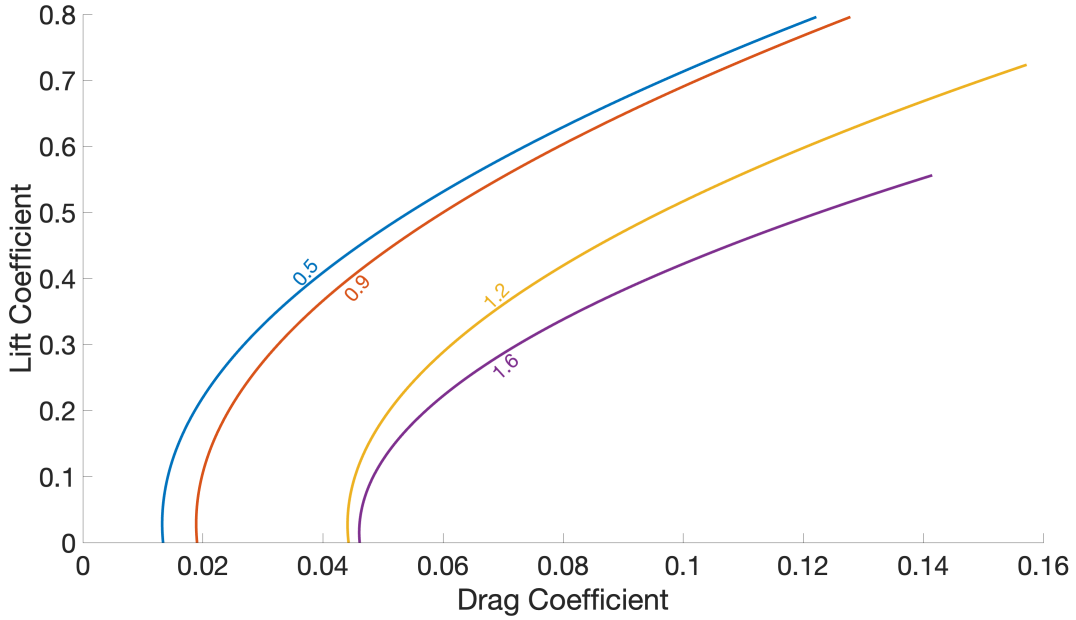

Figure 4.1: F-35 Drag Polar for different Mach numbers

4.1.2. Thrust

Publicly available information on the Pratt & Whitney F135, the engine installed in the F-35, is limited to the maximum thrust at both military and afterburner settings at sea level. The F-16 thrust model is scaled based on the maximum thrust settings of both engines. The entire thrust curve is multiplied by a corresponding multiplication factor, resulting in the same engine behavior across different Mach numbers and altitudes but with increased thrust production. The multiplication factor for the non-afterburner engine setting is 1.62, and the multiplication factor for the afterburner engine setting is 1.15 [44, 61].

$$T_{\text{F-35}} = T_{\text{F-16}} \cdot T_{\text{factor}} \tag{4.4}$$

The F-35 thrust plots are shown below in Figures A.10 and A.11. The values shown on the lines are the altitude values in meters. The altitude values represent steps of $10\,000$ ft, to allow for comparison with Appendix A.5, which explains the seemingly random altitudes in the figures.

Fuel Consumption

The Thrust Specific Fuel Consumption (TSFC) is used to calculate the fuel consumption. TSFC describes the fuel burned per second per Newton of thrust produced. Equation (4.5) shows how to calculate fuel burn for a specific thrust setting. The TSFC is assumed to be constant over Mach number and altitude, only changing based on engine setting. The TSFC values for the F135 are shown in Table 4.1. These TSFC values represent the best-case scenario for the F135, the real-life value could be significantly worse.

$$\text{Fuel use per second} = TSFC \cdot T \tag{4.5}$$

Table 4.1: Thrust Specific Fuel Consumption for F135 [62]

Engine Setting	Military Thrust	Afterburner
TSFC [mg/s/N]	19.8	55.2

4.1.3. Angle of Attack

The big difference in aspect ratio between the F-35 and F-16 means the lift curve has to be adjusted. A higher aspect ratio leads to a lower slope in the lift curve line. The lift curve slope for an infinite wing (a_0) is assumed to be the same for both aircraft. The (a_0) value depends on the airfoil, and since the F-16 and F-35 operate in similar flight regimes, the assumption is made that the airfoil used will also be similar between the aircraft. To determine the lift curve slope for a finite wing (a_{flap}) Equation (4.6) is used [52]. First, the data shown in Figure 3.6 is capped at the maximum lift coefficients shown in Figure 3.4b. Below these maximums, the lift curves are linear, allowing for an easy determination of the slope at all three Mach numbers. Once a_0 is calculated for the three Mach values for the F-16, the lift curve for the F-35 can be calculated using its aspect ratio and Equation (4.6).

$$a_{\text{flap}} = \frac{a_0}{1 + \frac{57.3 a_0}{\pi e AR}} \tag{4.6}$$

The date required to use Equation (4.6) is shown in Appendix A.7. The new lift curve is calculated using this data and Equation (4.7).

$$C_L = a_{\text{flap}}(\alpha - \alpha_{L=0}) \tag{4.7}$$

The lift curves for the F-16 and F-35 are shown in Figure 4.2. The effect of the lower aspect ratio of the F-35 can be seen in this figure, the lift curves have a shallower slope.

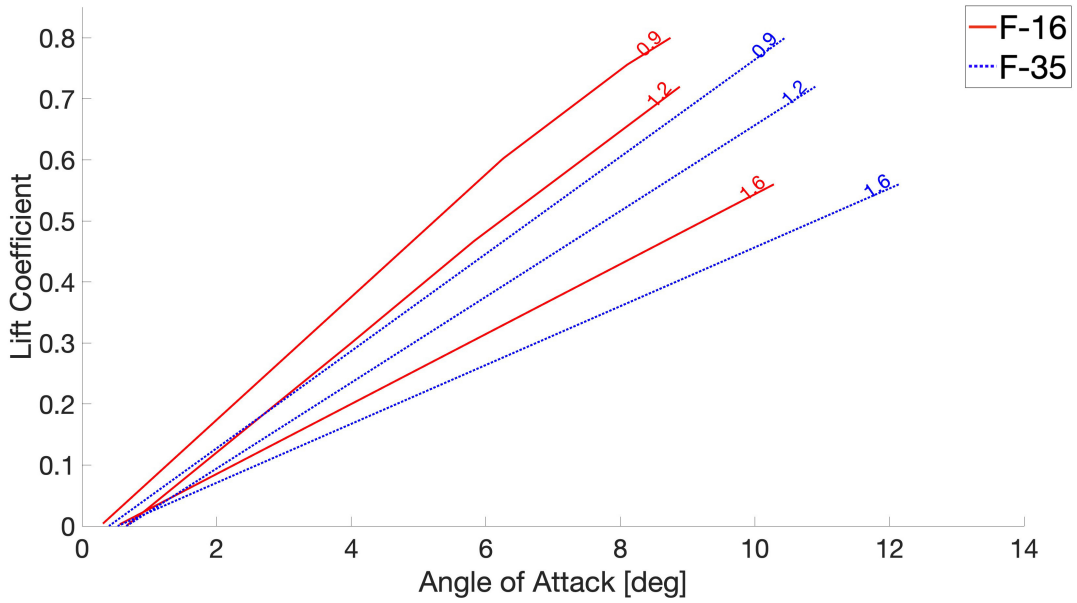

Figure 4.2: Lift Curves for F-16 and F-35

4.1.4. Drag Index

As mentioned in Section 3.7, the Drag Index (DI) due to stores is aircraft specific. The DI is determined relative to the reference surface area of the aircraft the store is attached to. That means every store's drag index must be scaled to match a new aircraft.

$$D_{\text{Store}} = \frac{1}{2}\rho v^2 S_{\text{Ref}} C_{D_{\text{Store}}} \tag{4.8}$$

The total aerodynamic drag of a store is calculated using the drag equation, shown in Equation (4.8). Combining Equation (4.8) with Equation (3.8) results in Equation (4.9). This equation calculates the total aerodynamic drag of a store based on its DI.

$$D_{\text{Store}} = \frac{1}{2}\rho v^2 S_{\text{Ref}} \frac{\text{DI}}{10^4} \tag{4.9}$$

The total drag of the store itself is constant, regardless of the aircraft to which it is attached. For now, the possible interference drag due to differences in aircraft geometry is ignored. For the same flight condition, the drag of a store underneath two separate aircraft is the same. This allows for two drag equations to be set as equal, as shown in Equation (4.10). The dynamic pressure cancels out on both sides, as the flight condition is identical.

$$S_{\text{Ref}_{\text{F-16}}} \cdot \frac{\text{DI}_{F-16}}{10^4} = S_{\text{Ref}_{\text{F-35}}} \cdot \frac{\text{DI}_{F-35}}{10^4} \tag{4.10}$$

Equation (4.10) can be rewritten as Equation (4.11), which is how the drag index will be scaled from the F-16 to the F-35.

$$\text{DI}_{\text{F-35}} = \frac{S_{\text{Ref}_{\text{F-16}}}}{S_{\text{Ref}_{\text{F-35}}}} \cdot \text{DI}_{\text{F-16}} \tag{4.11}$$

The drag index for the externally carried AIM-120 air-to-air missiles comes from the F-15 [46]. For this store, Equation (4.11) is used with the reference area of the F-15 instead of the F-16. The Drag Index data for the stores and adapters used in this thesis are shown in Appendix B.

4.1.5. Lift

A couple of assumptions are made to scale the lift production of the aircraft. First of all, the assumption is made that the F-16 and F-35 use similar airfoils. This assumption is based on the idea that they have similar flight envelopes and can perform similar missions. The assumption is made that the maximum lift coefficient of the F-35 is the same as for the F-16. This maximum lift coefficient is obtained from Figure 3.4b and depends on the Mach number. The maximum lift coefficient is linearly interpolated between Mach numbers. The lift coefficient required to calculate the required lift in every flight condition is calculated, and this lift coefficient is then checked not to exceed the maximum. Equation (4.12) shows how the lift coefficient is calculated.

$$C_{L_{\text{F-35}}} = \frac{L}{0.5\rho v^2 S_{\text{F-35}}} \tag{4.12}$$

4.1.6. Accuracy of scaled model

There is no way to confirm the scaled model's accuracy since no information is available to the public. The scaling method produces a reasonably accurate model that could be enhanced through further research and modeling of the F-35's aerodynamic shape or by accessing more information that may become available. To address the research questions, this thesis considers the verification data of the F-16 and scaling to be accurate enough to study this proof of concept.

4.2. Performance Matched Training System

With the F-35 aircraft model now complete, the development of the PMTS can begin. The PMTS will read the flight performance data of the loaded aircraft and adjust the performance of the aircraft it is installed on to match that of the loaded aircraft. This process is illustrated in Figure 4.3. The Energy Method used to calculate the performance of non-PMTS aircraft can still be used here but in reverse. Additionally, the effects of flaps need to be considered. Flaps will be utilized to match the angle of attack (AOA), covered in Section 4.2.1.

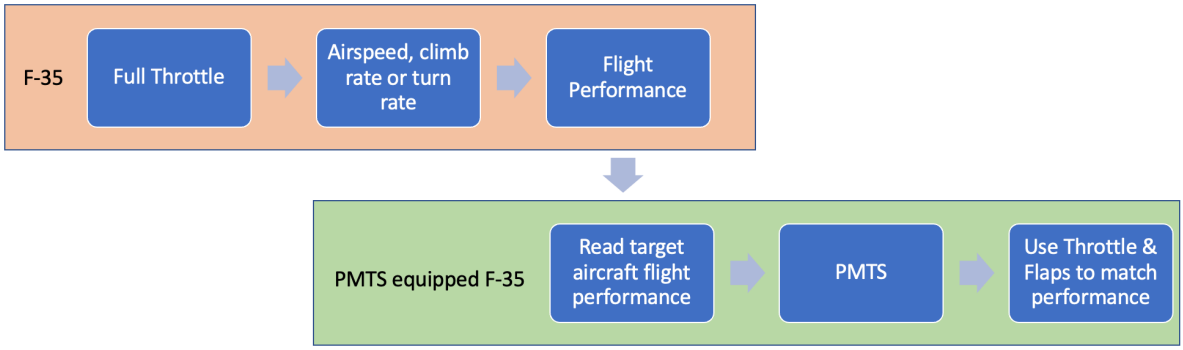

Figure 4.3: Flow Diagram of PMTS

4.2.1. Flaps

The first element that will be added to the equations of motion when using PMTS is the effect of trailing edge flaps. As PMTS aims to match the performance of an aircraft that will be heavier, the angle of attack will differ between these two aircraft. If an aircraft is heavier, it will fly at a higher angle of attack than a lighter aircraft in the same flight condition. PMTS will use the flaps to match the angle of attack. Flaps, also known as high-lift devices, are typically used to increase the lift production of the wing. PMTS uses flaps by deflecting them upwards to reduce lift production, similar to the function of a spoiler, which dumps lift. By reducing the lift production of the wing, the aircraft must increase its AOA to generate sufficient lift to maintain the same flight condition. By fine-tuning the negative flap deflection, PMTS will be able to match the angle of attack of the target aircraft. This will come at the cost of a slight increase in drag but will provide an increase in training realism.

First, the lift increment due to trailing edge flap deflection is calculated. A method by *Roskam* is used [63]. To simplify the process, several assumptions are made. First, it is assumed that a negative

deflection has the same, but opposite, effect as a positive flap deflection. This assumption is considered valid because the flap deflections are expected to be minimal, leading to similar but opposite effects when deflected in either direction. Due to the low flap deflections required by PMTS, it is assumed that flaps only affect the lift curve vertically, as displayed in Figure 4.4. The effect flaps could have on the slope of the lift curve is not considered for this thesis.

Equation (4.13) will be used to calculate the vertical displacement of the lift curve due to flap deflection [63]. This equation contains five different variables that need to be calculated or determined. The F-35 uses plain flaps with an assumed maximum flap deflection of $-15°$. The procedure to obtain each variable required to use Equation (4.13) is outlined in *Aircraft Design: Part VI* by *Roskam* [63]. The variables used are shown in Table 4.2.

$$\Delta C_L = K_b(\Delta c_l)(\frac{C_{L_{\alpha_W}}}{c_{l_\alpha}}) \left[\frac{\alpha_{d_{C_L}}}{\alpha_{d_{c_l}}}\right] \tag{4.13}$$

The two trailing edge flaps combined have an area of $4.28\,\text{m}^2$, and the flap represents $21\,\%$ of the total chord of the wing. These values were obtained by measuring them to scale in Figure A.14, which shows the F-35 trailing edge flap geometry.

Table 4.2: Variables for Flap Lift Increment Calculation F-35 [63]

K_b	$C_{L_{\alpha_W}}$	c_{l_α}	$\alpha_{d_{C_L}}/\alpha_{d_{c_l}}$	Max. Flap Deflection [deg]
0.58	0.065	0.1	1.13	-15

In Equation (4.13), the Δc_l represents the airfoil lift increment due to flaps. This value must be calculated for every possible flap deflection angle, the equation is shown in Equation (4.14). The variables include δ_f, the flap deflection angle in radians. The required variables are presented in Table 4.3 [63].

$$\Delta c_l = \delta_f \frac{c_{l_\delta}}{(c_{l_\delta})_{theory}} \cdot (c_{l_\delta})_{theory} \cdot k^{'} \tag{4.14}$$

Table 4.3: Variables for Airfoil Lift Increment due to flaps Calculation F-35 [63]

$\frac{c_{l_\delta}}{(c_{l_\delta})_{theory}}$	$(c_{l_\delta})_{theory}$	$k^{'}$
0.41	3.5	1

Using Equations (4.13) and (4.14), the wing lift coefficient reduction per flap deflection angle can be calculated. The AOA difference between the PMTS-equipped and target aircraft can be used to calculate the required difference in wing lift coefficient, this is done using the method described in Section 3.6 but then in reverse. The delta in AOA results in a delta in lift coefficient, which results in a required negative flap deflection to obtain the required delta lift coefficient.

Figure 4.4 shows the effect flaps have on the lift curve. There are three lift curves, showing a $0°$, $-5°$ and $-10°$ flap deflection. It shows that an aircraft can fly at a higher AOA while still producing the same lift coefficient if it uses negative flap deflection. The figure also shows the flaps only affect the lift curve vertically.

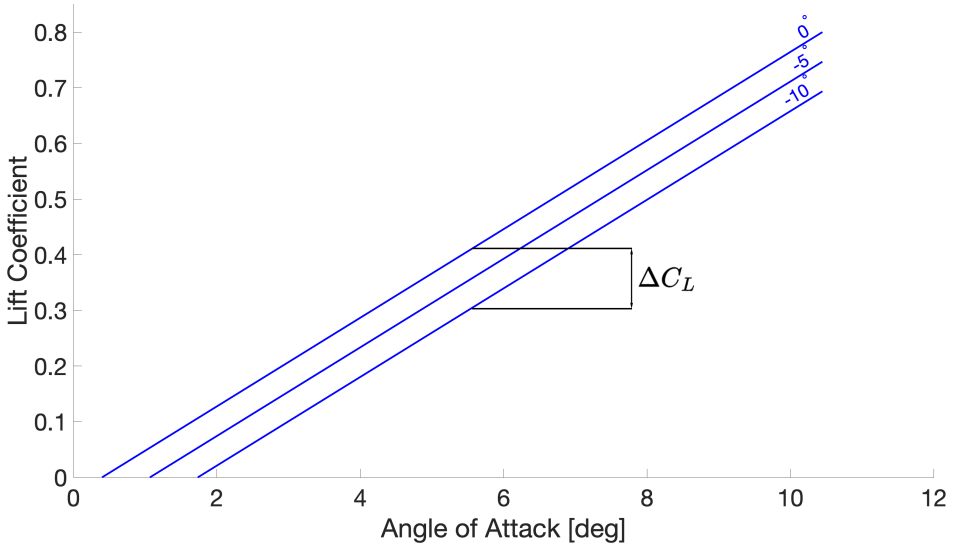

Figure 4.4: Effect of Flap Deflection on Lift Curve

Flaps generate drag, which must be accounted for in the equations of motion for the PMTS aircraft. The drag produced by flaps is calculated using section 4.6 from *Aircraft Design: Part VI* by *Roskam* [63]. The drag produced by a flap is split up into profile drag and induced drag, plain flaps do not produce interference drag [63]. The drag coefficient due to flap deflection can be calculated using Equation (4.15), this equation is only valid in the subsonic regime. Since flap deflections will be very small at supersonic speeds, this is deemed acceptable for this thesis. Like the lift increment calculation, the drag produced by the flap depends on the geometry of the aircraft, with some variables obtained from graphs and others from simple calculations. These values can be easily reproduced using the Roskam book mentioned earlier.

$$C_{D_{flap}} = \Delta C_{D_{prof_{flap}}} + \Delta C_{D_{i_{flap}}} \tag{4.15}$$

The profile drag due to flap deflection is calculated using Equation (4.16), where the first variable is the two-dimensional profile drag increment. This variable depends on the flap deflection, thus ensuring the profile drag changes depending on the amount of deflection.

$$\Delta C_{D_{prof_{flap}}} = (\Delta C_{D_{p_{\Lambda_{c/4}=0}}})(\cos(\Lambda_{c/4})\frac{S_{wf}}{S} \tag{4.16}$$

The induced drag due to flap deflection is calculated using Equation (4.17). $\Delta C_{L_{\text{flap}}}$ represents the incremental lift coefficient due to the flap, which changes the induced drag based on the amount of flap deflection.

$$\Delta C_{D_{i_{\text{flap}}}} = K^2(\Delta C_{L_{\text{flap}}})^2 \cos(\Lambda_{c/4}) \tag{4.17}$$

The variables required to use Equations (4.16) and (4.17) are shown in Table 4.4. $\Delta C_{D_{p_{\Lambda_{c/4}=0}}}$ is not shown, as this is a function of the flap deflection, which is calculated by multiplying the flap deflection in RAD by 0.0012.

Table 4.4: Flap Drag Increment Variables [63]

$\Lambda_{c/4} = 0$ [RAD]	S_{wf} $[m^2]$	K
0.42	4.28	0.3

Using the equations and methods outlined in this section, PMTS can identify the difference in AOA between the target and PMTS-equipped aircraft. Subsequently, it calculates the necessary difference in lift coefficient to compensate for the AOA difference. PMTS then determines the required flap deflection to achieve this difference in lift coefficient and computes the amount of drag generated by the flaps at that deflection angle.

4.2.2. Equations of Motion for PMTS

Equations (3.9) to (3.11) must be updated to incorporate the effect of flaps and to remove the influence of stores. Instead of determining the achievable performance with a maximum thrust setting, PMTS receives performance data that it must match and calculates the flap and thrust settings required to match this performance. Equations (4.18) and (4.19) are the rewritten force equilibrium and equation of motion for an aircraft equipped with PMTS. The energy method is still used but in reverse. Equation (4.20) shows how performance data from the target aircraft is used to calculate the required performance from the PMTS-equipped aircraft using the energy method.

$$L_{\text{F-35}} + T_{\text{F-35}} \sin(\alpha_{\text{F-35}}) = W \tag{4.18}$$

$$T_{\text{F-35}} \cos(\alpha) - (D_{\text{F-35}} + D_{\text{Flaps}}) = m\frac{dv}{dt} \tag{4.19}$$

$$P_s = \left\{ \frac{T_{\text{F-35}} \cdot v - (D_{\text{F-35}} + D_{\text{Flaps}}) \cdot v}{W} \right\}_{\text{PMTS Aircraft}} = \left\{ \frac{dh}{dt} + \frac{v}{g}\frac{dv}{dt} \right\}_{\text{Target Aircraft}} \tag{4.20}$$

To match performance, the performance data is obtained from the loaded aircraft and fed into PMTS. The delta can be an acceleration, altitude change, or a combination of the two. The delta in performance results in a delta SEP that the matching aircraft needs to overcome. The next step is to determine the flap deflection required to match AOA, after which the thrust setting required to match both AOA and performance can be calculated. The AOA iteration between AOA, lift, and thrust is also performed using the same iterative process described in Section 3.5.1. The effect of flaps, as outlined in Section 4.2.1, are now a part of that iteration. This all results in a thrust setting and flap deflection, at which the performance and AOA of the loaded aircraft are matched.

4.2.3. PMTS in turns

PMTS must be capable of matching the loaded aircraft's turn performance, which necessitates a different calculation than for non-turning flights. The turn rate and load factor during the turn need to be matched to match turn performance.

To match the turn performance of the target aircraft, the turn rate, load factor, and flight conditions are obtained from the loaded aircraft's performance data. Equation (3.14) demonstrates that the velocity will also be the same when turn rate and load factor are matched. Equation (3.15) reveals that for the same velocity and load factor, a lighter aircraft will require a lower lift coefficient to execute the same turn. During turns, flaps are utilized to match AOA, as previously described. Since PMTS matched both turn rate and load factor, the velocity it flies at is also the same, as shown in Equation (3.14). There will be a difference in lift coefficient since the matching aircraft is lighter. This lower lift coefficient leads to less drag production and, subsequently a lower thrust setting.

4.2.4. The limits of PMTS

There could be a situation where due to specific aircraft and flight parameters, PMTS will not be able to match AOA anymore. These areas will be highlighted, and PMTS will generate a message indicating this happened during the mission or test. To test how far PMTS can go regarding matching performance and AOA, each of the three missions will be flown at a maximum take-off weight configuration. The same number of stores are released, but the aircraft will bring more weight a take-off. The rest of the mission is identical. This is done to test the limits of PMTS. The maximum takeoff weight for the three missions is $30\,000$ kg [15]. The results will be discussed after the three missions in Section 6.4.

4.3. PMTS Test Missions

In this chapter, the F-16 model created earlier has been scaled up to represent an F-35 based on several scaling parameters. Additionally, the theory behind PMTS has been explained, and the workings of a PMTS-equipped aircraft are now clear. However, it might still be challenging to envision what PMTS does and how it impacts aircraft performance. In this section, PMTS will be used on three smaller test cases to demonstrate the workings of PMTS and how a PMTS-equipped aircraft compares to a loaded or clean aircraft.

Table 4.5 displays three different configurations of the F-35. The table shows a clean configuration consisting of only the aircraft, a pilot, and a full fuel load. The PMTS-equipped aircraft is identical to the clean configuration, the only additional item is the PMTS software. The loaded aircraft, in this case, represents a configuration for a Close Air Support mission, which will be covered in more detail in Chapter 5. The configuration, and the loadout, are shown in Appendix C.3.

The test cases will provide a better understanding of the system's behavior and the differences between a PMTS-equipped, clean, and loaded aircraft in various scenarios. To maintain the organization of this thesis, the relevant figures for this section can be found in Appendix D.

Table 4.5: Configuration for PMTS tests (all values are in kg besides the DI, which is unitless) [15, 46]

	Clean	PMTS	Loaded
W_{Clean}	13290	13290	13290
W_{Fuel}	8278	8278	8278
$W_{\text{Weapons + Adapters}}$	-	-	2904
W_{Total}	21568	21568	24472
Drag Index	-	-	44.14

The three test cases used to explain the workings of PMTS are presented in Table 4.6. The results will show all three configurations flying the same task, and the performance difference between the three will be highlighted and discussed. The missions have been chosen to represent a different aspect of aircraft performance. Since the clean configuration is not weighed down by the extra weight or drag of stores, an adjustment has to be made to make the tests fair. If the clean configuration finishes the test quicker than the loaded configuration, it will cruise at a fixed speed until the other aircraft are finished. That way, the tests can compare fuel burn and derate fairly.

Table 4.6: PMTS Test Missions

Type of Mission	M_{Start}	M_{End}	$\text{Altitude}_{\text{Start}}$ [m]	$\text{Altitude}_{\text{End}}$ [m]	Duration [sec]
Level Acceleration	0.5	1.3	4572	4572	120
Climb and Acceleration	0.5	1.2	3048	10668	250
Sustained Turn	0.9	0.9	4572	4572	270

4.3.1. PMTS Test 1: Level Acceleration

The first test for PMTS will be a level acceleration from Mach 0.5 to Mach 1.3 at an altitude of 4572 m with the engine set to full afterburner. Figure D.1 illustrates the increase in Mach number and Thrust value throughout this test. The clean configuration reaches M_{End} in a notably shorter time than the other two configurations. This is evident as the clean configuration spends about 40 seconds cruising while it waits for the loaded configuration to complete the test. This is a logical outcome, as the clean configuration is neither restricted by PMTS nor the additional weight and drag caused by stores. The PMTS-equipped aircraft matches the acceleration of the loaded configuration while using less thrust to achieve the same performance. This first mission demonstrates the effectiveness of PMTS.

In Figure D.2, the angle of attack of all three aircraft are presented, as well as the flap deflection required by the PMTS-equipped aircraft to match the performance of the loaded aircraft. The flap deflection never exceeds $-4.5°$ and becomes smaller throughout the mission. There are two explanations for this observation. First, the loaded aircraft has a higher thrust setting, leading to a higher fuel burn rate than the PMTS aircraft. The weight of these two aircraft converges throughout the mission due to differences in fuel burn rate, leading to a more similar weight and a lower delta AOA and, thus, lower flap deflection. Second, as the aircraft accelerates, the increased velocity causes the required flap deflection to decrease.

The results of test 1 are presented in Table 4.7. The PMTS-equipped aircraft uses less fuel than the loaded and clean aircraft. The derate, mentioned in Table 4.7, is calculated by comparing the average thrust setting over the entire mission of the PMTS aircraft relative to either the loaded or clean aircraft. The derate value significantly impacts maintenance intervals and cost for aircraft engines, as covered in Section 2.3.1. This first test shows the potential of PMTS, as it matches performance and AOA while reducing fuel burn and engine thrust setting.

Table 4.7: PMTS Test 1 Results

	Clean	PMTS	Loaded
Fuel Used [kg]	885	818	920
Difference in fuel use	$8\,\%$	-	$12\,\%$
Derate when using PMTS	$-8\,\%$	-	$-11\,\%$

4.3.2. PMTS Test 2: Climb and Accelerate

The second test involves both acceleration and climbing, with the aircraft accelerating from Mach 0.5 to Mach 1.2 while simultaneously climbing from $3048\,\text{m}$ to $10\,668\,\text{m}$. The engine is set to full afterburner. Figure D.3 shows the progression of the Mach number and altitude for the three configurations. Like the first PMTS test results, the clean configuration completes the segment in a shorter time and has to wait until the end.

The flap deflection required to match the angle of attack is illustrated in Figure D.4. PMTS can match the AOA across the entire mission with reasonable flap deflections, never exceeding $-3.6°$ during this test. The data shown in Table 4.8 indicates that PMTS uses less fuel to perform the same mission again. The derate is again in the double digits.

Table 4.8: PMTS Test 2 Results

	Clean	PMTS	Loaded
Fuel Used [kg]	1118	1088	1243
Difference in fuel use	$3\,\%$	-	$14\,\%$
Derate when using PMTS	$-3\,\%$	-	$-13\,\%$

4.3.3. PMTS Test 3: Maximum Sustained Turn Rate

The final PMTS test is a continuous turn at the initial maximum sustained turn rate. This turn takes place at Mach 0.9 at $4572\,\text{m}$ with full afterburner. The maximum sustained turn rate is determined at the start of the test, and that constant turn rate is maintained for five full circles ($1800°$). As lighter aircraft have higher maximum sustained turn rates, the clean configuration completes the five full circles first and spends the remainder of the test cruising straight and level at the same flight condition.

Since the aircraft become lighter throughout the test, they no longer fly at their maximum sustained turn rate. Consequently, the AOA decreases as the turn rate drifts further from the maximum attainable performance at that moment. PMTS is again able to match the performance and AOA of the loaded aircraft. In Figure D.5, the thrust setting and fuel burn of the three configurations are presented. Table 4.9 shows that the PMTS-equipped aircraft again uses less fuel. The derate percentage is the highest of the three tests.

Figure D.6 illustrates the angle of attack for the three aircraft and flap deflection required by PMTS. The flap deflection never exceeds $-6°$ and decreases throughout the test. The aircraft becomes lighter during the test while maintaining the same turn performance; hence their angle of attack reduces.

Table 4.9: PMTS Test 3 Results

	Clean	PMTS	Loaded
Fuel Used [kg]	1473	1359	1710
Difference in fuel use	$8\,\%$	-	$26\,\%$
Derate relative to	$-10\,\%$	-	$-21\,\%$

4.3.4. PMTS Tests: Discussion

The three PMTS tests have shown a couple of things. First, PMTS can match performance and angle of attack in all three tests. PMTS does this while burning less fuel, even compared to the clean configuration. PMTS allows the matching aircraft to obtain high derate values. While it is challenging to estimate the exact benefits of such a derate accurately, the information in Section 2.3.1 suggests that the derate offered by PMTS in these tests would significantly extend the maintenance interval of the F135.

5

Missions and Configurations

This chapter will introduce the missions the F-35 will fly, as well as the corresponding configurations. The RNLAF and NLR have verified all three missions and configurations proposed in this chapter to represent realistic and attainable training scenarios. To recap, each of the missions will be flown virtually by three different configurations. A clean configuration with no stores represents how training missions are currently flown by the RNLAF. A loaded configuration represents how the actual mission would be flown during a combat mission. And a PMTS-equipped configuration is an aircraft with a clean configuration but where PMTS restricts performance to enable the aircraft to match the performance and AOA of the loaded aircraft.

Each mission in this thesis adheres to a few standard rules. Each mission starts at 3048 m ($10\,000$ ft). This is to ensure the safety of the pilot and the aircraft. A fuel fraction is used to account for the takeoff and climb to the safety altitude. The landing phase of the mission is not simulated. When a mission profile mentions that a store is released, this can mean a physical store on the loaded aircraft or a virtual store for the aircraft's onboard training system.

5.1. Mission 1: Air-to-Air Combat

The first training mission mimics an air-to-air combat scenario. In this scenario, there is one enemy aircraft and one F-35. During this mission, the F-35 will take six AIM-120 missiles and carry them internally. Internal storage is chosen to keep the radar cross-section of the F-35 as low as possible, which is critical in air-to-air combat. The F-35 will perform a series of combat maneuvers. The maneuvers consist of three sets of three attack runs. During each set, the F-35 fires five of the six AIM-120 missiles at the enemy aircraft. The F-35 will always keep one AIM-120 as a backup in case the aircraft runs into trouble on the way home.

PMTS, together with OTS, provides a unique opportunity to virtually reload the aircraft in-flight. This mission consists of 3 sets of 3 runs, during which 15 missiles could be fired. Virtual reloading maximizes training efficiency and has been common practice for the Air Force for years. This virtual reloading will only be done for this first mission. It also means the loaded aircraft has to be virtually reloaded to set a performance target for PMTS to match. The mission consists of a climb and cruise to the start of the training area, a combat phase, and then a cruise back to the edge of the training area.

5.1.1. Configuration

The configuration for an air-to-air mission is focused on missiles and radar cross-section. Lockheed Martin is developing an upgrade allowing the F-35 to carry six internal missiles instead of the usual four [64]. To keep the radar cross section as small as possible while still providing maximum possibilities, this mission's configuration will consist of six AIM-120 missiles carried internally. The configuration is shown in Figure 5.1. A summary of the configuration data is shown in Table 5.1, and a complete breakdown can be found in Appendix C.

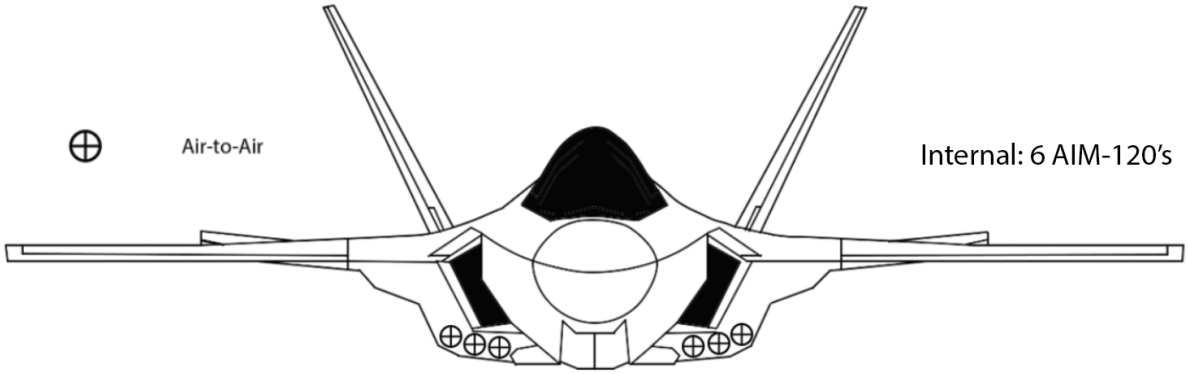

Figure 5.1: Mission 1: Air-to-Air Combat Configuration

Table 5.1: Air to Air configuration data [15, 46, 47, 48]

W_{Aircraft} [kg]	W_{Fuel} [kg]	$W_{\text{Stores + Adapters}}$ [kg]	DI
13,290	8278	1104	0

5.1.2. Mission Profile

The F-35 first climbs to 9144 m while accelerating at the same time. The aircraft then cruises 45 NM at full military power. After reaching the beginning of the combat area, an enemy aircraft appears at 80 NM distance. The F-35 flies toward the enemy aircraft at full military power. Once the enemy is within 40 NM, the F-35 switches to full afterburner and arms its air-to-air missiles. Once the enemy aircraft is within 30 NM, the F-35 fires two air-to-air missiles. It then performs a maximum sustained turn at full afterburner to turn $180°$ and flies away from the enemy at full military power for 2 minutes. The aircraft then turns back towards the enemy at the max sustained turn rate and flies towards the enemy for one minute at military power and one minute at full afterburner before firing another two missiles. It makes this whole loop again for a third time, but it only fires one missile on the final run. After the third run, the aircraft flies back to the start of the combat area at full military power. The mission profile is shown in Figure 5.2.

For the loaded aircraft, this would be the end of the mission, and it would have to return to the base to reload. One more store is available, but it needs to keep this as a backup. At this point, the aircraft is virtually reloaded. This happens twice during this mission, resulting in three sets of three attack runs in which fifteen missiles are fired. To provide PMTS with flight performance data of a loaded aircraft performing this mission, the loaded aircraft will also be reloaded in-flight.

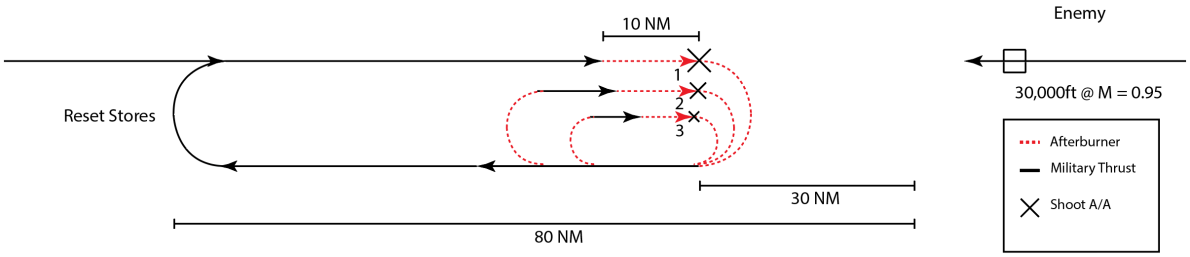

Figure 5.2: Mission 1: Air-to-Air Combat

5.2. Close Air Support

The second mission used to test the effectiveness of PMTS is a close air support (CAS) mission. A CAS mission is used to help troops on the ground once air superiority has been reached. Since air and surface threats are not as significant here, there is no longer the requirement to keep the radar cross-section as small as possible. Therefore, for this mission, both internal and external stores will be used. The F-35 will still bring air-to-air missiles in case an enemy aircraft appears. Some evasive

maneuvers have been added to the mission profile. These can be interpreted as a quick evasion of an enemy surface-to-air missile (SAM) site. The aircraft flies at a lower altitude in this mission as it wants to be able to use the onboard cameras and other sensors to gain situational awareness of what is happening on the ground.

5.2.1. Configuration

The configuration for the CAS mission is focused on carrying as many air-to-ground weapons as possible while still having a couple of air-to-air missiles, just in case. The external storage of stores for this configuration means that this configuration will see the effect of the Drag Index on aircraft performance. In the CAS configuration, the aircraft carries four GBU-39, five GBU-49, and four AIM-120. To carry four GBU-39 internally, it uses a BRU-61 adapter [49]. A visualization of the configuration is shown in Figure 5.3. A summary of the configuration data is shown in Table 5.2, a complete breakdown can be found in Appendix C. This mission will highlight the performance impact of external stores as well as a much heavier configuration. Table 5.2 shows that this configuration carries more than twice as many stores in terms of weight compared to the first configuration, there are even heavier configurations possible, but the choice was made to keep these configurations realistic.

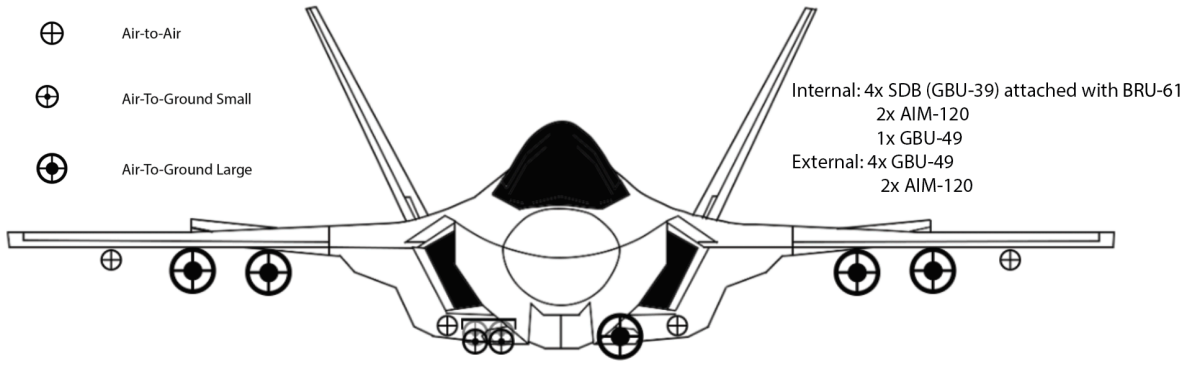

Figure 5.3: Mission 2: CAS Combat Configuration

Table 5.2: Close Air Support configuration data [15, 46, 47, 48, 49]

W_{Aircraft} [kg]	W_{Fuel} [kg]	$W_{\text{Stores + Adapters}}$ [kg]	DI
13,290	8278	2752	44.14

5.2.2. Mission Profile

The aircraft climbs to 6096 m and accelerates to Mach 0.9. It then cruises to the start of the mission area for about 25 minutes, after which combat begins. Over the span of an hour, all nine air-to-ground weapons will be dropped. In between, the aircraft performs three evasive maneuvers. These are max sustained turns at Mach 0.85 that last 90 seconds. The stores are dropped in an alternating pattern, alternating between heavy and lighter weapons. If the aircraft has the same type of weapon, both internally and externally, the external store will be dropped first. At the end of the mission, the four AIM-120s will still be attached to the aircraft. The mission profile is shown in Figure 5.4.

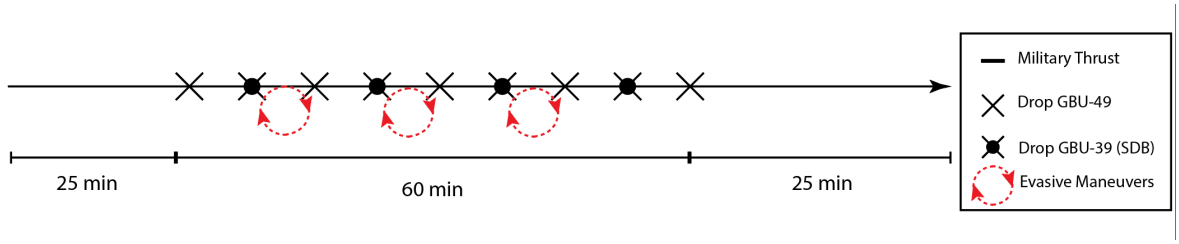

Figure 5.4: Mission 2: Close Air Support

5.3. Red Flag

Red Flag is a two-week-long aerial combat training exercise that happens multiple times a year. The goal of Red Flag is to provide a realistic training exercise for the U.S. Air Force and its partners. The RNLAF frequently participates. The missions flown in Red Flag often represent realistic combat missions and sometimes involve live munitions. Live munitions are expensive, so using PMTS to simulate the effect of munition while not having to drop actual stores would be beneficial in terms of cost. The Red Flag mission chosen to test PMTS is a specific air-to-ground combat mission. In this scenario, there is no aerial superiority, so minimizing the radar cross-section is essential. The aircraft will enter enemy airspace, fly to the target as fast as it can without drawing too much attention, drop its stores, and fly back. During this mission, the aircraft will perform a couple of evasive maneuvers to avoid enemy SAM sites or enemy aircraft.

5.3.1. Configuration

The Red Flag configuration consists of two large air-to-ground stores and two air-to-air missiles. All are carried internally to minimize the radar cross-section. The air-to-air missiles are brought as a defensive weapon. Ideally, during this mission, no aerial threats are encountered. A summary of the configuration data is shown in Table 5.3, and a complete breakdown can be found in Appendix C. The air-to-ground stores that are chosen for this mission are GBU-31. These weigh almost a 1000 kg per store, resulting in a very heavy but still entirely internal configuration [65]. This configuration will highlight the heavy stores' impact without the additional drag of external stores. The configuration is visualized in Figure 5.5.

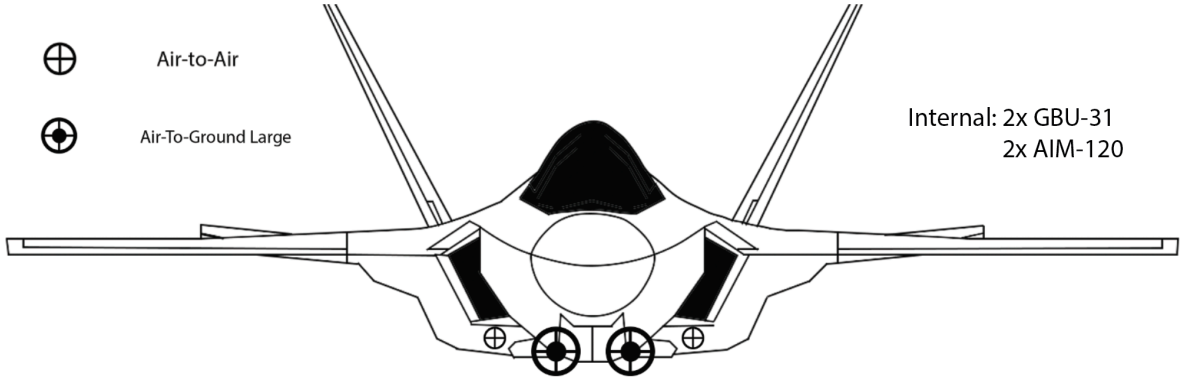

Figure 5.5: Mission 3: Red Flag Configuration

Table 5.3: Red Flag configuration data [15, 48, 46, 47]

W_{Aircraft} [kg]	W_{Fuel} [kg]	$W_{\text{Stores + Adapters}}$ [kg]	DI
13,290	8278	2294	0

5.3.2. Mission Profile

The Red Flag mission profile is quite simple. The F-35 climbs to 9144 m while accelerating at the same time. It then cruises for 45 minutes at full military power. During the cruise phase, the aircraft performs two evasive maneuvers, which are 90 seconds of max sustained turn rate at full afterburner. After the cruise to the target, the combat maneuver starts. Combat consists of dropping two air-to-ground weapons for 5 minutes. The weapons are dropped from cruise altitude. Then the aircraft turns around and cruises back for 45 minutes at full military power, performing two evasive maneuvers on the way back. The mission profile is shown in Figure 5.6.

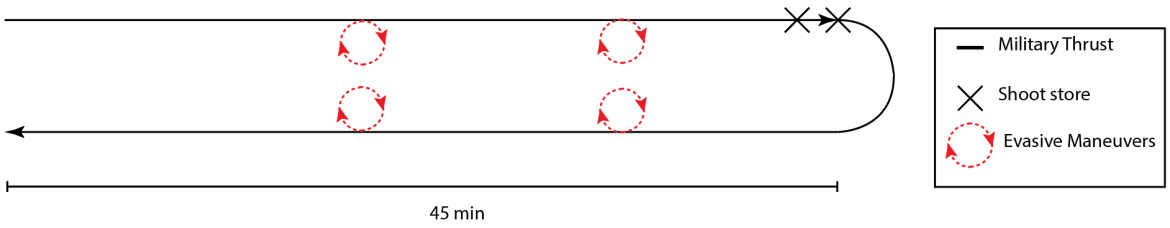

Figure 5.6: Mission 3: Red Flag

5.4. Discussion of the Missions and Configurations

This chapter covered three very distinct missions with different configurations. The idea was to create representative scenarios regarding mission requirements and configurations. Before moving on to the results, it is important to highlight these differences, as they will affect the outcome of this thesis. The first main difference between the missions is how the aircraft cruises, which might seem trivial but significantly impacts the performance. Missions 1 and 3 have an unspecified cruise speed. The engine is set to max military thrust, resulting in an airspeed. Mission 2 has a specified fixed cruise speed. The difference here is that for missions 1 and 3, the aircraft is at max power during cruise, while for mission 2, the loaded aircraft is already derated due to the specified cruise speed. Due to the difference in weight and drag between configurations, a cruise at maximum military power results in different cruise speeds. This will lead to differences between configurations in the time to complete specific segments, how much fuel can be saved, and the total derate.

The choice between internal, external, or a combination of the two mounting locations will significantly impact performance. Mission 2 is the only mission with external stores. It will be interesting to see the difference in fuel savings when matching an externally loaded configuration versus only internally.

6

Results and Discussion

This chapter will present the results of the three missions flown virtually for this thesis. The effectiveness of PMTS will be judged based on a few key parameters. These parameters are Thrust Setting, Mach number, Total Weight, Fuel Burn, AOA, and flap deflection. The last parameter, flap deflection, only applies to the aircraft equipped with PMTS, as the flaps are used to match AOA. Some of the less intriguing figures have been moved to Appendix E to create more room for the exciting figures in this section. Since the clean configuration is lighter, it will complete specific segments faster. At the end of the mission, if the clean configuration has completed tasks faster, it will cruise at the final flight condition until its mission length is identical to the loaded configurations. This is done to make the comparison fair. After the three missions, a test case to show the limits of PMTS is discussed.

6.1. Mission 1: Air to Air

The first mission is the air-to-air mission introduced in Section 5.1. The loaded configuration for this mission, as shown in Figure 5.1, only carries internal stores. One unique feature of this mission is including virtual reload moments, made possible through onboard training systems (OTS). The virtual reloading feature allows pilots to complete three sets of air-to-air (A/A) setups during the mission. Each set simulates a new mission in terms of virtual stores onboard and their performance impact on the aircraft.

The total weight line of the loaded aircraft, shown in Figure 6.1, displays vertical drops whenever stores are released. The total weight of the matching and clean aircraft is initially the same, but as the mission progresses, the two total weights start to diverge due to the lower fuel burn of the matching aircraft. The reduced fuel burn is due to a lower thrust setting, visible in Figure 6.3. The two virtual reload moments during the mission can be observed as vertical increases in the total weight data of the loaded aircraft.

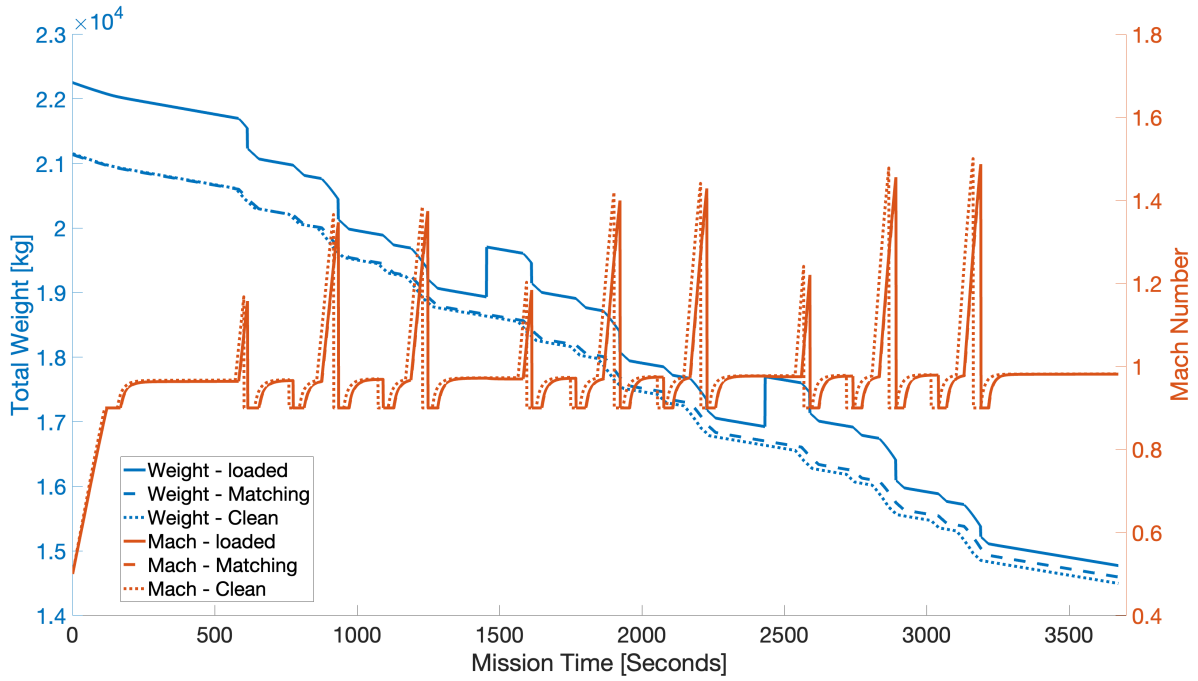

Figure 6.1: Mission 1: Total Weight and Mach number

The Mach numbers of the three aircraft are shown in Figure 6.1. The different mission segments become very clear when analyzing the Mach number. The initial climb and acceleration are visible, with a small part of the climb flown at a constant Mach number towards the end. During the climb, the pilot limits the aircraft to a maximum Mach number of 0.9. Once the aircraft reaches that Mach number and hasn't finished climbing, the pilot continues the climb at that constant Mach number till the aircraft reaches the desired altitude. Since the speed of sound reduces with altitude, the aircraft slowly decelerates toward the end of its climb. This deceleration is very small and lasts for less than a minute; it happens for both the clean and loaded configurations.

At cruise altitude, both the clean and loaded aircraft fly at maximum military power, resulting in a top speed slightly below the speed of sound for both configurations. The clean aircraft reaches a slightly higher Mach number because it produces less drag due to its lower weight. It is evident when the afterburner is activated, as Mach numbers quickly rise and the aircraft goes supersonic. As before, the clean configuration reaches a higher top speed than the loaded configuration. Since parts of this mission are specified by distance or altitude, as covered in Section 5.1, the clean aircraft will complete these segments in less time. The lower weight and resulting higher cruise speed and climb rate lead to the clean aircraft completing specific mission segments in less time. For that reason, the data for the clean aircraft looks out of phase with the matching/loaded aircraft. The clean configuration makes up for this time at the end of the mission.

The matching aircraft can use PMTS to match the performance of the loaded aircraft throughout the entire mission. The data for the matching aircraft overlaps with the loaded aircraft's data in Figure 6.1, displaying the effectiveness of PMTS.

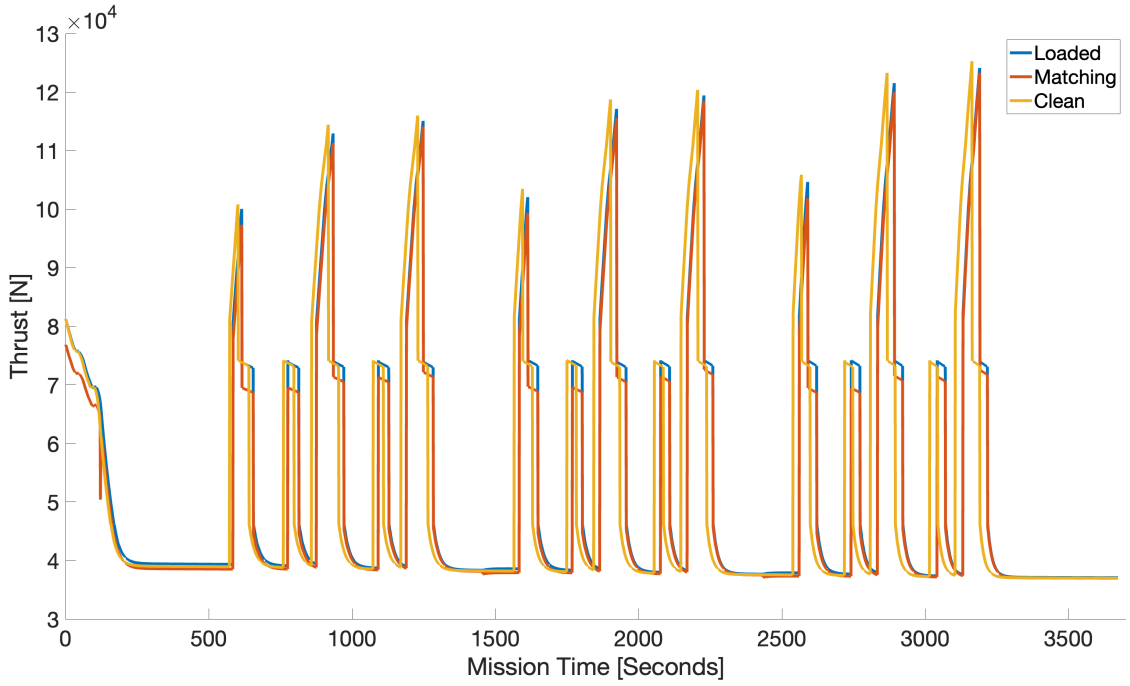

Figure 6.2: Mission 1: Thrust Setting

Figure 6.2 depicts the engine thrust setting during the first mission for all three configurations. The same out-of-phase behavior is visible in Figure 6.1 is seen here, as expected. The three sets, each consisting of three runs, are visible in the thrust data. The second and third runs have higher maximum thrust values than the first. This is due to the length first run of each set being defined by distance, while the second and third are defined by time. This allows the aircraft to reach a higher top speed on the first run than on the second and third. Importantly, Figures 6.1 and 6.2 show that the matching aircraft equipped with PMTS can replicate the performance of the loaded aircraft across the entire mission while keeping its engine at a lower thrust setting.

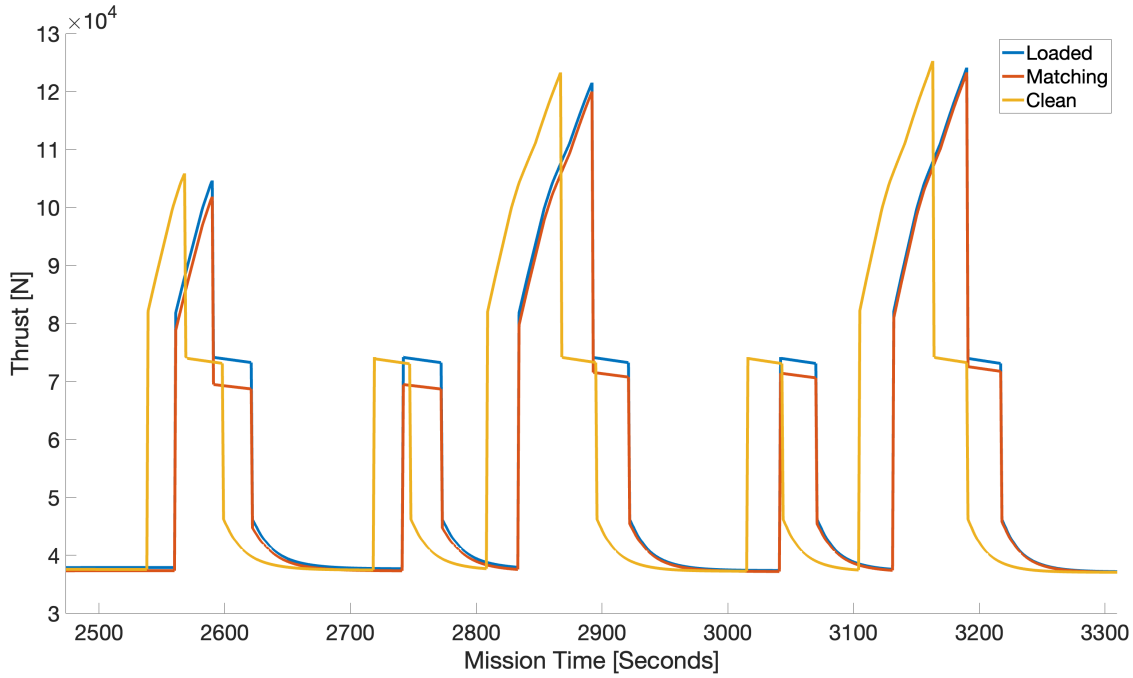

Figure 6.3: Mission 1: Thrust Setting for Final set

The reduction in thrust values might not be visible in Figure 6.2; therefore, Figure 6.3 displays the thrust values for the third set. This image displays several things worth discussing that might not be immediately visible in Figure 6.2. The phase shift between the clean and matching/loaded aircraft is visible. The lower thrust setting required by the matching aircraft over the entire mission, specifically in high-performance maneuvers, is also visible. The matching aircraft has an overall derate but also drastically reduces peak thrust values. The clean aircraft can produce more thrust because it can reach a higher Mach number due to its lower weight and subsequent performance advantages.

Finally, during the maximum sustained turn rate turns, the thrust value reduces during the maneuver. The maximum sustained turn rate is determined at the beginning of the maneuver and then held till the aircraft turns $180°$. Since the aircraft burns fuel during this maneuver, it becomes lighter and no longer flies at its maximum sustained turn rate. That leads to the aircraft continuously reducing thrust to keep the turn rate constant, this behavior is visible in the turns shown in Figure 6.3.

6.1.1. Flaps and Angle of Attack

The data presented above shows that PMTS can effectively match the performance of the loaded aircraft throughout the entire mission. However, PMTS is specifically designed to match not only performance but also the angle of attack. Figure 6.4 illustrates how the clean aircraft consistently flies at lower AOA than the loaded aircraft. This is due to the clean aircraft's reduced weight, lower lift requirement, and slightly higher maximum speed, which allows for a lower AOA.

The clean and loaded aircraft fly at almost the same AOA during turns. Although they produce similar lift coefficients by flying at similar AOA, their turn rates are not identical. The clean aircraft is lighter and can achieve a higher maximum sustained turn rate than the heavier-loaded aircraft. The expectation would be that a light aircraft could fly at a higher AOA. Still, the difference in total weight is not big enough to allow for a significant difference in maximum AOA.

Figure 6.4 also presents the flap deflection required by the matching aircraft to match the AOA of the loaded aircraft. The most significant flap deflection occurs during the maximum sustained turn rate turns. The required flap deflection reduces throughout the mission since the weight of the loaded and matching configurations converge.

The results from the first mission show that PMTS is effective in matching the performance and AOA of the loaded aircraft.

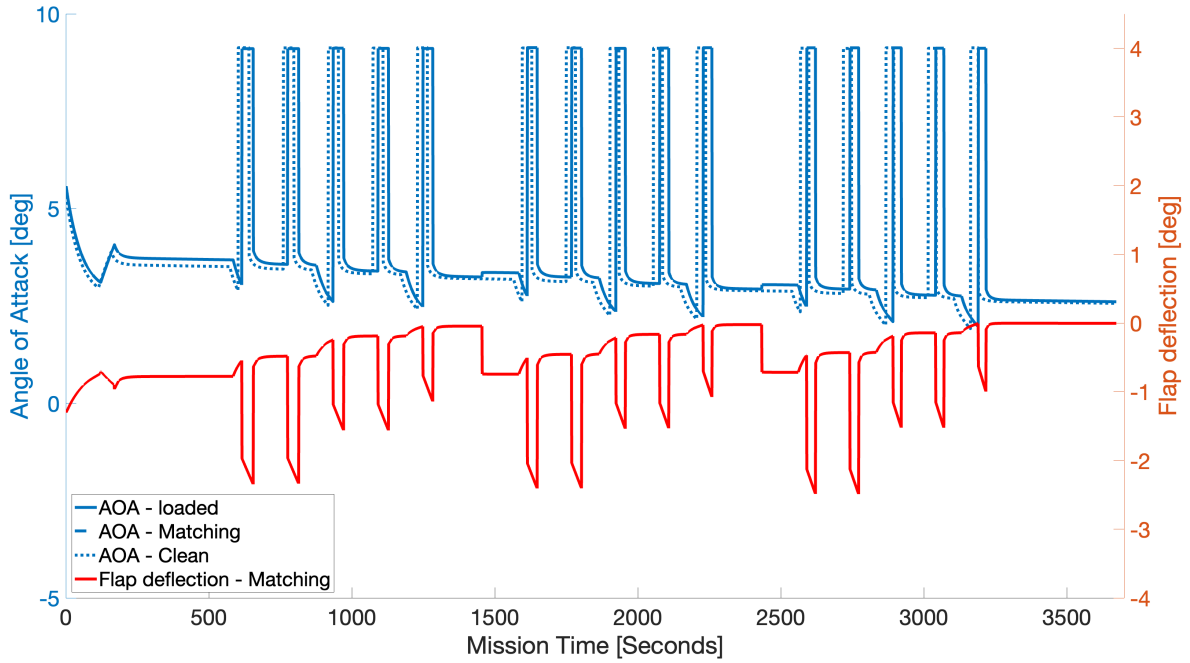

Figure 6.4: Mission 1: Flap Deflection and Angle of Attack

6.1.2. Fuel and Derate

The previous sections have established that PMTS can match the performance and angle of attack during the first mission. The fuel burn reduction and derate represent an additional benefit to using PMTS. Figure E.1 shows the progression of fuel burn during the mission. The fuel burn data does not begin at zero since the aircraft burns fuel to get to the start of the mission area. The fuel required for this is estimated as a fraction of the total fuel onboard. As anticipated, the fuel burn progression reveals that the matching aircraft uses less fuel than the clean and loaded aircraft. Table 6.1 shows the data for the first mission. The matching configuration outperforms the loaded and clean configuration regarding derate percentage and fuel burn. The matching aircraft achieves a fuel saving of $2.4\,\%$ and a derate of $2.2\,\%$ relative to the loaded configuration. When compared to the clean configuration, the matching configuration saves $1.7\,\%$ of fuel at a derate of $1.6\,\%$. Although this derate percentage is small, as mentioned in Section 2.3.1, it can significantly impact maintenance intervals and cost. The derates shown in Table 6.1 are the average derate percentages. The top two peak derate values comparing the clean and matching configuration are $24.5\,\%$ and $6.4\,\%$. That first value happens during the climb, and the second happens during the third set of attack runs. The average derate shows positive results already, but the reduction in peak thrust values could further increase the impact PMTS has on the engine's life and maintenance. The peak derates are only compared to the clean configuration, as this represents the current training configuration. Thus comparison with the current training configuration is most important to analyze when it comes to the effectiveness of PMTS. In conclusion, for the first mission, PMTS has demonstrated its ability to match performance and AOA while reducing engine wear and fuel consumption.

Table 6.1: Fuel Burn and Derate data for Mission 1

	Loaded	Matching	Clean
Fuel Used [kg]	7121	6956	7071
Difference in fuel burn w.r.t. matching configuration	$2.4\,\%$	N/A	$1.7\,\%$
Average derate w.r.t. matching configuration	$-2.2\,\%$	N/A	$-1.6\,\%$

6.2. Mission 2: Close Air Support

The second mission is the Close Air Support (CAS) mission. As explained in Chapter 5, this configuration differs significantly from the first mission. The CAS configuration is significantly heavier and carries its stores internally and externally. The external stores increase the total drag of the aircraft, with the drag increase calculated using the drag index, as discussed in Section 3.7. Figure 6.5 displays the total weight and Mach number of all three configurations throughout the second mission. Although this graph is less dynamic than the first mission, it offers interesting insights. The total weight data reveal a substantial difference in starting weight between the clean and loaded configurations. The second mission's loaded configuration represents the heaviest configuration in this thesis. The total weight data for the loaded aircraft displays when stores are dropped, represented as vertical drops in the total weight data. The clean and matching aircraft share the same starting weight, with their total weights diverging as the mission progresses due to differences in fuel burn.

Compared to the first mission, there is a much smaller difference in total mission duration between the loaded and clean aircraft. Since the second mission specifies a cruise speed, the total duration of that segment is the same for any configuration. The clean configuration is only faster than the loaded configuration during the climb and acceleration phase, a minor portion of the total mission. The Mach number data in Figure 6.5 highlights the three evasive maneuvers executed during the mission. During these maneuvers, the clean and loaded aircraft perform a maximum sustained turn at full afterburner for 90 seconds. Since the clean aircraft is lighter and has a higher sustained turn rate, the clean configuration performs more turns during that time than the loaded aircraft. PMTS is again able to match performance and AOA throughout the entire mission.

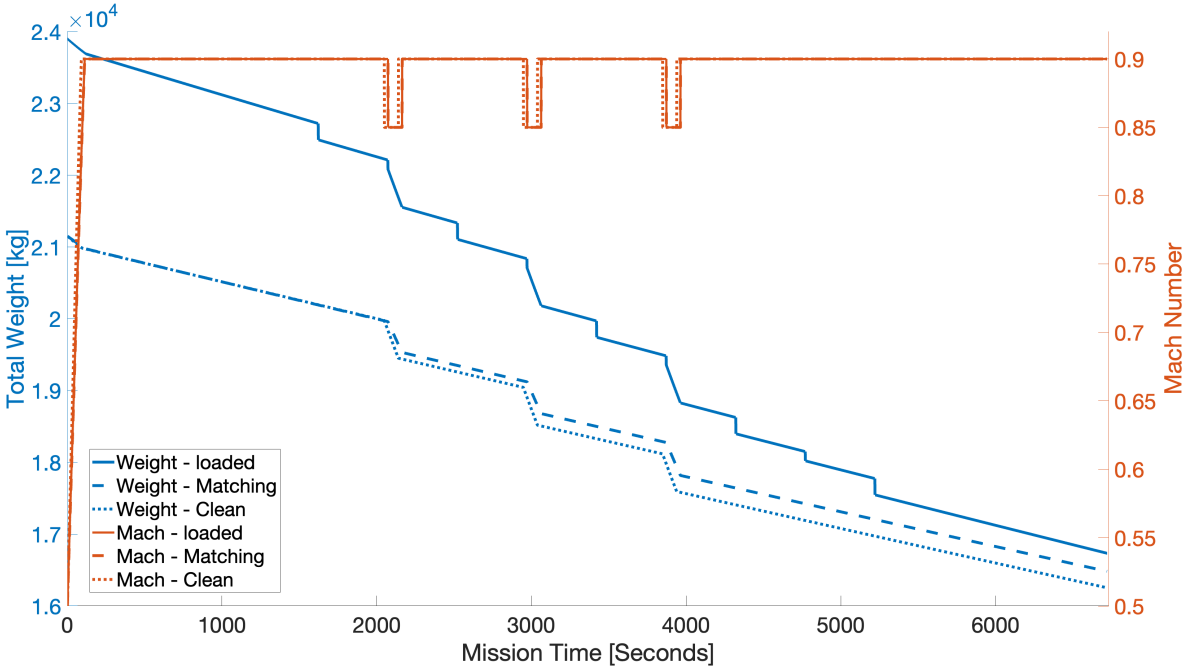

Figure 6.5: Mission 2: Total Weight and Mach number

Figure 6.6 depicts the engine thrust setting throughout the mission. There is a significant difference between the thrust setting for the clean and loaded configuration during the cruise phase. Each time a store is dropped, the difference in thrust decreases as the store no longer generates drag on the loaded aircraft. This behavior is evident as a downward staircase pattern in the thrust data of the loaded aircraft. Towards the end of the mission, the loaded configuration still requires more thrust than the clean aircraft. This can be attributed to the adapters and A/A missiles still present on the aircraft. These adapters have their own drag index and weight, thus increasing the total drag of the aircraft even after stores have been dropped. The three evasive maneuvers stand out as massive spikes in thrust production due to full afterburner being used during these maneuvers.

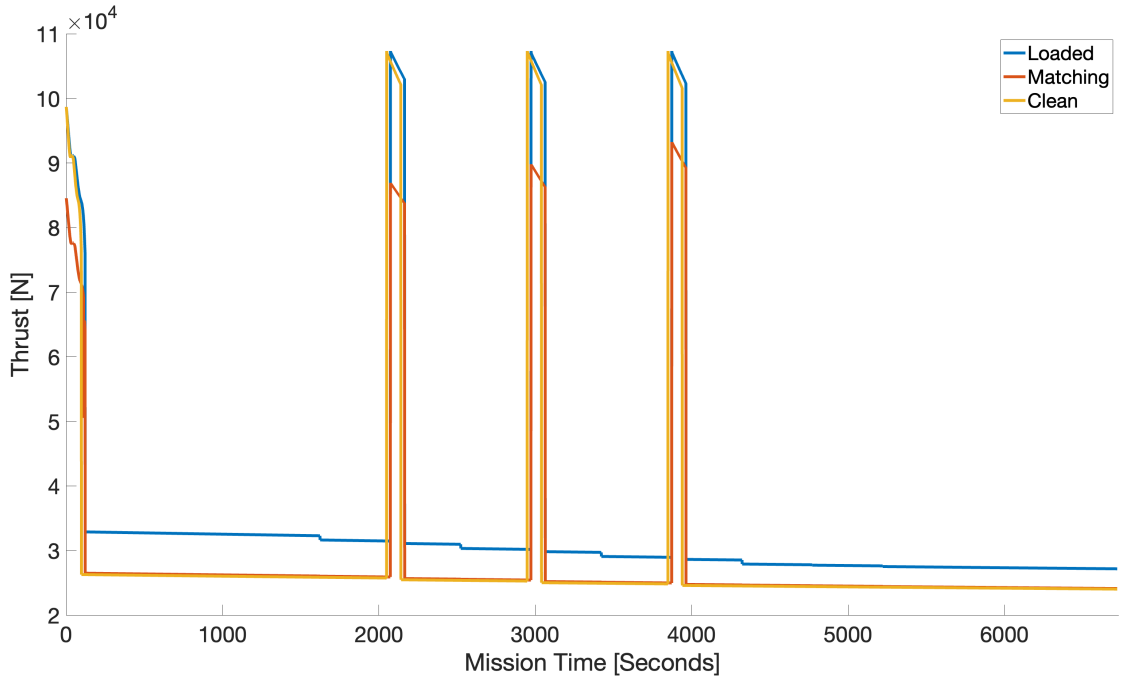

Figure 6.6: Mission 2: Thrust Setting

Figure 6.7 illustrates the thrust setting during the first evasive maneuver. A couple of observations stand out: first, the thrust settings for the clean and loaded aircraft are the same. Since both aircraft fly at the same altitude and velocity, they have the same maximum thrust available at that flight condition. As previously mentioned, there is a difference in turn performance due to weight differences between the two configurations. Second, the matching aircraft can match performance across the maneuver using less thrust. Figure 6.7 highlights the significantly lower thrust setting of the matching aircraft during this evasive maneuver. The thrust setting during cruise is also visible before and after the maneuver shown in Figure 6.7, which shows the matching aircraft uses significantly less thrust during cruise.

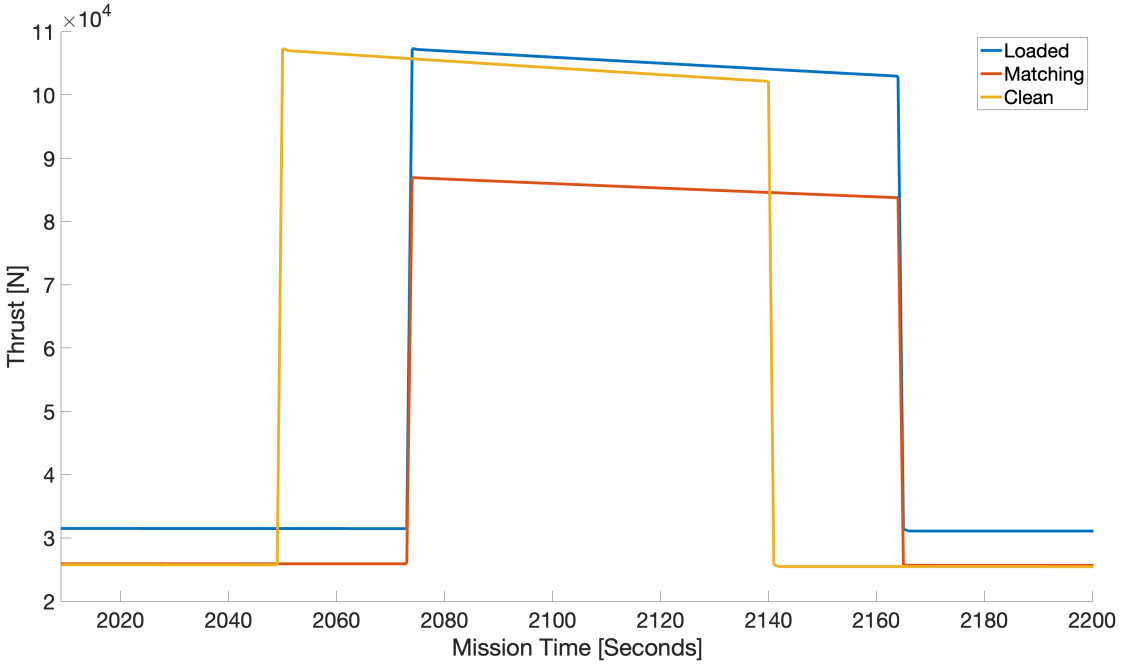

Figure 6.7: Mission 2: Thrust Setting during Evasive Maneuver 1

6.2.1. Flaps and Angle of Attack

PMTS can match the performance of the loaded aircraft for the second mission. This section evaluates if PMTS can also match the angle of attack. Figure 6.8 displays the angle of attack for all three configurations and the flap deflection required by the matching aircraft to match the loaded configurations AOA. The AOA data during the evasive maneuvers stand out. The maximum AOA of the clean aircraft is higher than that of the loaded aircraft, which did not occur during the first mission. This can be explained by the external stores creating so much drag that it limits the amount of lift-induced drag that can be added by the aircraft before the thrust is no longer sufficient to maintain airspeed. This limits the maximum angle of attack the loaded aircraft can fly at and is only a limitation during evasive maneuvers. PMTS successfully matches the AOA of the loaded configuration throughout the entire mission. It does this with reasonable flap deflections, never exceeding $-6°$. As anticipated, the flap deflection decreases during the mission as the matching and loaded configuration weights converge.

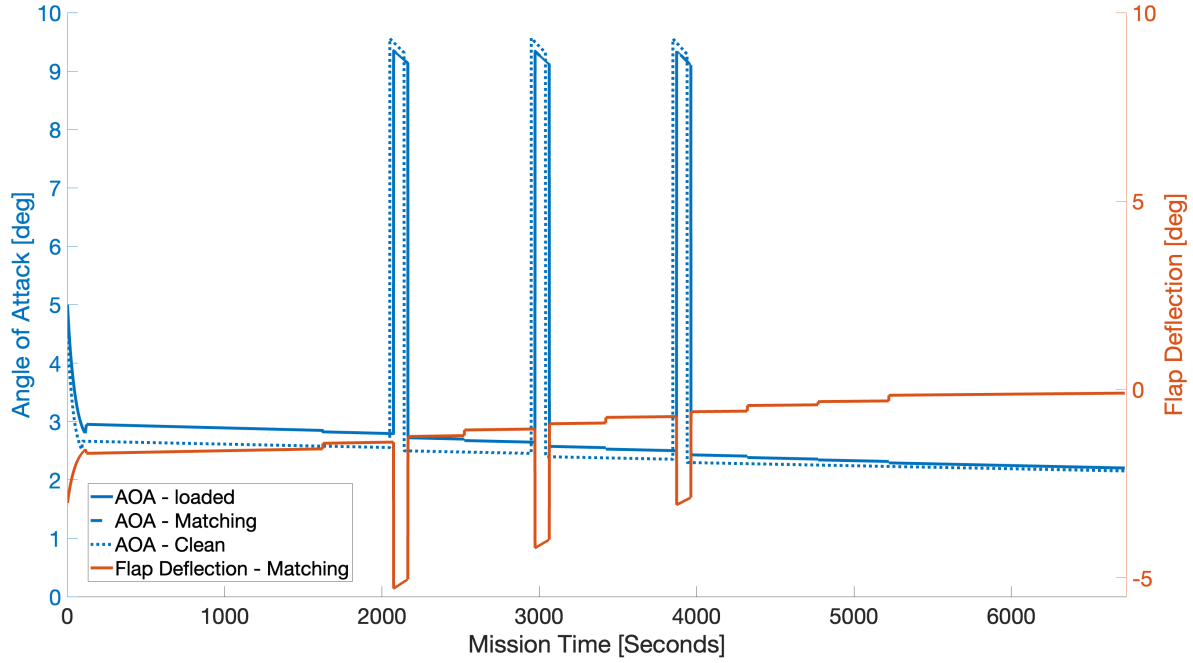

Figure 6.8: Mission 2: Angle of Attack and Flap Deflection Setting

6.2.2. Fuel and Derate

PMTS can match AOA and performance while operating at a lower thrust setting. Figure E.2 displays the fuel used during the mission. The differences in fuel consumption are considerably more significant than those observed during the first mission, which can be attributed to more stores on the aircraft and their external mounting leading to more drag. The divergence in fuel use between the clean and matching configurations is also visible due to PMTS limiting thrust on the matching configuration, which leads to a lower fuel burn.

The derate and fuel savings resulting from the lower thrust setting are presented in Table 6.2. The Fuel savings are significantly higher than those observed for the first mission, with the matching configuration achieving double-digit savings compared to the loaded aircraft. Compared to the clean configuration, the PMTS-equipped configuration saves over $4\,\%$ in fuel, a considerable amount. The average derate of the engine relative to the loaded configuration is significant and higher than for the first mission. The average derate relative to the clean configuration is similar to the first mission. The two highest peak derate values when comparing the matching and clean configuration are $18\,\%$ and $15\,\%$. The first occurs during the climb, similar to the first mission. The second value occurs during the first evasive maneuver. As was the case during the first mission, the peak derate values are significantly higher than the average. This could positively impact engine life and maintenance intervals.

Table 6.2: Fuel Burn and Derate data for Mission 2

	Loaded	Matching	Clean
Fuel Used [kg]	5933	5085	5314
Difference in fuel burn w.r.t. matching configuration	16.7 %	N/A	4.5 %
Average derate w.r.t. matching configuration	−15.2 %	N/A	−1.9 %

6.3. Mission 3: Red Flag Mission

The third and final mission is the Red Flag mission, which mimics a real-life air-to-ground mission with the added threat of potential SAM sites or enemy aircraft. For this reason, the configuration consists of only internally carried stores to maintain the lowest possible radar cross-section for the aircraft. Figure 6.9 displays the total weight and Mach number throughout the entire mission for all three configurations.

Examining the Mach number data, some interesting things stand out. During the climb and acceleration phase, the Mach number remains constant for a period of time. This behavior is also observed during the first mission and is explained in Section 6.1. At cruise altitude, the aircraft cruises at maximum military power, leading to different cruise speeds for the loaded and clean configurations. Similar to the first mission, the heavier configuration has a lower cruise speed at full power Once the stores are dropped, the weights of the two configurations become closer, resulting in similar cruise speeds. The clean aircraft can complete the climb and acceleration segment faster, leading to a slight 'phase shift' in the data. Four evasive maneuvers are visible, consisting of maximum sustained turn rates at a fixed Mach number. The moments the stores are dropped are visible as two vertical drops in the total weight data of the loaded configuration. The clean and matching aircraft begin with the same weight, and as anticipated, their total weights diverge towards the end of the mission due to a difference in thrust setting.

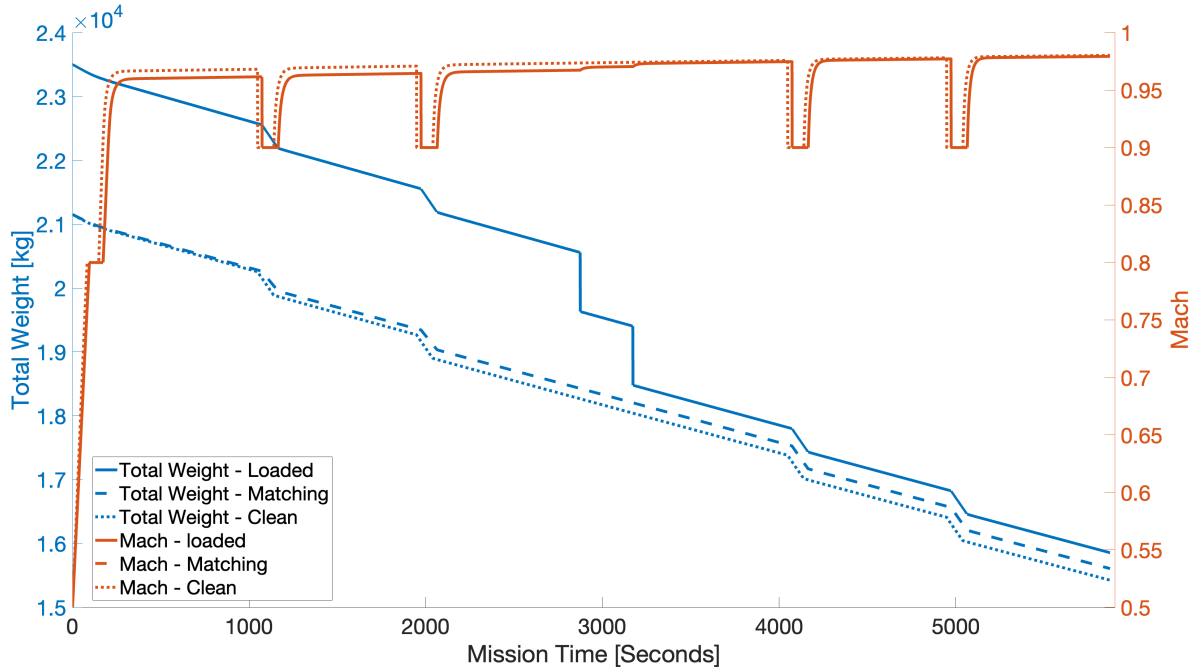

Figure 6.9: Mission 3: Total Weight and Mach number

Figure 6.10 illustrates the thrust values for all three configurations throughout the mission. The two evasive maneuvers before the store drops reveal a significant difference between the thrust settings for loaded and matching configuration. And even during cruise, the matching aircraft has a significantly lower thrust setting. After the stores are dropped, the total weight of these two configurations converges, and the difference in thrust becomes much smaller. The matching aircraft can match performance while maintaining a lower thrust setting during the entire mission.

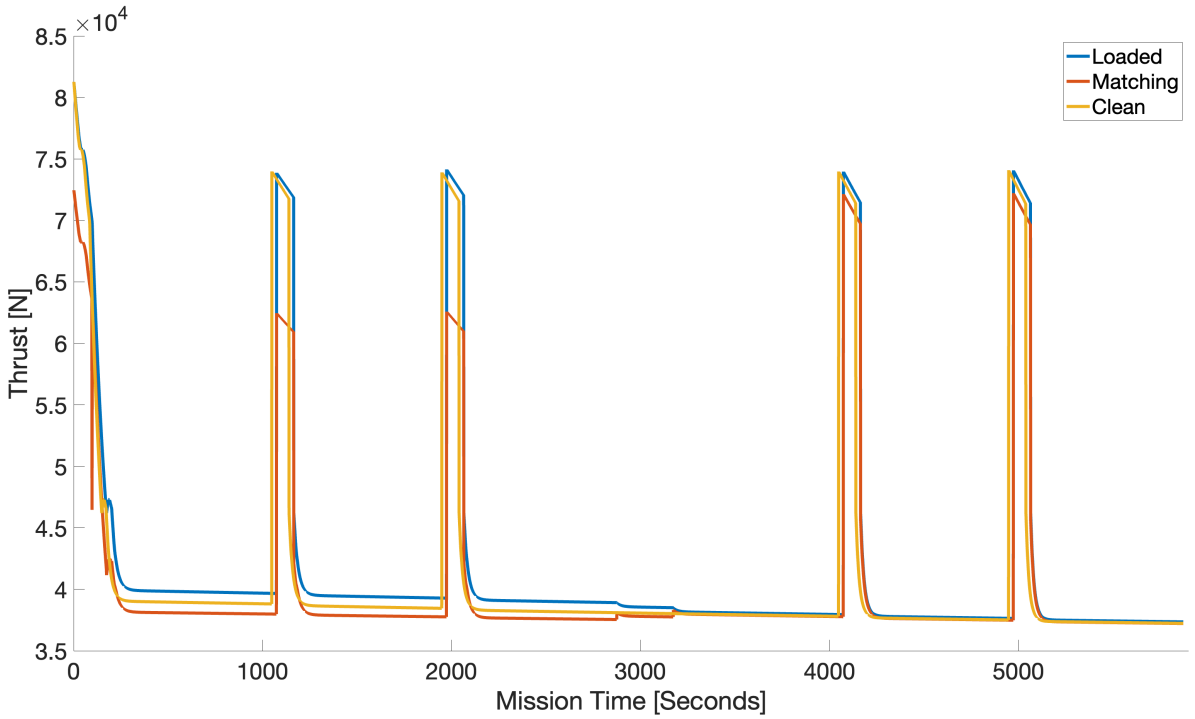

Figure 6.10: Mission 3: Thrust Setting

6.3.1. Flaps and Angle of Attack

The AOA and flap deflection data is presented in Figure 6.11. As the loaded configuration for this mission carries only internal stores which produce no external drag, the difference in maximum AOA is minimal. Before the store drops, the difference in weight between the clean and loaded configuration is visible as a difference in AOA at the same velocity. PMTS can match the angle of attack throughout the entire mission. It achieves this with a very modest flap deflection, with flap deflections remaining below $-6°$ for the entire mission.

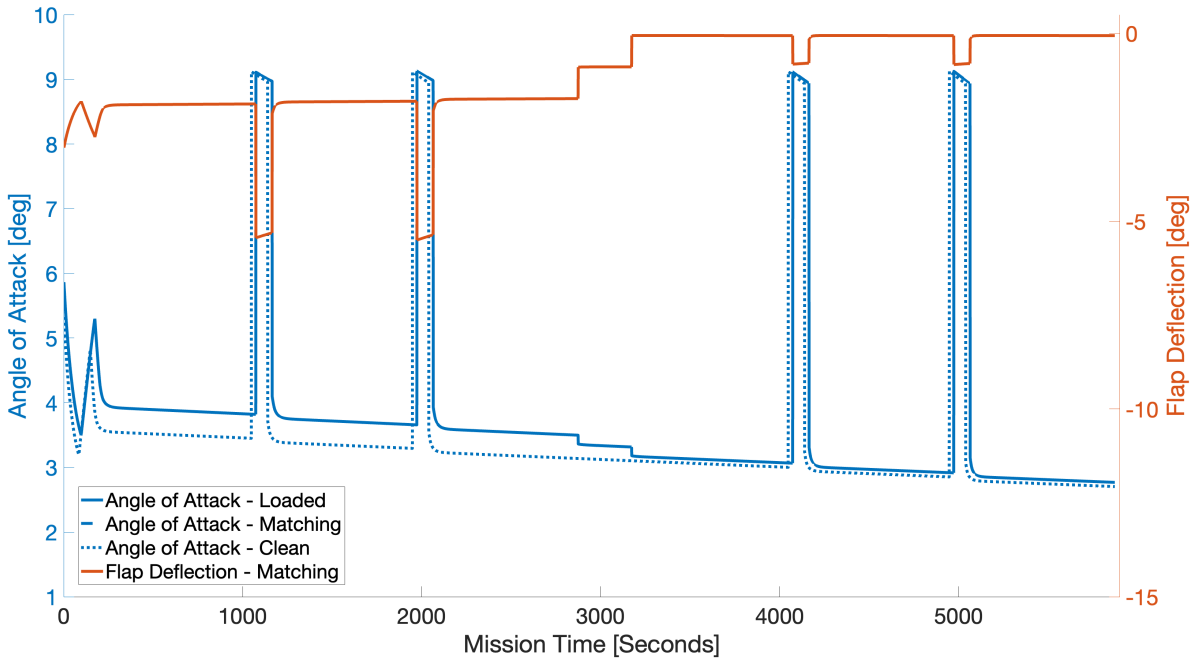

Figure 6.11: Mission 3: Angle of Attack and Flap Deflection Setting

6.3.2. Fuel and Derate

The progression of fuel use displayed in Figure E.3 is expected, with sharp increases in fuel burn rate when the afterburner is activated.

All three configurations' fuel use and derate data are presented in Table 6.3. PMTS reduces fuel use by $4.2\,\%$ compared to the loaded configuration and $3.1\,\%$ compared to a clean configuration. The average derate ranges from $-3.4\,\%$ to $-2.1\,\%$. The two highest peak derates values when comparing the matching and clean configuration are $27\,\%$ and $15\,\%$. They occur during the climb and the second evasive maneuver.

Table 6.3: Fuel Burn and Derate data for Mission 2

	Loaded	Matching	Clean
Fuel Used [kg]	6210	5961	6143
Difference in fuel burn w.r.t. matching configuration	$4.2\,\%$	N/A	$3.1\,\%$
Average derate w.r.t. matching configuration	$-3.4\,\%$	N/A	$-2.1\,\%$

6.4. PMTS limits

To test the limits of PMTS, each of the three missions described earlier has been flown with a maximum take-off weight (MTOW) configuration in addition to the original three missions. This is done to test if the PMTS-equipped aircraft can still match performance and AOA at bigger differences in weight and, if so, what the flap deflections would be. This test shows if PMTS still works when the AOA delta is the largest it can be. All three missions still burn fuel and drop the same amount of stores as before, becoming lighter during the mission. PMTS can match performance and angle of attack for all three missions. The flap deflections become significantly larger, with maximum deflections ranging between -14.8° and -15.2°. This means that the maximum flap deflection of -15°, stated for this thesis, is exceeded. However, the real-life maximum flap deflection limit might well be higher. The derate values and fuel savings numbers become significantly higher, as expected. This shows that if the maximum flap deflection angle allows it, PMTS can match the F-35's performance and AOA across these missions regardless of the configuration weight. Please keep in mind that if additional performance matching metrics are incorporated into PMTS, this may change.

6.5. Effectiveness of PMTS

After three different missions, PMTS has shown to match performance and AOA over the entire mission. PMTS achieves this result at a lower thrust setting, leading to a reduction in fuel burn. It can outperform both the clean and loaded configuration regarding fuel use and derate values. While hard to quantify, the average and peak derate values indicate a potentially significant impact on engine life and maintenance intervals. Combining the impact derate has on training and operating costs with the reduction in fuel burn, PMTS could significantly impact training costs. The fact that PMTS outperforms a loaded configuration in terms of fuel use and derate was expected. It is much more important that PMTS can do this compared to a clean configuration, as this represents the current most flown training configuration. PMTS outperforms the clean configuration in all three missions. This means PMTS allows for more realistic training while reducing training costs simultaneously. As mentioned in Section 4.1.2, the TSFC used in this thesis is likely for the most optimal condition, the real-life TSFC could be significantly higher. This would increase the fuel-saving potential of PMTS.

If Onboard Training Systems (OTS) can accurately simulate non-performance related aspects of training missions (which they already do), PMTS could complete the OTS package with performance-matching capabilities. PMTS would be an invaluable addition to the OTS package on modern fighter aircraft. Increasing training realism while at the same time reducing training costs.

7

Conclusion and Recommendations

This study aimed to show that fighter training realism could be enhanced by using flap and thrust scheduling to match the performance of a combat-configured aircraft. The Performance Matched Training System (PMTS) allows a clean training aircraft to match the performance of a loaded combat aircraft. PMTS uses the engine management system (EMS) and flaps to match a loaded aircraft's performance and angle of attack. The EMS effectively derates the engine, while the flaps are used to reduce lift production of the clean aircraft and allow it to fly at a higher angle of attack while maintaining the same flight condition. The effectiveness of PMTS was evaluated using three typical combat missions: Air-to-Air, Close Air Support, and a Red Flag mission. Each mission has its unique configuration, consisting of internal and external stores. Depending on where stores are mounted, they affect the aircraft's performance differently.

7.1. Conclusion

The effect of stores on aircraft performance can be simulated using flap and thrust scheduling. Negative flap deflections are used to reduce lift production of the clean aircraft, allowing it to fly at a higher angle of attack while keeping other flight parameters equal. This allows the clean aircraft to match AOA with heavier aircraft. Thrust scheduling is used to match performance. By derating the engine, the performance of a heavier aircraft can be matched during most phases of flight. PMTS can match performance across all three missions in this thesis within the limitations set for this research.

During the three test missions, there was a notable reduction in fuel consumption ranging from $1.7\,\%$ to $4.5\,\%$. Additionally, the average derate ranged from $1.6\,\%$ to $2.1\,\%$, while the peak derate was between $18\,\%$ and $27\,\%$. The values are relative to the current clean training configuration and thus show potential benefits to current training methods. Derate and fuel use differences were higher when compared to the loaded configuration. The impact derate has on engine life is difficult to quantify, but the impact can be estimated to be in the double-digit range in terms of life extension. This would also have a positive effect on, for example, spare parts and other maintenance-related factors.

Compared to current training methods, PMTS would be able to be used with any of the current Onboard Training Systems (OTS) available. Whether in virtual training missions offered by Embedded Training or in actual red/blue air training flights, PMTS can enhance training efficacy. Although untested on actual pilots, it is reasonable to assume that adding PMTS to OTS will improve training outcomes. Moreover, PMTS can function independently as a standalone system. Its integration into the current set of OTS is not expected to result in any significant alterations to the training techniques.

PMTS impacts training efficacy in several ways. By matching the performance and AOA of a loaded aircraft, it is reasonable to assume that training realism is enhanced. This claim can be made based on the improvements in the perceived effectiveness that other OTS currently offer. Matching the performance and AOA of the aircraft a pilot is training to fly during combat should enhance training realism, efficacy, and perceived effectiveness. PMTS can match airspeed, AOA, climb and turn rate across all three of the missions in this thesis, including climb and turn rates. Furthermore, PMTS reduces training expenses in multiple ways, allowing for more frequent training or extended training missions due to the reduced fuel burn.

7.2. Recommendations for future work

This thesis has shown that PMTS can match the specific performance parameters chosen for this thesis. Therefore, the recommendation for future work and research would be to continue implementing PMTS on operational F-35. The roadmap to implementation on an actual F-35 is still long. This thesis has covered the proof-of-concept phase of the roadmap but has done no work in the direction of the actual implementation for the F-35. The current F-35 model is enough to prove the proof-of-concept, but a significantly more detailed and realistic model is required for actual implementation. There is still a lot of work to do to implement PMTS. First, PMTS needs to be expanded to include every aspect of a store's impact on performance. Right now, the scope of this thesis is limited to certain aspects. Performance metrics like deceleration, descent, and matching AOA of a lighter configuration are not included. By using flaps as intended to produce more lift, the aircraft should be able to match a lighter aircraft's lower AOA. Furthermore, by using flaps as speed brakes, PMTS could be able to match the deceleration of a heavier and draggier configuration. This needs to be researched and implemented. The effect of stores on angular rates and accelerations should also be included, as well as un-symmetrical store loading effects and the possible effect releasing stores has on the flight condition. What this relates to is what a pilot feels when they release stores. On top of that, the implementation and interaction with the F-35's Flight Control Systems need to be researched and tested. The F-35 FCS is especially suited for PMTS implementation, but this needs to be proven. The integration into the pilot vehicle interface, as well as the safety implications of PMTS, require further elaboration and research.

On top of these technical development required to implement PMTS research into the additional benefits and cost of the system should be done. First of all, the effect PMTS has on engine and airframe life is not quantified right now. An educated guess is made regarding the order of magnitude of improvements. Still, significantly more research is necessary to accurately predict the impact PMTS has on the longevity of the engine and airframe. The TSFC is also not accurately modeled due to a lack of information. The expectation is that the actual TSFC is significantly higher than the one used in this thesis, which needs to be determined as it would make the case for PMTS even better. These benefits also help in the cost estimation of PMTS and the expected return on investment duration. Just in terms of performance, PMTS saves fuel and thus cost, but the reduction in maintenance and training costs should also be quantified. A study into flying an F-35 with a constant negative flap deflection should be done. This configuration could have unintended consequences, or the control actuators for these flaps might not have been rated for these types of movements. This should be studied to ensure the safety of the aircraft.

This thesis also showed that PMTS is still capable of matching performance and AOA when the loaded configuration takes off at maximum takeoff weight. However, more research is needed as to where PMTS can no longer match performance. When adding new performance-matching metrics, this point might change depending on the phase of flight. For example, PMTS might be able to match during a climb but not during a descent for the same weight. These limits need to be determined, and if they affect training realism.

Additionally to the technical and cost aspects of PMTS, the effectiveness of PMTS itself should be studied. Research should be done to determine the increase in perceived effectiveness that PMTS could offer. Right now, it is assumed to offer a benefit, but testing with pilots should be done to determine if this conclusion holds in real life. This type of testing has already been done for Embedded Training and can also be done for PMTS.

References

[1] *Cover Image*. url: https://www.flickr.com/photos/lockheedmartin/8030769554/.

[2] Bryan Frederick et al. *Understanding the Deterrent Impact of U.S. Overseas Forces*. 2020. doi: 10.7249/rr2533. url: https://www.rand.org/pubs/research_reports/RR2533.html.

[3] Gosse Wedzinga. "E-CATS: First time demonstration of embedded training in a combat aircraft". In: *Aerospace Science and Technology* 10.1 (2006), pp. 73–84. issn: 1270-9638. doi: 10.1016/j.ast.2005.08.005. url: https://dx.doi.org/10.1016/j.ast.2005.08.005.

[4] J.J. Roessingh and G.G. Verhaag. *Training Effectiveness of Embedded Training in a (Multi-) Fighter Environment*. Tech. rep. Defense Technical Information Center, 2009, p. 9. url: https://apps.dtic.mil/sti/citations/ADA567736.

[5] B Brady et al. "The basics of on-board simulation and embedded training". In: *24th Aerospace Sciences Meeting*. Aerospace Sciences Meetings. American Institute of Aeronautics and Astronautics, Jan. 1986. doi: doi:10.2514/6.1986-493. url: https://doi.org/10.2514/6.1986-493.

[6] DCS. *DCS F-16 Cockpit Instruction Manual*. url: https://dcs-docs.lordvesel.win/en/f16/03.cockpit/.

[7] Conrad G. Bills et al. *F-35 Embedded Training*. 2009. url: https://apps.dtic.mil/sti/citations/ADA567738.

[8] Ministerie van Defensie. *Luchtmachtoefeningen*. url: https://www.defensie.nl/onderwerpen/vliegbewegingen/oefenen.

[9] Lockheed Martin. *F-35 Media Kit*. url: https://www.smugmug.com/gallery/n-5tnXV4/i-fVt8WgM.

[10] A E Sheridan and R Burnes. "F-35 program history – from JAST to IOC". In: *2018 Aviation Technology, Integration, and Operations Conference*. American Institute of Aeronautics and Astronautics Inc, AIAA, 2018. isbn: 9781624105562. doi: 10.2514/6.2018-3366.

[11] Lockheed Martin. *F-35 Lightning II - 5th Generation Capabilities*. url: https://www.lockheedmartin.com/en-us/products/f-35/f-35-capabilities.html.

[12] Lockheed Martin. *Everything You Need to Know about the F-35*. url: https://www.lockheedmartin.com/f35/news-and-features/everything-you-need-to-know-about-the-f-35c.html.

[13] Transcript of U.S. Congress Hearing. *Pentagon's F-35 Fighter Under Fire in Congress*. 2010.

[14] Lockheed Martin. *The Global F-35 Enterprise*. url: https://www.lockheedmartin.com/en-us/products/f-35/f-35-global-partnership.html.

[15] Jane's Information Group. *Janes*. 2022. url: https://www.janes.com/.

[16] Jamie Hunter. *The Truth About The Air Force's Biggest Changes To Pilot Training Since The Dawn Of The Jet Age*. url: https://www.thedrive.com/the-war-zone/41789/the-truth-about-the-air-forces-biggest-changes-to-pilot-training-since-the-dawn-of-the-jet-age.

[17] Guy Birchall. *RAF jets shoot down 53 drones in largest air-to-air missile mass firing exercise*. Oct. 2022. url: https://news.sky.com/story/raf-jets-shoot-down-53-drones-in-largest-air-to-air-missile-mass-firing-exercise-12726554.

[18] Eric Tegler. *A Drone With A Small Bizjet Engine Might Let The U.S. Air Force Simulate 5th Generation Fighters For Cheap*. May 2022. url: https://www.forbes.com/sites/erictegler/2022/03/30/a-drone-with-a-small-bizjet-engine-might-simulate-5th-generation-fighters-for-cheap/?sh=6069853c7f82.

[19] Herbert H. Bell and Wayne L. Waag. “Evaluating the effectiveness of flight simulators for training combat skills: A review”. In: *International Journal of Aviation Psychology* 8.3 (1998). issn: 10508414. doi: 10.1207/s15327108ijap0803{_}4. url: https://apps.dtic.mil/dtic/tr/fulltext/u2/a484153.pdf.

[20] JW Jacobs et al. “A meta-analysis of the flight simulator training research”. In: *Naval training systems center: human factors division* (1990). url: https://apps.dtic.mil/sti/pdfs/ADA228733.pdf.

[21] Hyunsik Joe et al. “Air-to-air and air-to-ground engagement modeling for the KAI Embedded Training System”. In: *AIAA Modeling and Simulation Technologies Conference and Exhibit*. 2008. isbn: 9781563479458. doi: 10.2514/6.2008-6859.

[22] M.F.R. Keuning. *Embedded Training and LVC*. Tech. rep. National Aerospace Laboratory NLR, 2011, p. 15. url: https://reports.nlr.nl/xmlui/bitstream/handle/10921/185/TP-2010-469.pdf?sequence=1&isAllowed=y.

[23] Conrad G. Bills et al. *F-35 Embedded Training*. Tech. rep. Lockheed Martin Corporation, 2009, p. 11.

[24] Steven P. Wurth and Mark S. Smith. “F-35 propulsion system integration, development, and verification”. In: *2018 Aviation Technology, Integration, and Operations Conference*. 2018. doi: 10.2514/6.2018-3517.

[25] Dario Leone. *F135 Engine Issues force USAF F-35 Demo Team to cut the number of 2021 shows by eight performances*. Feb. 2021. url: https://theaviationgeekclub.com/f-135-engine-issues-force-usaf-f-35-demo-team-to-cut-the-number-of-2021-shows-by-eight-performances/.

[26] Valerie Insinna. *An engine shortage is the newest problem to hit the F-35 enterprise*. Feb. 2021. url: https://www.defensenews.com/air/2021/02/12/an-engine-shortage-is-the-newest-problem-to-hit-the-f-35-enterprise/.

[27] Pratt & Whitney. *F135 Engine Core Upgrade*. url: https://www.prattwhitney.com/en/products/military-engines/f135/engine-core-upgrade.

[28] F.E. Wu. *Aero engine life evaluated for combined creep and fatigue, and extended by trading-off excess thrust*. Tech. rep. Cranfiel University, Jan. 1994. url: http://dspace.lib.cranfield.ac.uk/handle/1826/10517.

[29] Patrick Chiles. “AeroSAfetyworld”. In: *Flight Safety Foundation* (2011), pp. 11–13. url: https://flightsafety.org/asw/mar11/asw_mar11_p11-13.pdf.

[30] Earl Dowell et al. “Transonic Nonlinear Aeroelasticity”. In: *Encyclopedia of Aerospace Engineering* (2010). doi: 10.1002/9780470686652.eae151. url: http://10.0.3.234/9780470686652.eae151%20https://dx.doi.org/10.1002/9780470686652.eae151.

[31] Ilie Nicolin and Bogdan Adrian Nicolin. “The fly-by-wire system”. In: *INCAS BULLETIN* 11.4 (2019), pp. 217–222. issn: 2247-4528. doi: 10.13111/2066-8201.2019.11.4.19. url: http://10.0.51.55/2066-8201.2019.11.4.19%20https://dx.doi.org/10.13111/2066-8201.2019.11.4.19.

[32] Stuart Bennett. “A Brief History of Automatic Control”. In: *IEEE Control Systems* 16.3 (1996), pp. 17–25. issn: 1066033X. doi: 10.1109/37.506394. url: https://web.archive.org/web/20160809050823/http://ieeecss.org/CSM/library/1996/june1996/02-HistoryofAutoCtrl.pdf.

[33] S.H. Lane and R.F. Stengel. “Flight control design using non-linear inverse dynamics”. In: *Automatica* 24.4 (1988), pp. 471–483. doi: 10.1016/0005-1098(88)90092-1.

[34] Skander Taamallah. *The use of Nonlinear Dynamic Inversion (NDI) within Flight Control Systems*. Tech. rep. National Aerospace Center (NLR), 0, p. 9.

[35] Gertjan Looye. “Design of robust autopilot control laws with nonlinear dynamic inversion”. In: *At-Automatisierungstechnik* 49.12 (2001). issn: 01782312. doi: 10.1524/auto.2001.49.12.523.

[36] J.J. Harris and J.R. Stanford. “F-35 flight control law design, development and verification”. In: *2018 Aviation Technology, Integration, and Operations Conference*. 2018. isbn: 9781624105562. doi: 10.2514/6.2018-3516.

[37] Ken Bordignon and John Bessolo. “Control allocation for the X-35B”. In: *2002 Biennial International Powered Lift Conference and Exhibit*. 2002. isbn: 9781624101090. doi: 10.2514/6.2002-6020.

[38] S. Antony Snell, Dale F. Enns, and William L. Garrard. “Nonlinear inversion flight control for a supermaneuverable aircraft”. In: *Journal of Guidance, Control, and Dynamics* 15.4 (1992), pp. 976–984. issn: 07315090. doi: 10.2514/3.20932.

[39] Daniel G. Canin, Jeffrey K. McConnell, and Paul W. James. “F-35 high angle of attack flight control development and flight test results”. In: *AIAA Aviation 2019 Forum*. 2019. doi: 10.2514/6.2019-3227. url: https://arc-aiaa-org.tudelft.idm.oclc.org/doi/pdf/10.2514/6.2019-3227.

[40] Fabian Grondman et al. “Design and Flight Testing of Incremental Nonlinear Dynamic Inversion-based Control Laws for a Passenger Aircraft”. In: *2018 AIAA Guidance, Navigation, and Control Conference*. Reston, Virginia: American Institute of Aeronautics and Astronautics, Jan. 2018. isbn: 978-1-62410-526-5. doi: 10.2514/6.2018-0385. url: http://10.0.9.210/6.2018-0385%20https://dx.doi.org/10.2514/6.2018-0385%20https://arc.aiaa.org/doi/10.2514/6.2018-0385.

[41] Charles Justiz and Suresh Patel. “NASA Shuttle Training Aircraft flight simulation overview”. In: *Flight Simualtion Technologies Conference*. Guidance, Navigation, and Control and Co-located Conferences. American Institute of Aeronautics and Astronautics, Sept. 1988, pp. 182–190. doi: doi:10.2514/6.1988-4608. url: https://doi.org/10.2514/6.1988-4608.

[42] D Rohlf, D Schafranek, and K Wilhelm. “Recent results with ATTAS in-flight simulator”. In: *Flight Simualtion Technologies Conference*. Guidance, Navigation, and Control and Co-located Conferences. American Institute of Aeronautics and Astronautics, Sept. 1988. doi: doi:10.2514/6.1988-4606. url: https://doi.org/10.2514/6.1988-4606.

[43] Joe Stout. *Vista F-16*. url: https://web.archive.org/web/20091020104940/http://www.codeonemagazine.com/archives/1991/articles/jan_91/jan2a_91.html.

[44] Falcon 4, Mav-JP, and Raptor One. “High Fidelity Flight Models”. In: (2004). url: https://www.scribd.com/document/99184372/HFFM-Manual.

[45] T. S. Webb, D. R. Kent, and J. B. Webb. “Correlation of F-16 aerodynamics and performance predictions with early flight test results”. In: *AGARD Conf Proc* 242 (1977).

[46] David A Shlapak et al. *A Global Access Strategy for the US Air Force*. Tech. rep. RAND CORP SANTA MONICA CA, 2002.

[47] John Pike. *Globalsecurity.org Weapon Data*. url: https://www.globalsecurity.org/military/systems/munitions/smart.htm.

[48] L3 Harris. *L3Harris Release Systems Product Catalog*. L3 Harris, 2019.

[49] Cobham Mission Systems. *BRU-61/A Small Diameter Bomb Carriage System*. Tech. rep. 2009. url: www.cobham.com/missionsystems.

[50] *F-16 and F-35 Illustrations*. url: https://www.pinterest.com%20https://upload.wikimedia.org/wikipedia/commons/d/d3/F-35A_three-view.PNG.

[51] Jane’s Information Group. *Jane’s Aero-Engines*. 2022. url: https://janes.ihs.com/AeroEngines/Reference.

[52] John D. Anderson Jr. *Introduction to Flight - International Edition*. 7th ed. McGraw-Hill Higher Education, 2012.

[53] Ray Whitford. *Design for Air Combat*. 1st ed. Janes Information Group, 1987, p. 224. isbn: 978-0710604262.

[54] Egbert Torenbeek. *Advanced Aircraft Design: Conceptual Design, Analysis and Optimization of Subsonic Civil Airplanes*. Wiley, 2013, pp. 1–410. isbn: 9781118568118. doi: 10.1002/9781118568101.

[55] Lockheed Martin. *F-35A CTOL Variant*. 2011. url: https://web.archive.org/web/20110317113904/http://www.lockheedmartin.com/products/f35/f-35A-ctol-variant.html.

[56] Peter Sucio. *This Is What An F-35 In 'Beast Mode' Looks Like*. June 2021. url: https://www.19fortyfive.com/2021/06/this-is-what-an-f-35-in-beast-mode-looks-like/.

[57] Lockheed Martin. *F-35 Weaponry*. url: https://web.archive.org/web/20190418155950/https://f35.com/about/carrytheload/weaponry.

[58] J.N. Hefner and D.M. Bushnell. "An overview of concepts for aircraft drag reductions". In: *Document ID 19770025148*. 1977.

[59] John Robert Wilson. *The Doghouse Plot: History, Construction Techniques, and Application*. Tech. rep. ARIZONA STATE UNIVERSITY, Dec. 2017.

[60] Mirabel Cerqueira Rezende et al. "Radar Cross Section Measurements (8-12 GHz) of Magnetic and Dielectric Microwave Absorbing Thin Sheets". In: *Revista de Física Aplicada e Instrumentação* (2002). url: http://www.sbfisica.org.br/rfai/Vol15/Num1/v15_24.pdf.

[61] Pratt & Whitney. *F135 Specs Charts*. url: https://web.archive.org/web/20150924005241/http://www.f135engine.com/docs/B-2-4_F135_SpecsChart.pdf.

[62] *Pratt & Whitney F135-PW-100 Augmented Turbofan*. url: https://web.archive.org/web/20080516195621/http://www.turbokart.com/about_f135.htm.

[63] Jan Roskam. *Airplane Design Part VI: Preliminary Calculation of Aerodynamic, Thrust and Power Characteristics*. DARcorporation, 2017. isbn: 1884885527.

[64] Sea Power. *Lockheed Develops Rack to Make F-35A/C a Six-Shooter*. 2019. url: https://seapowermagazine.org/lockheed-develops-rack-to-make-f-35a-c-a-six-shooter/.

[65] USAF. *Joint Direct Attack Munition GBU- 31/32/38*. 2003. url: https://www.af.mil/About-Us/Fact-Sheets/Display/Article/104572/joint-direct-attack-munition-gbu-313238/.

A

Aircraft Model Data

A.1. Drag Polars

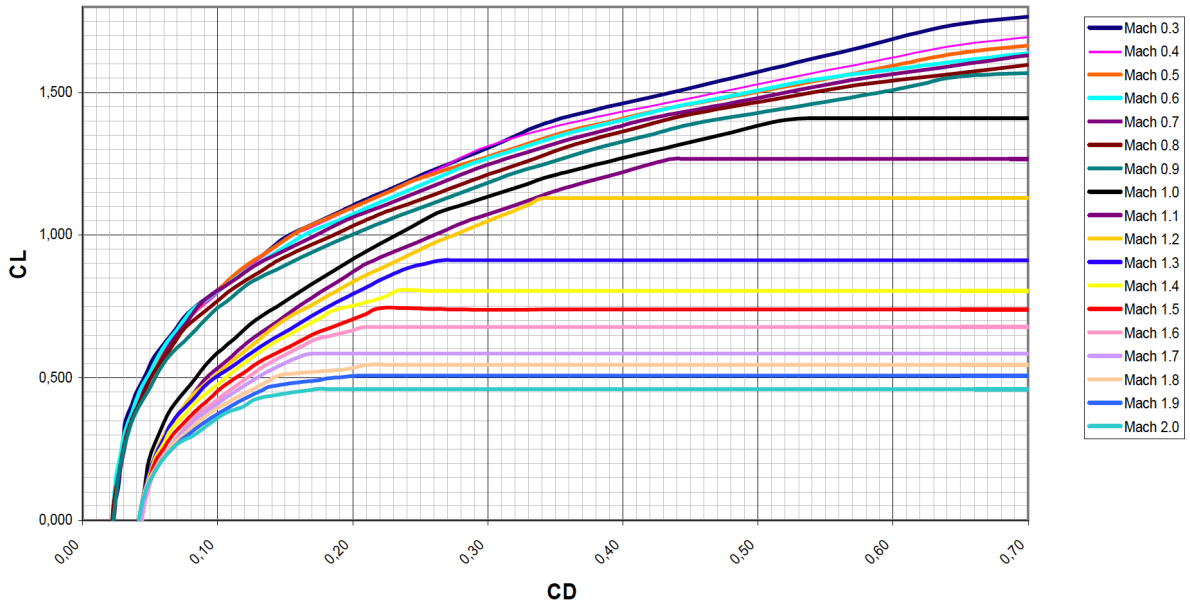

Figure A.1: F-16 Drag polar [44]

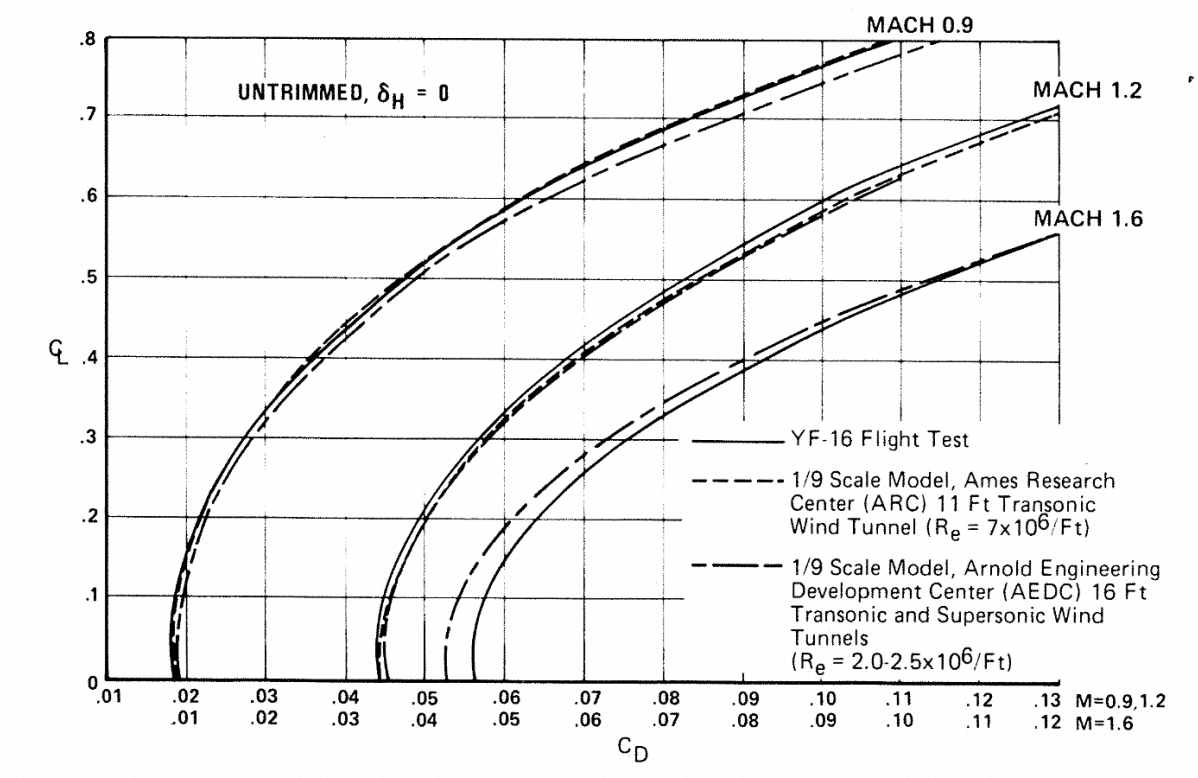

Figure A.2: YF-16 Drag Polar [45]

A.2. Drag Polar Variables

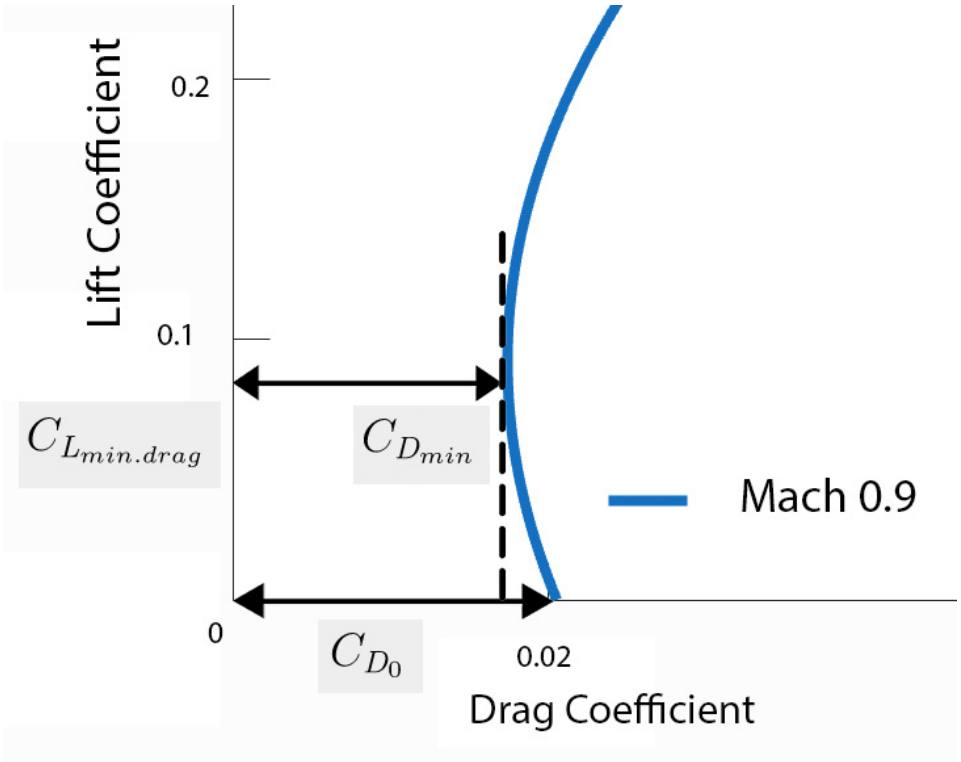

Figure A.3: Drag polar Variables

A.3. Drag Polar Variables for Thesis Model

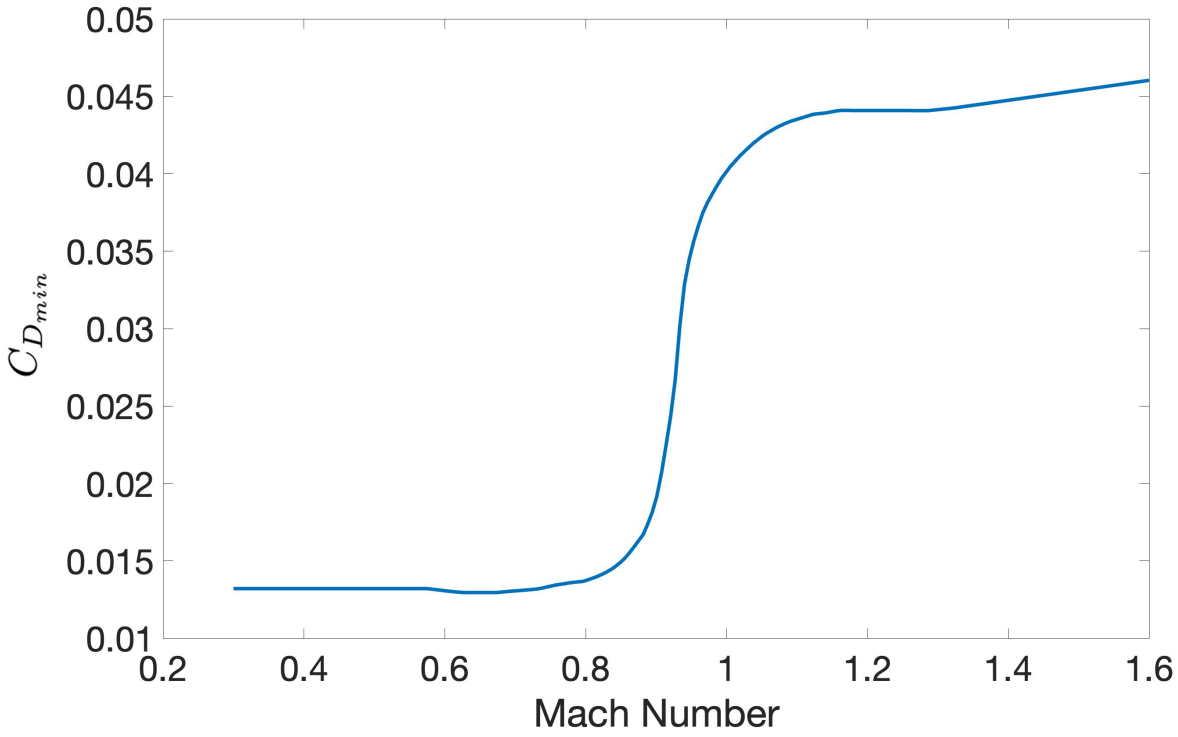

Figure A.4: $C_{D_{\text{min}}}$ Distribution

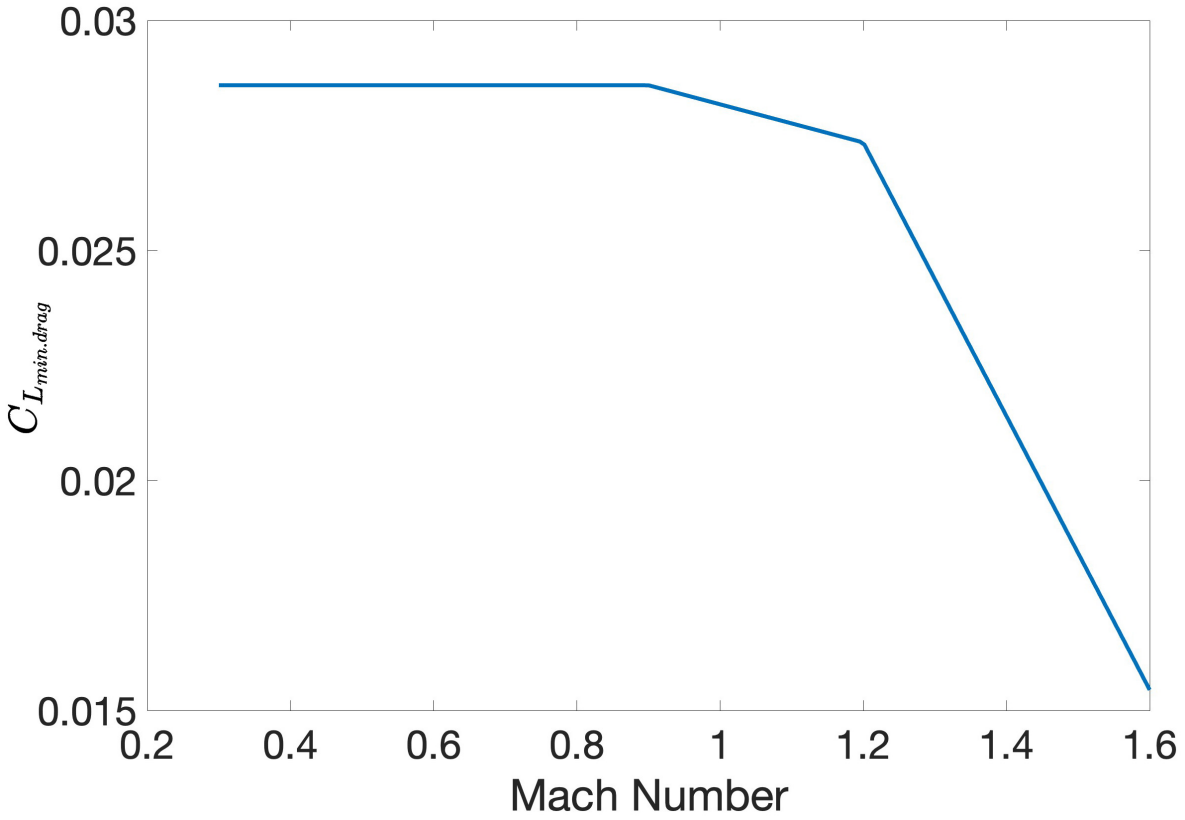

Figure A.5: $C_{L_{\text{min.drag}}}$ Distribution

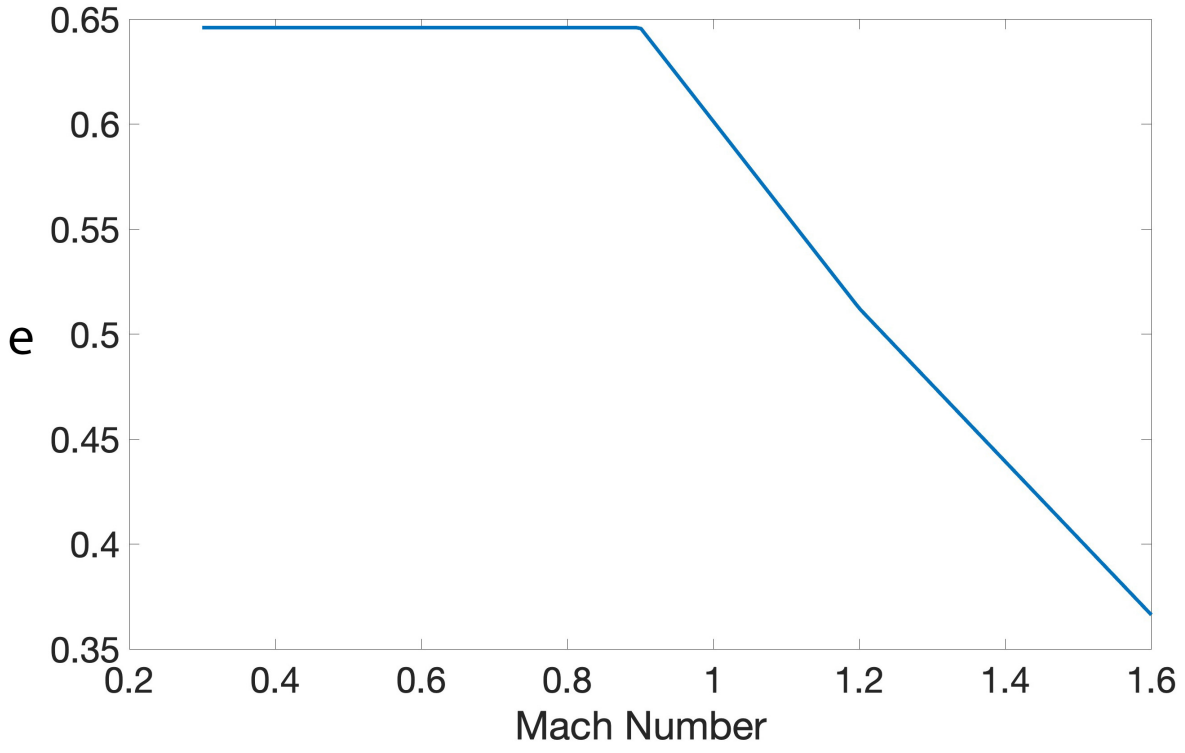

Figure A.6: e Distribution

A.4. Drag Polar Comparison of F-35 and F-16 Thesis Model

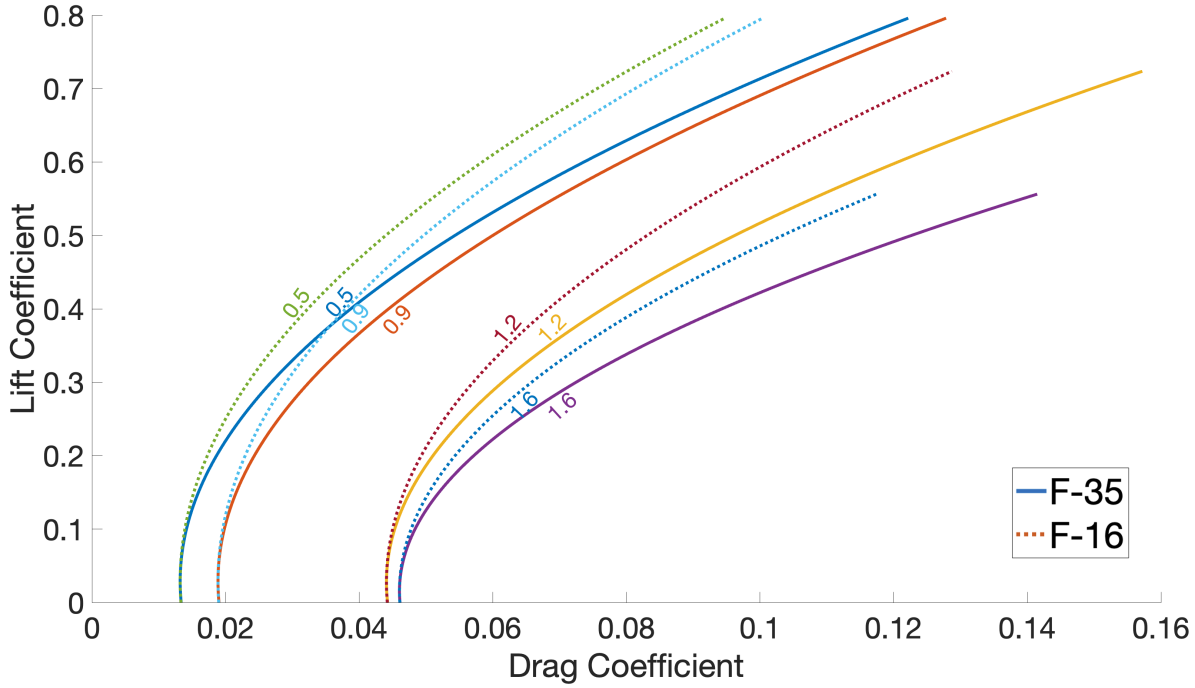

Figure A.7: Drag Polar Comparison for thesis F-16 model and F-35 after

A.5. F-16 Thrust Data: F110-GE-129

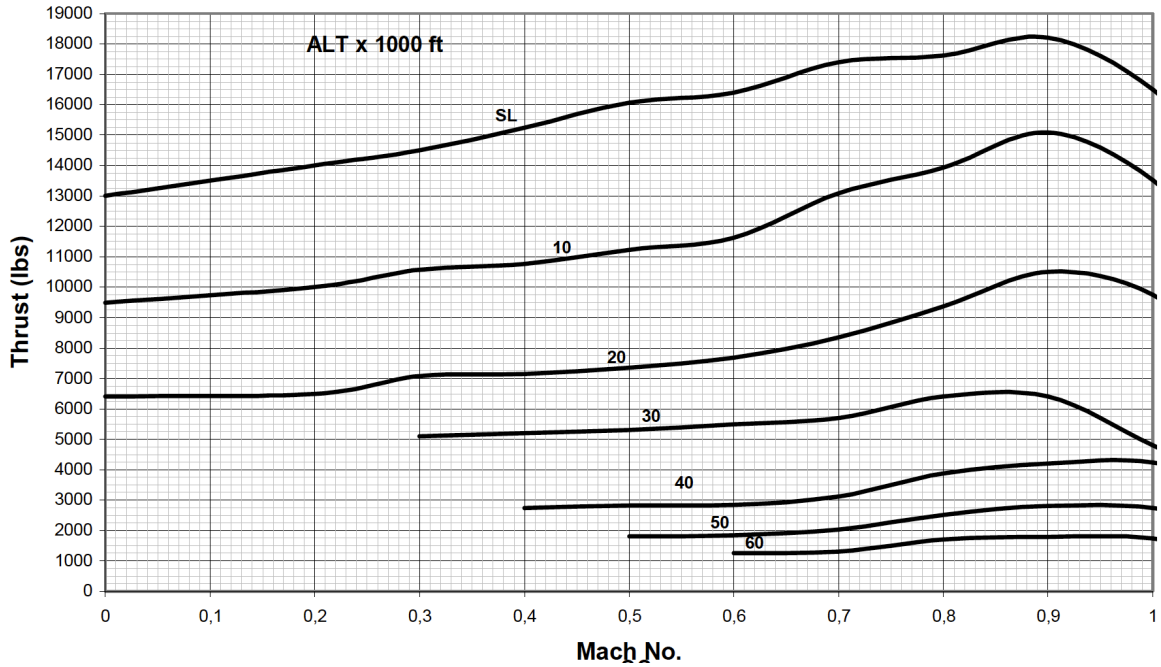

Figure A.8: Thrust plot for F110-GE-129 - Military Thrust [44]

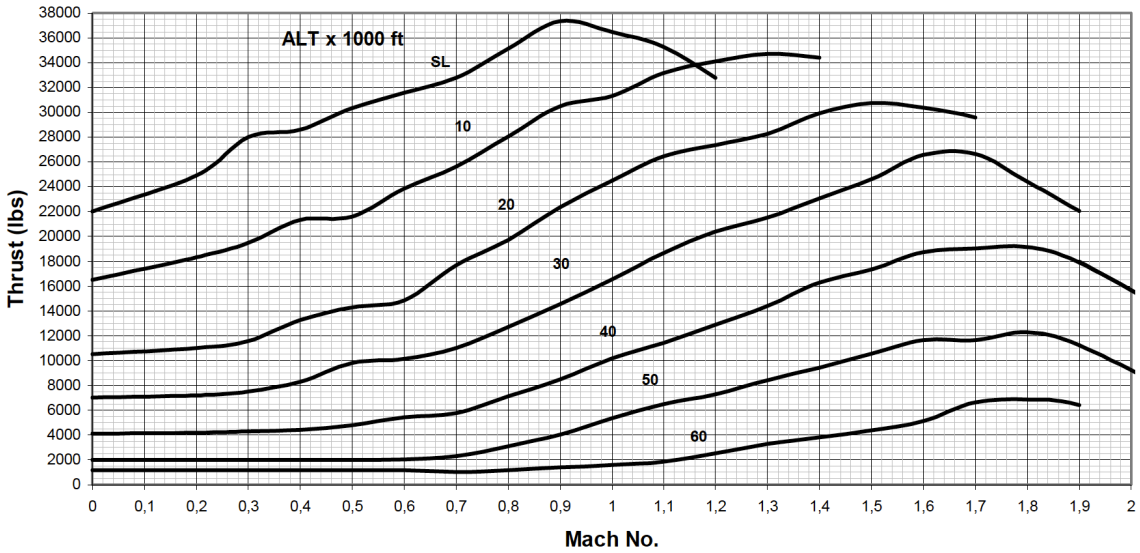

Figure A.9: Thrust plot for F110-GE-129 - Afterburner Thrust [44]

A.6. F-35 Thrust Model (scaled): F135

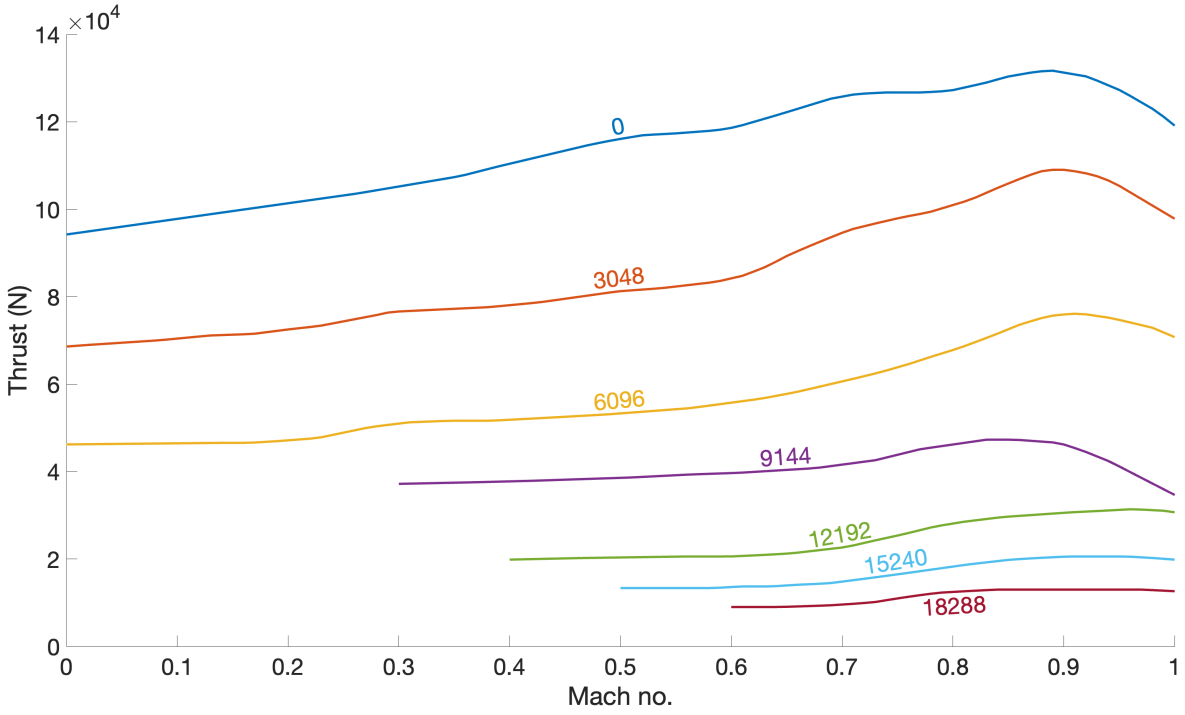

Figure A.10: F-35 Thrust Plot - Military Power

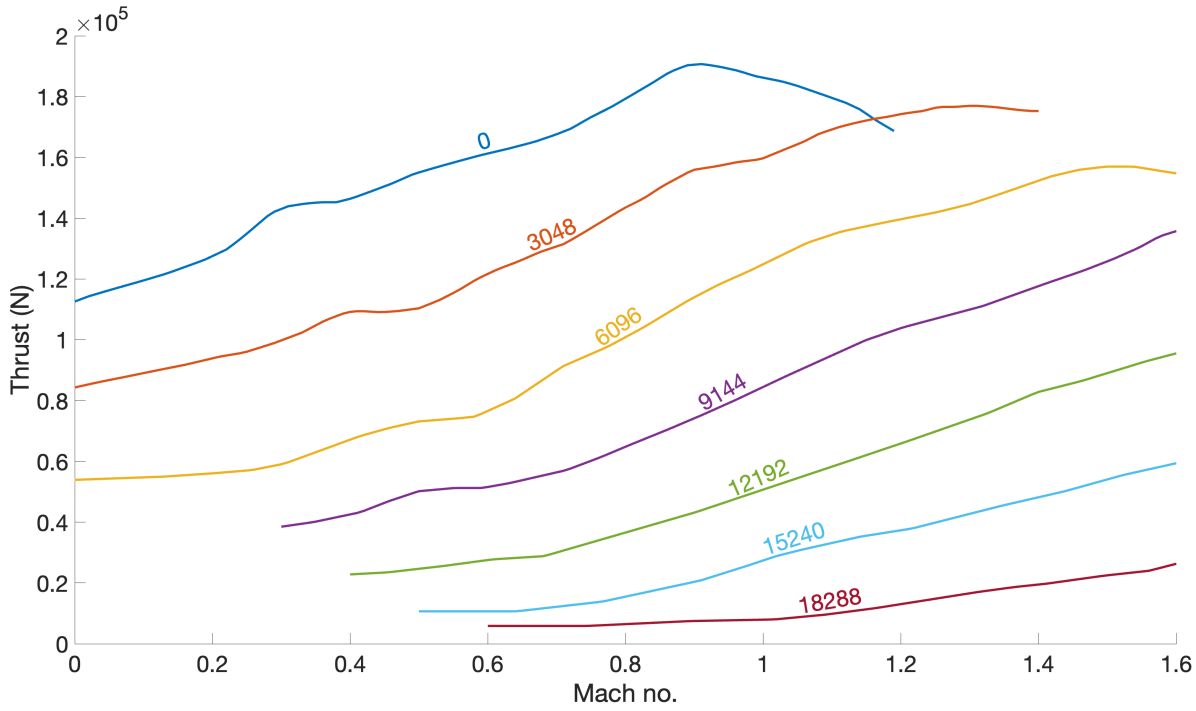

Figure A.11: F-35 Thrust Plot - Afterburner

A.7. Lift Curves YF-16

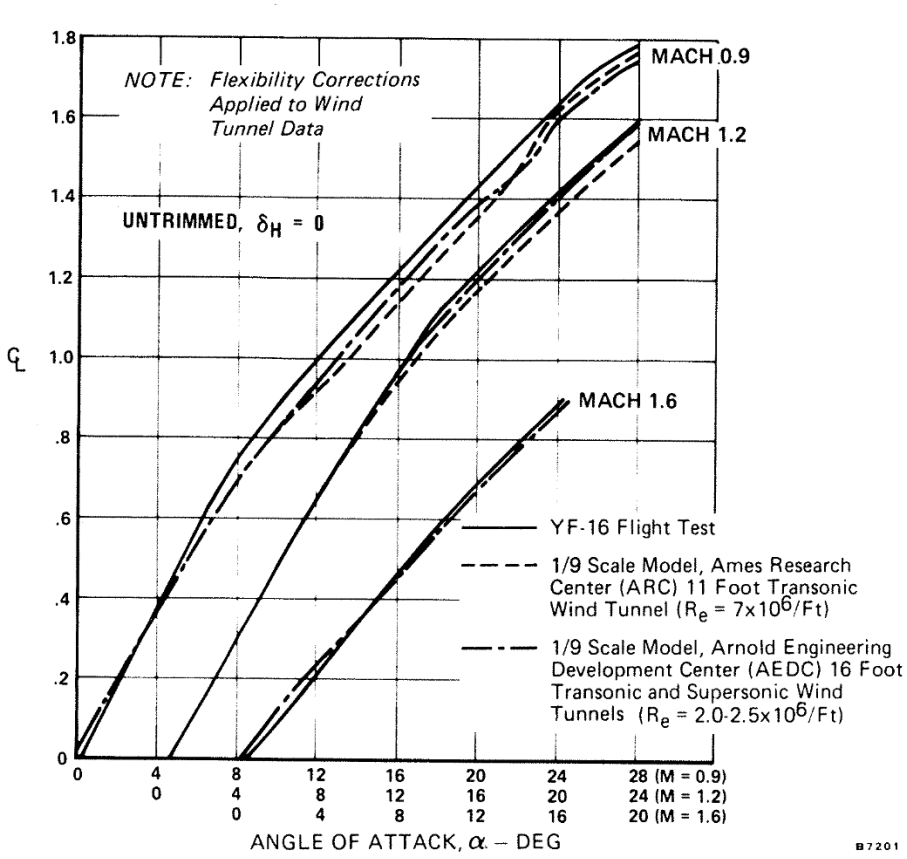

Figure A.12: Comparison of Flight Test With Wind Tunnel Lift Curves for YF-16 [45]

A.8. Angle of Attack - Linear model capped at Maximum Lift Coefficient

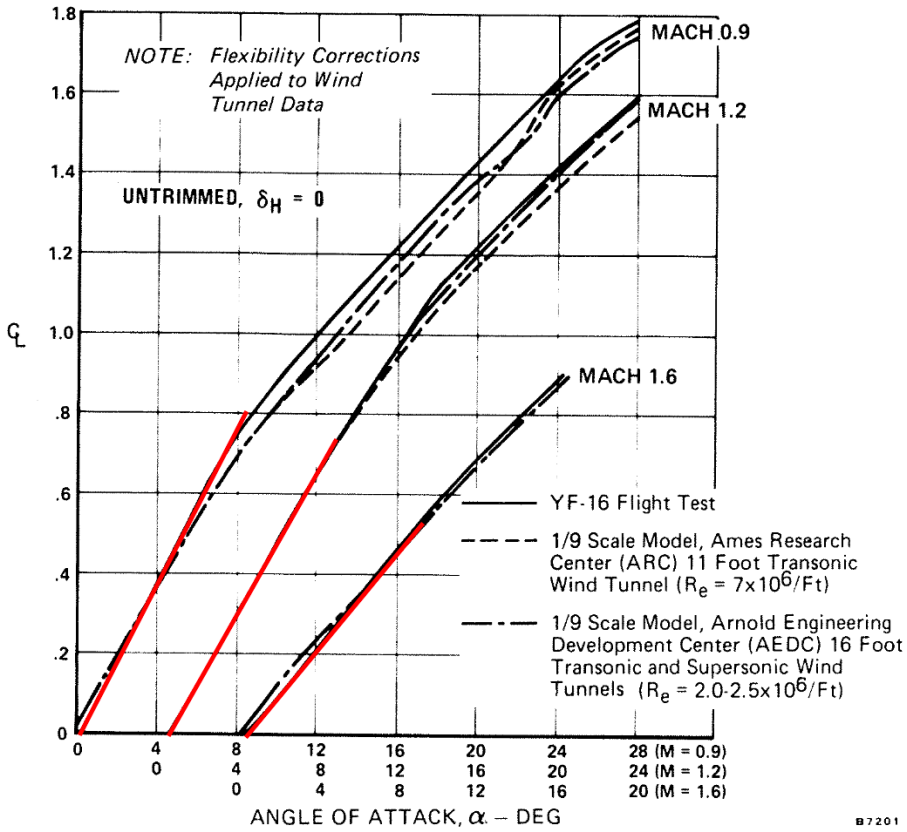

Figure A.13: Linear approximation of YF-16 data, capped at maximum value for Lift Coefficient at that Mach number [45]

Table A.1: Variables used to scale Lift Curve between F-16 and F-35

Variable/Mach number	0.9	1.2	1.6
F-16 a_{flap}	0.10	0.09	0.06
F-16 a_0	0.52	1.2	0.50
F-35 a_{flap}	0.08	0.07	0.05
$\alpha_{L=0}$	0.4	0.66	0.53

A.9. Trailing Edge Flap Geometry F-35

Figure A.14: Trailing Edge Flap Layout F-35

A.10. Doghouse Plots with thesis model overlay

Turn Performance - 10000 Feet

DATA BASIS: ESTIMATED

AIRCRAFT: F-16C Block 50
ENGINE: F110-GE-129

CONDITIONS:
- **STANDARD DAY**
- **MAX AB**

CONFIGURATION:
- **DRAG INDEX = 38**
- **GW = 28670 POUNDS**

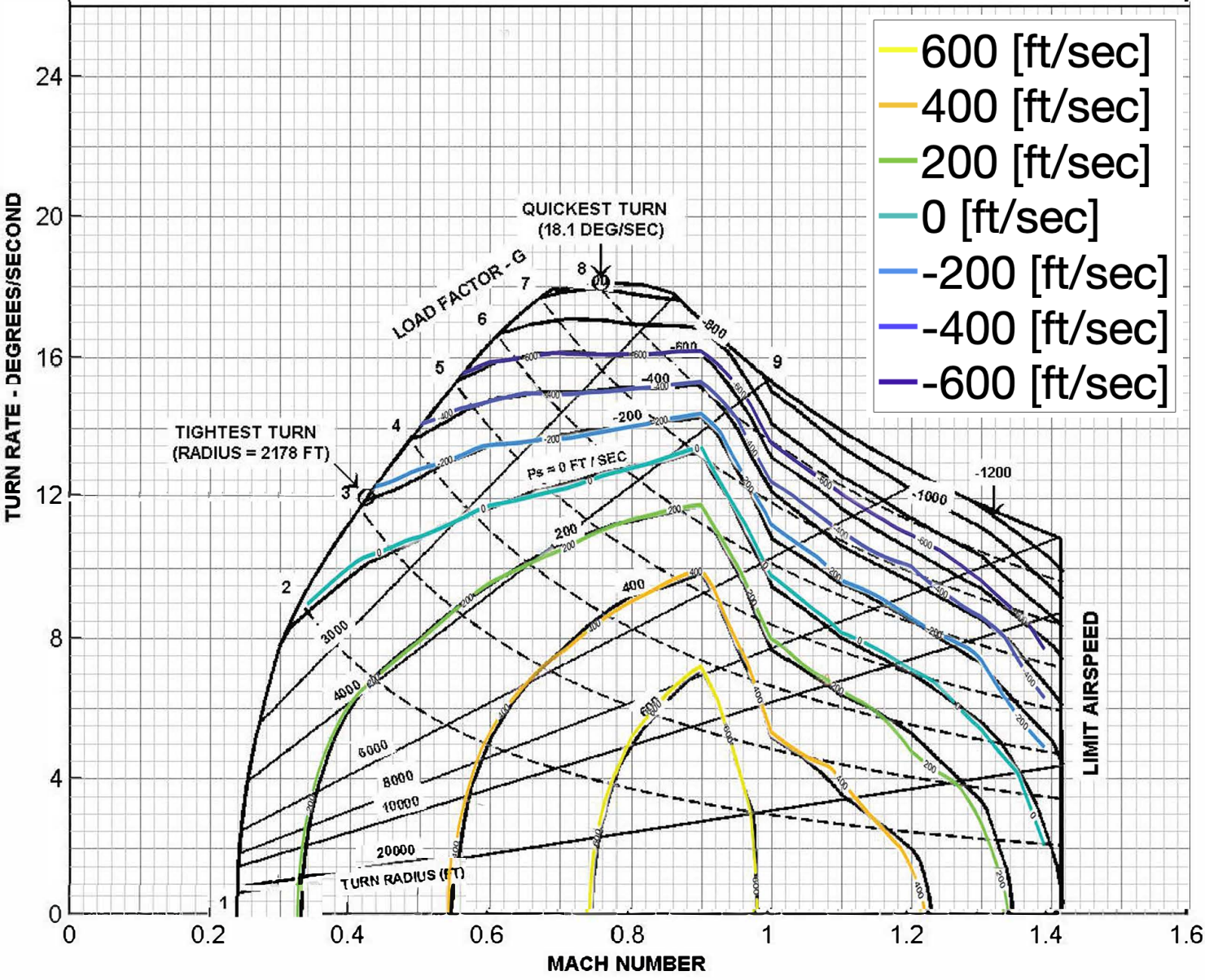

Turn Performance - 20000 Feet

DATA BASIS: ESTIMATED

AIRCRAFT: F-16C Block 50
ENGINE: F110-GE-129

CONDITIONS:
- **STANDARD DAY**
- **MAX AB**

CONFIGURATION:
- **DRAG INDEX = 38**
- **GW = 28670 POUNDS**

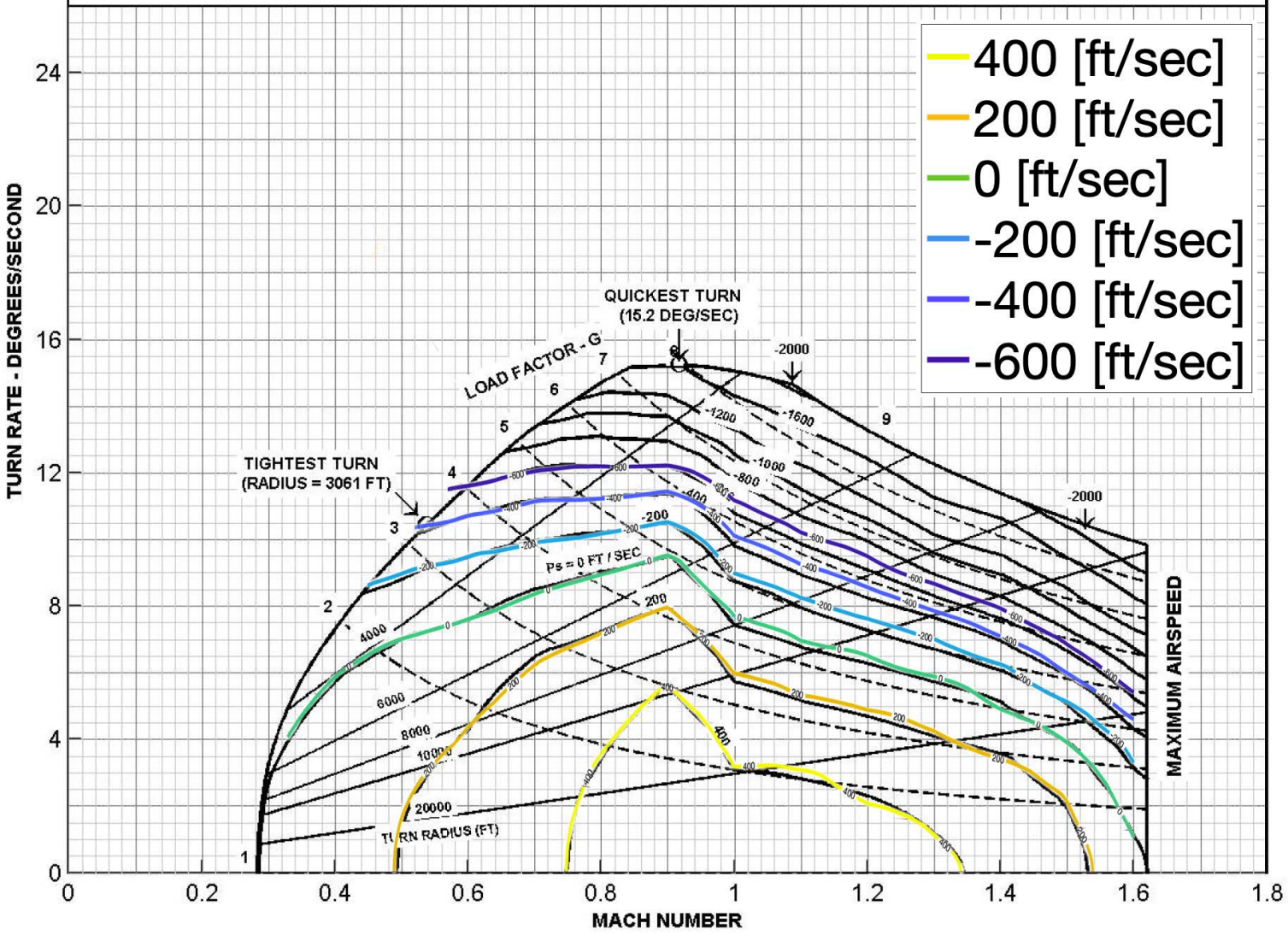

Turn Performance - 30000 Feet

DATA BASIS: ESTIMATED

AIRCRAFT: F-16C Block 50
ENGINE: F110-GE-129

CONDITIONS:
- **STANDARD DAY**
- **MAX AB**

CONFIGURATION:
- **DRAG INDEX = 38**
- **GW = 28670 POUNDS**

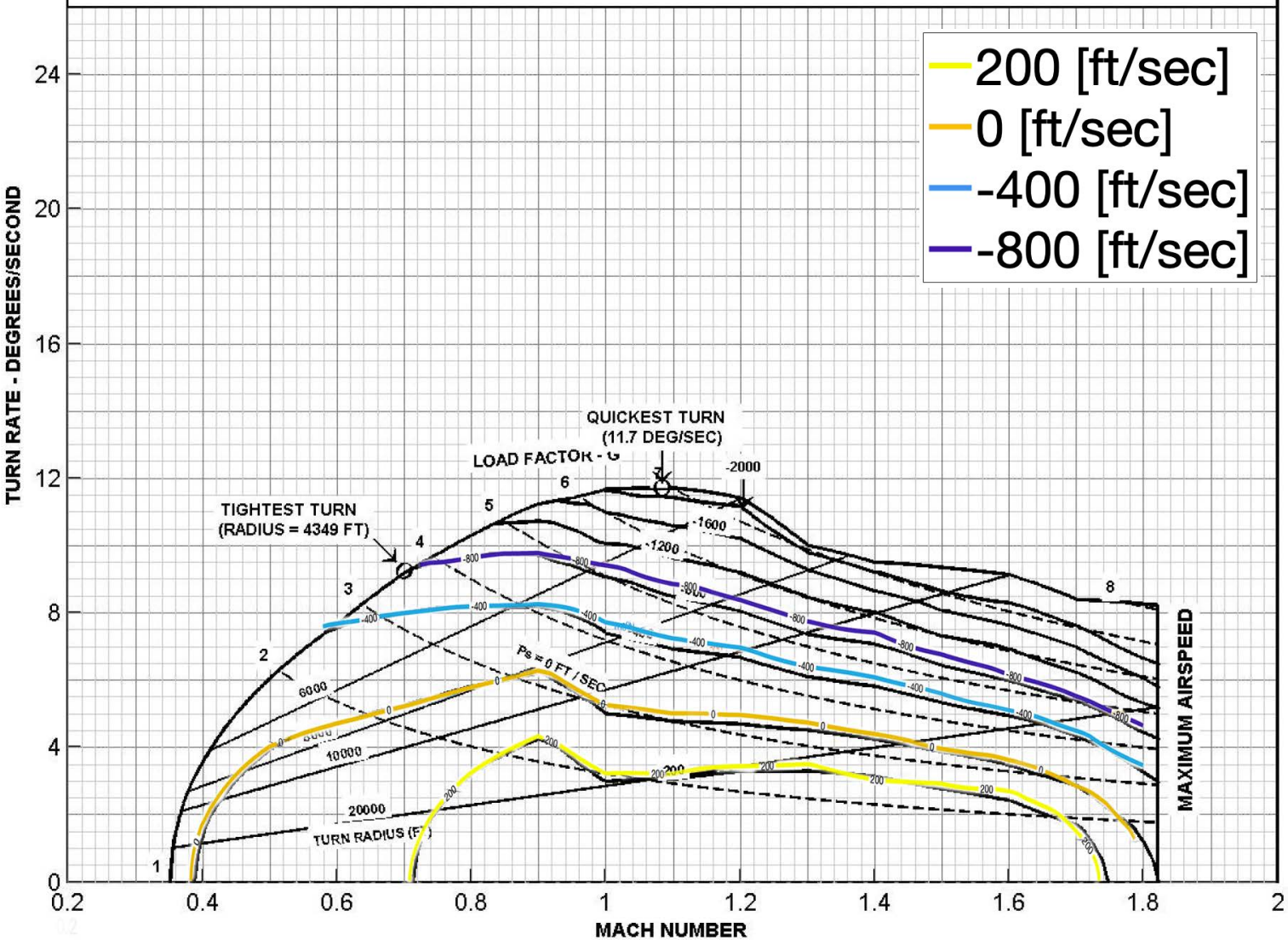

B

Store and Adapter Data

B.1. Internal Stores and Adapters

Table B.1: Data regarding internal stores [46, 47, 48, 49]

Name	Type	W_{Store} [kg]	$W_{Adapter}$ [kg]	DI_{Store}	$DI_{Adapter}$
GBU-12	A/G	277	39	0	0
GBU-31	A/G	924	39	0	0
GBU-39	A/G	129	39	0	0
GBU-49	A/G	227	39	0	0
AIM-120	A/A	155	29	0	0
BRU-61	Carriage System	0	150	0	0

B.2. Conversion Factors Drag Index From Other Aircraft

Table B.2: Conversion factors for Drag Index [15]

Conversion Aircraft	S_{Ref} [m^2]	Conversion Factor DI to F-35
F-16	28	0.65
F-15	56.5	1.31

B.3. External Stores and Adapters

Table B.3: Data regarding external stores, all weights are in kg, all DI are w.r.t. the F-35A [46, 48, 47]

Name	Type	W_{Store}	$W_{Adapter}$	DI_{Store}	$DI_{Adapter}$	Conversion Aircraft
AIM-120	A/A	155	39	2.23	3.58	F-15
GBU-24	A/G	1066	39	13	3.58	F-16
GBU-49	A/G	227	39	4.55	3.58	F-16

C

Configuration Data

C.1. Clean

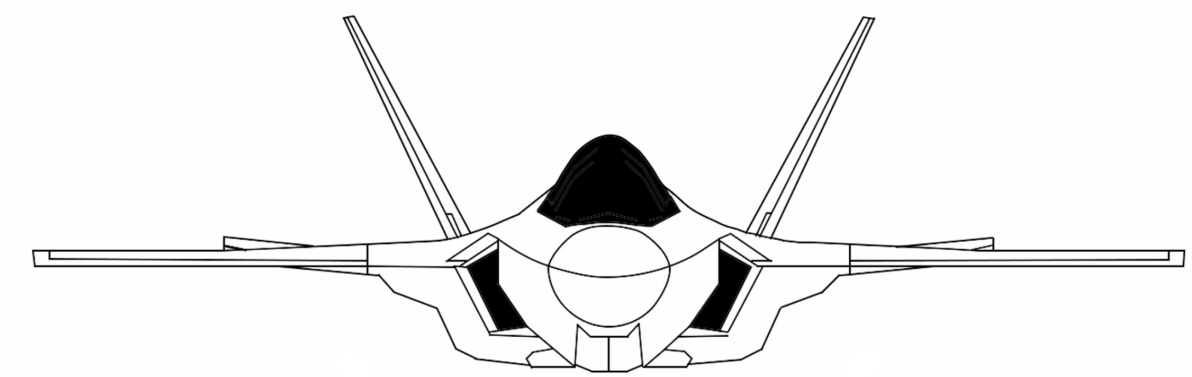

Figure C.1: Clean Configuration

Table C.1: Clean Aircraft data

Name	Weight [kg]	Weight Adapter [kg]	DI	DI Adapter
F-35A Clean	13290			
F-35A Fuel	8278			
Total	21568	0	0	0

C.2. Air to Air

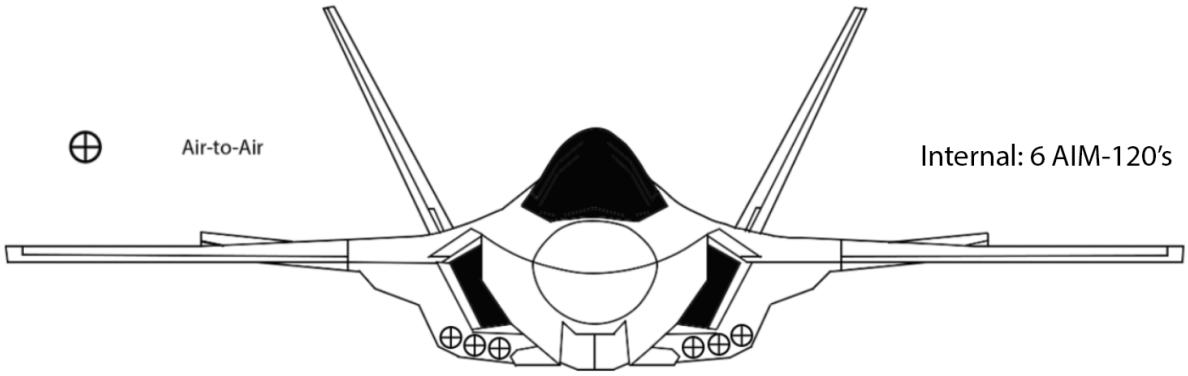

Figure C.2: Mission 1: Air-to-Air Combat Configuration

Table C.2: Mission 1: Aircraft and Stores data

Name	Amount	Weight [kg]	Weight Adapter [kg]	DI	DI Adapter	Location
F-35A Clean	1	13290				
F-35A Fuel	1	8278				
AIM-120	6	930	174	0	0	Internal
Total		22498	174	0	0	

C.3. Close Air Support

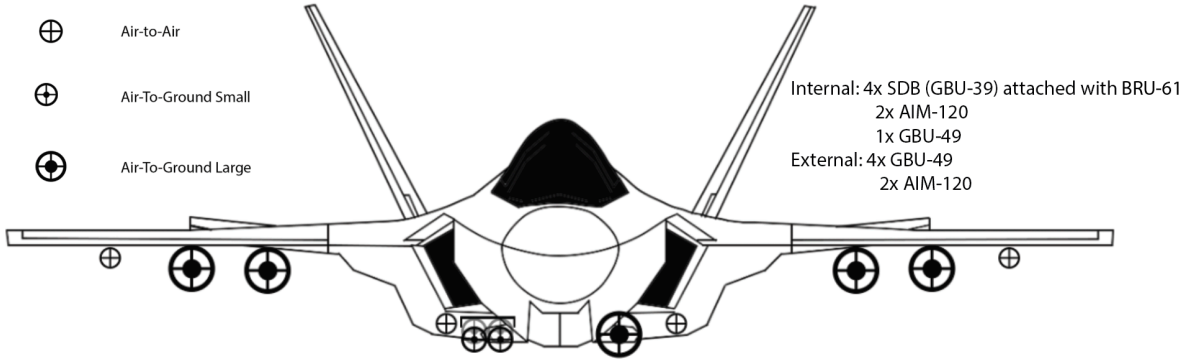

Figure C.3: Mission 2: CAS Combat Configuration

Table C.3: Mission 2: Aircraft and Stores data

Name	Amount	Weight [kg]	Weight Adapter [kg]	DI	DI Adapter	Location
F-35A Clean	1	13290				
F-35A Fuel	1	8278				
AIM-120	2	310	58	0	0	Internal
GBU-39	4	516	0	0	0	Internal
BRU-61	1	0	150	0	0	Internal
GBU-49	1	227	39	0	0	Internal
GBU-49	4	908	156	18.2	14.32	External
AIM-120	2	310	78	4.46	7.16	External
Total		23839	481	22.66	21.48	

C.4. Red Flag

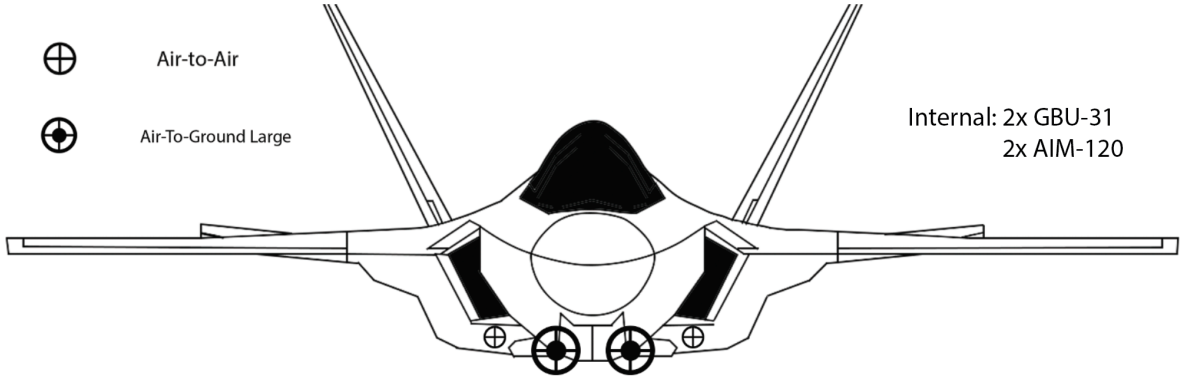

Figure C.4: Mission 3: Red Flag Configuration

Table C.4: Mission 3: Aircraft and Stores data

Name	Amount	Weight [kg]	Weight Adapter [kg]	DI	DI Adapter	Location
F-35A Clean	1	13290				
F-35a Fuel	1	8278				
AIM-120	2	310	58	0	0	Internal
GBU-31	2	1848	78	0	0	Internal
Total		23726	136	0	0	

D

PMTS Test Data

D.1. PMTS Test 1: Level Acceleration

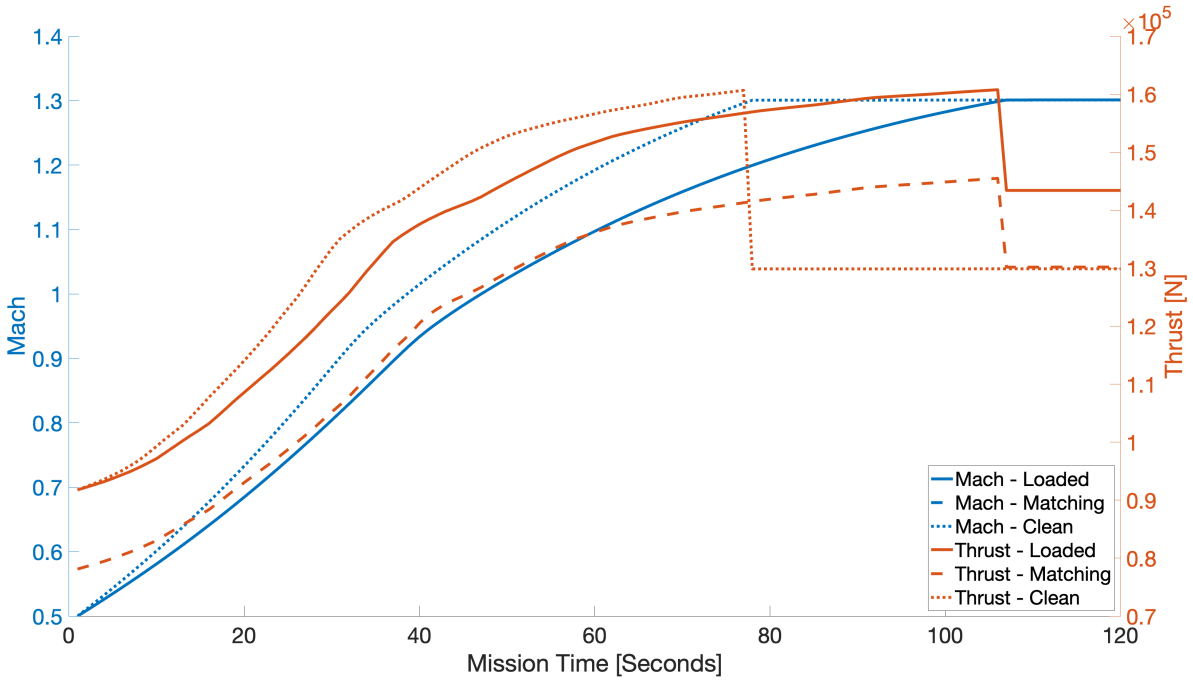

Figure D.1: PMTS Test 1 - Mach and Thrust setting

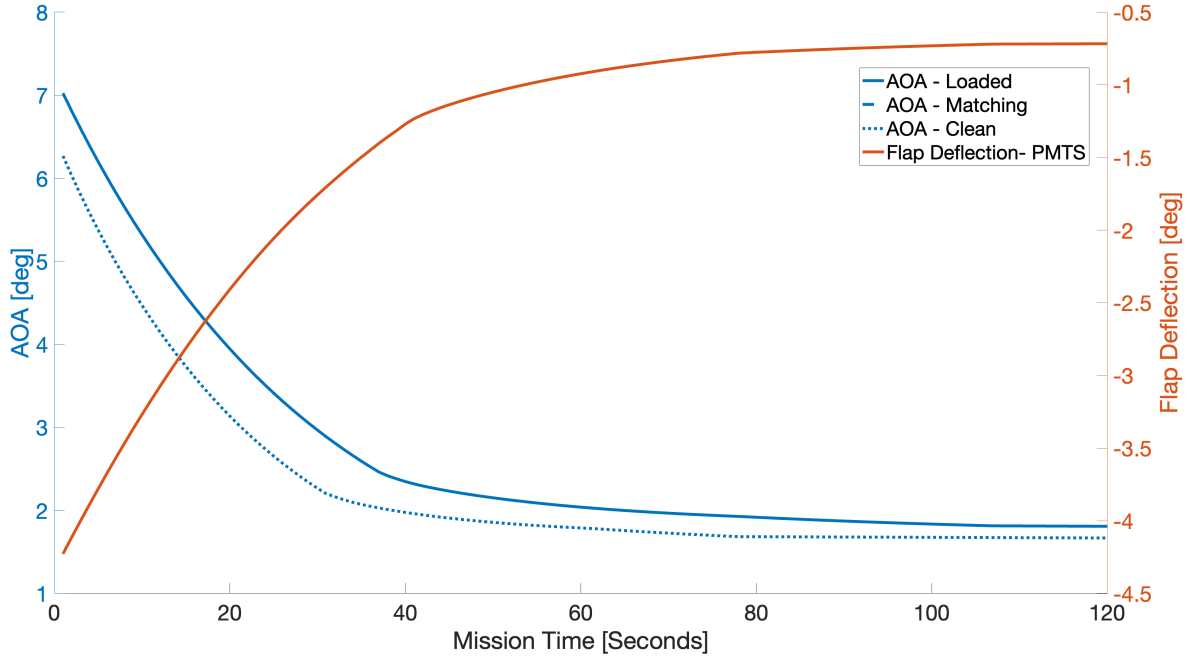

Figure D.2: PMTS Test 1 - Angle of Attack and flap deflection

D.2. PMTS Test 2: Climb and Accelerate

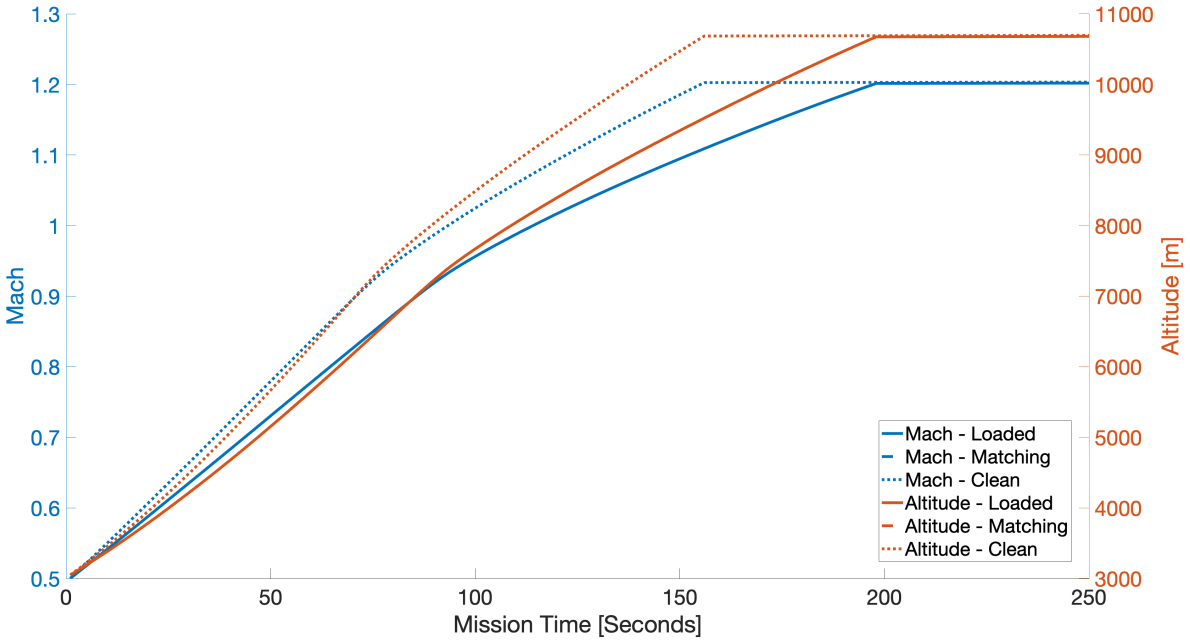

Figure D.3: PMTS Test 2 - Mach and Altitude

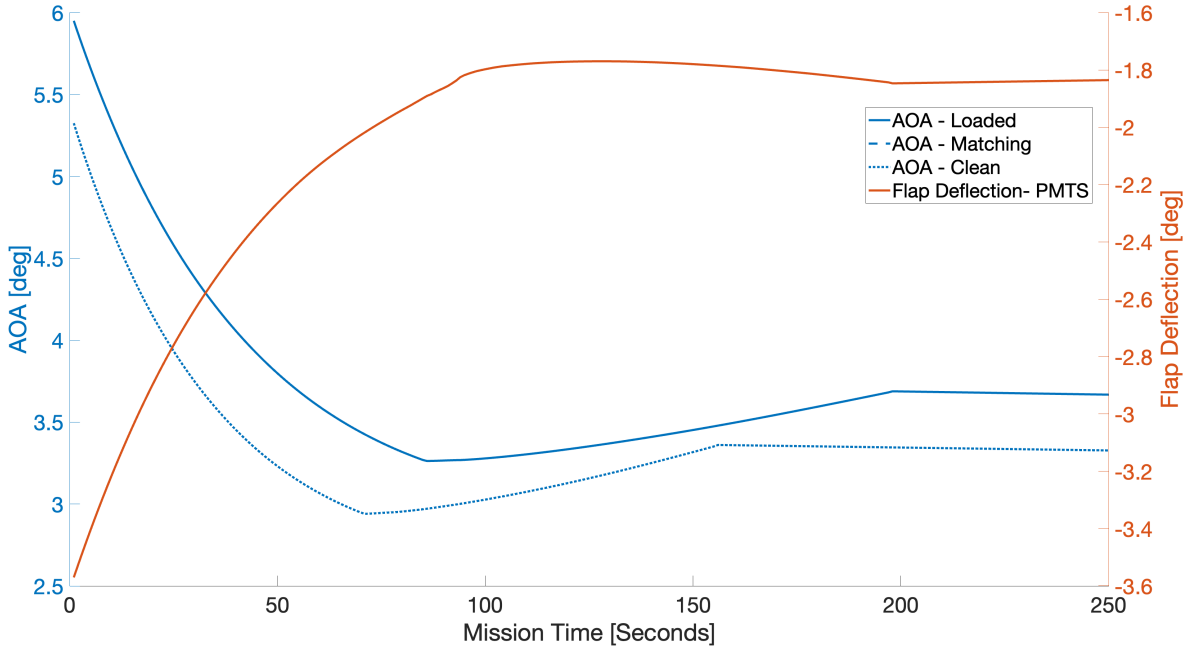

Figure D.4: PMTS Test 2 - Angle of Attack and flap deflection

D.3. PMTS Test 3: Maximum Sustained Turn Rate

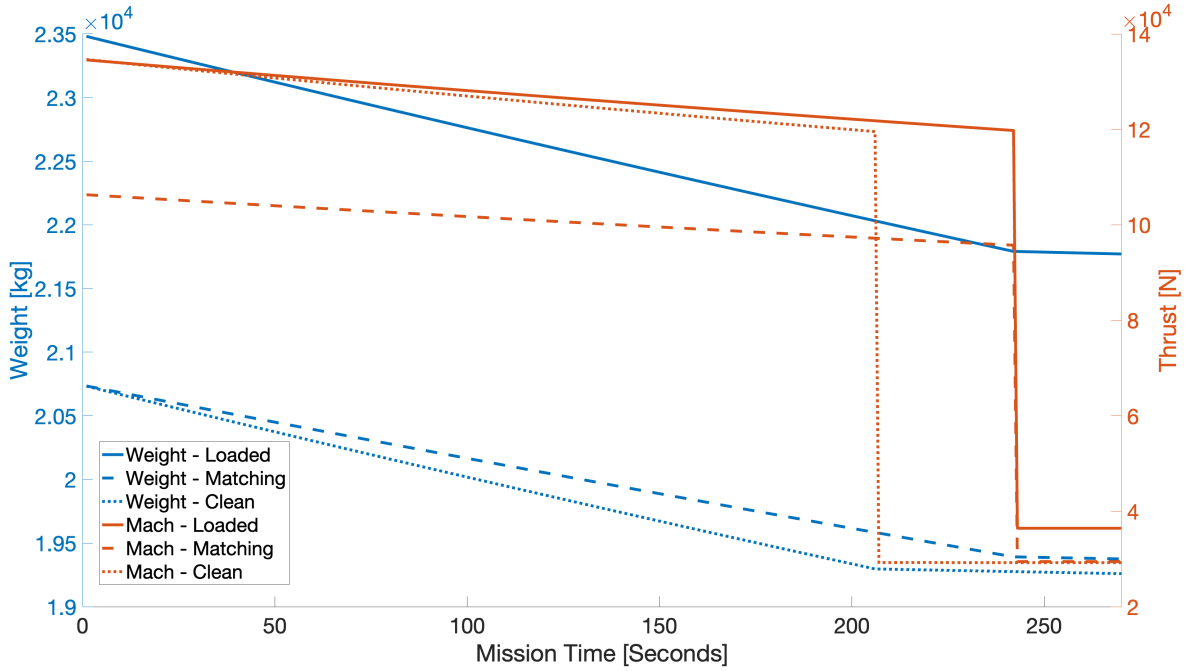

Figure D.5: PMTS Test 3 - Total Weight and Thrust Setting

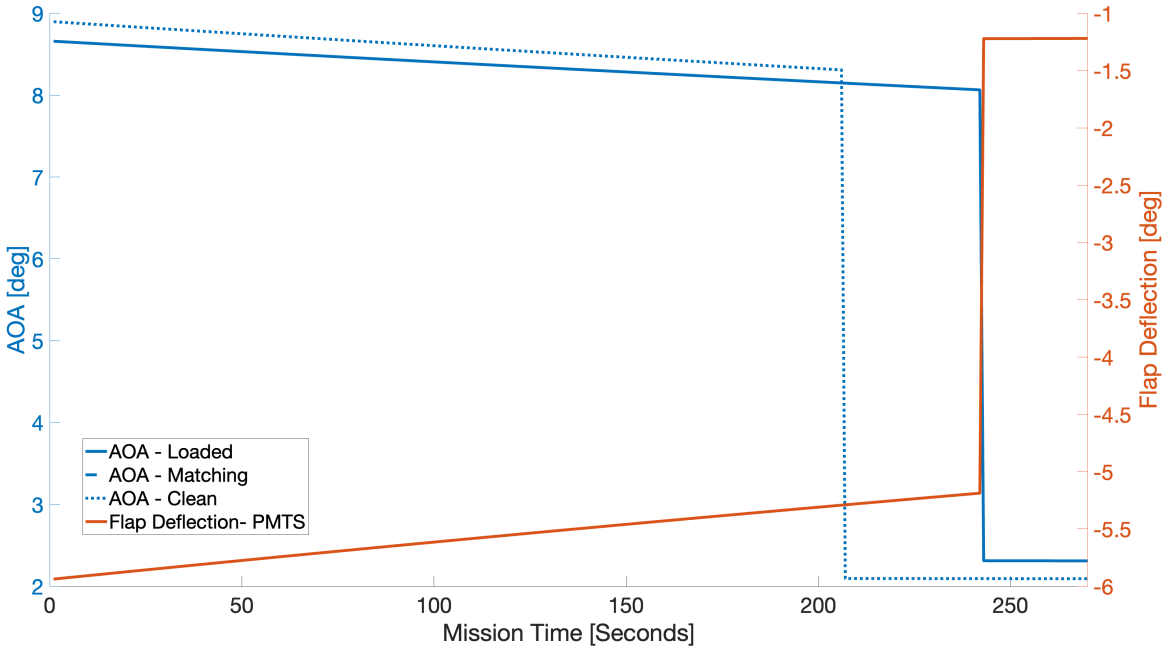

Figure D.6: PMTS Test 3 - Flap deflection angle and Angle of Attack

E

Mission Results Figures

E.1. Fuel Use

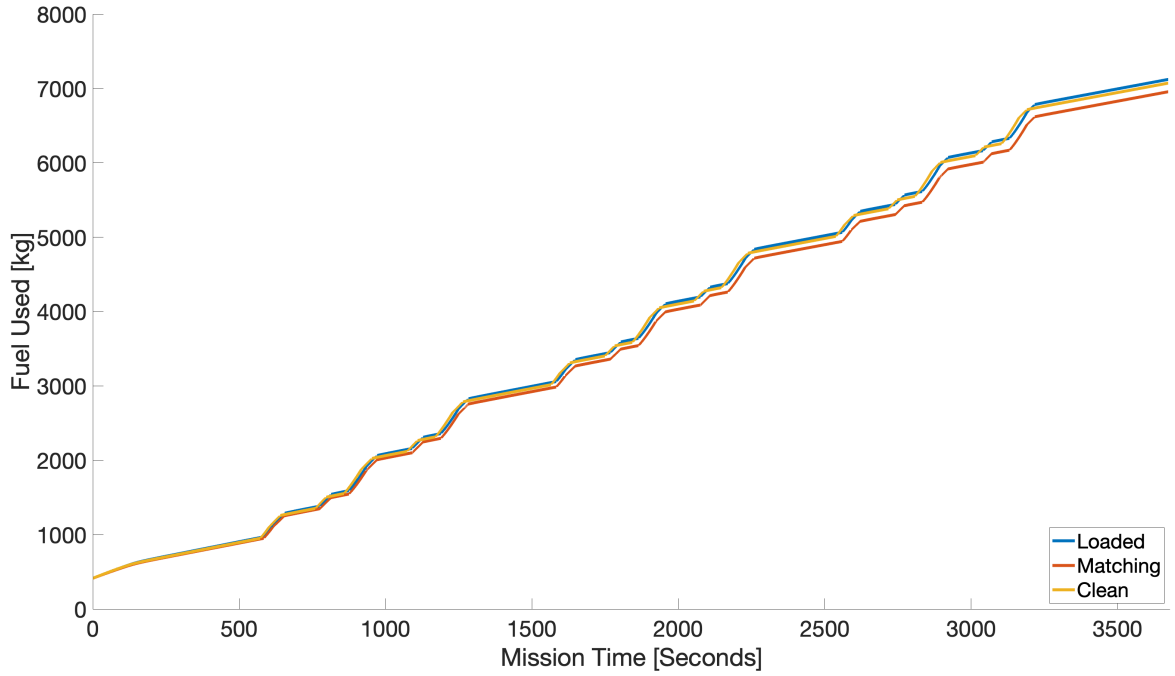

Figure E.1: Mission 1: Fuel Used

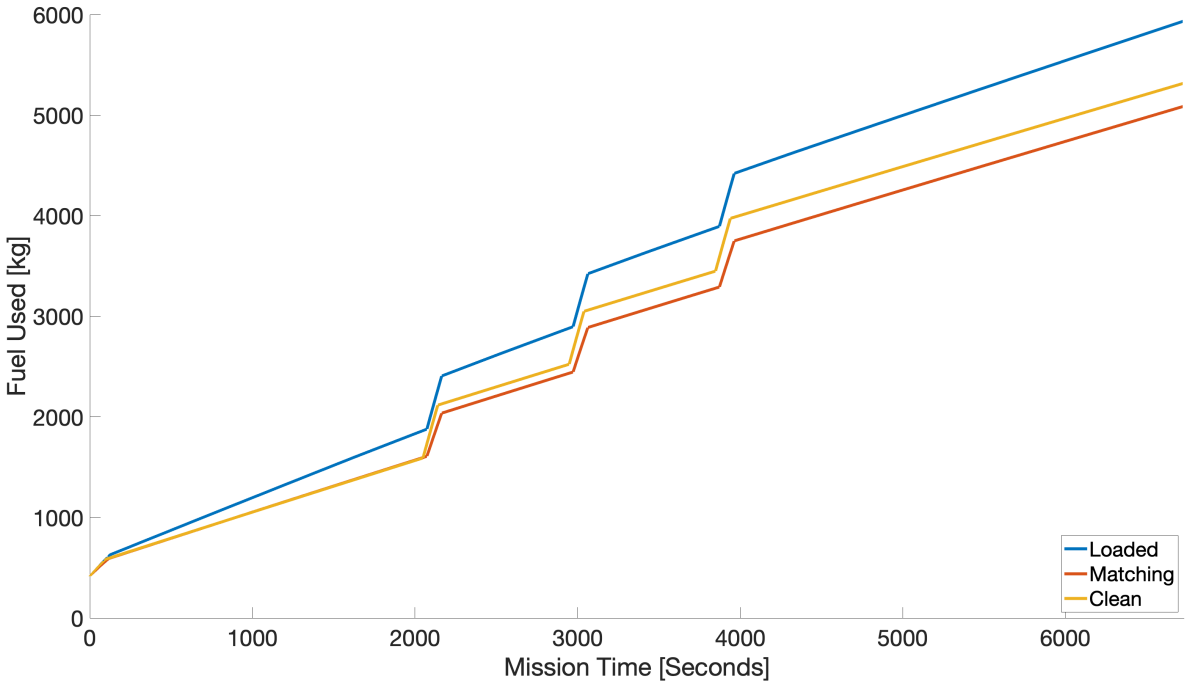

Figure E.2: Mission 2: Fuel Used

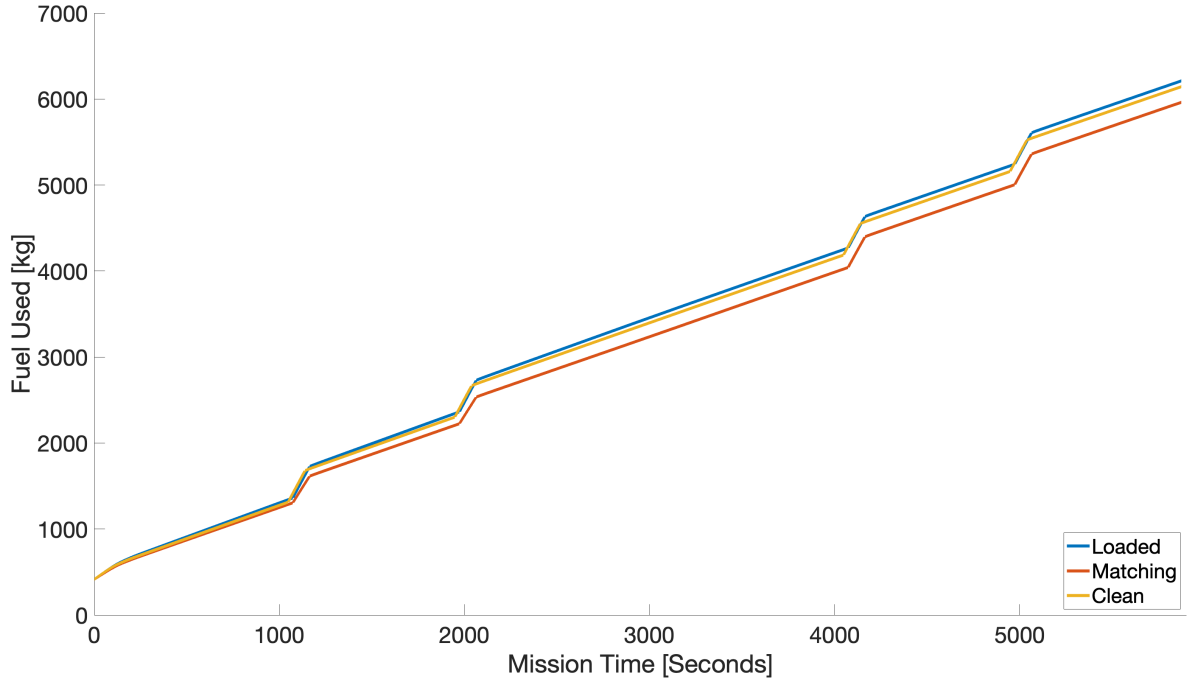

Figure E.3: Mission 3: Fuel Used